

***IN SITU* TEM INVESTIGATION OF DEFORMATION AND FRACTURE
MECHANISM IN NANOCRYSTALLINE NICKEL**

by

Zhiwei Shan

BS, Jilin University, 1996

MS, Institute of Metal Research, CSSA, 1999

Submitted to the Graduate Faculty of
the School of Engineering in partial fulfillment
of the requirements for the degree of
Doctor of Philosophy

University of Pittsburgh

2005

UNIVERSITY OF PITTSBURGH

SCHOOL OF ENGINEERING

This dissertation was presented

by

Zhiwei Shan

It was defended on

July 15, 2005

and approved by

Minking K. Chyu, Professor, Department of Mechanical Engineering

William S. Slaughter, Associate Professor, Department of Mechanical Engineering

Judith C. Yang, Associate Professor, Department of Materials Science & Engineering

Jörg M. K. Wiezorek, Associate Professor, Department of Materials Science & Engineering

Dissertation Director: Scott Mao, Professor, Department of Mechanical Engineering

IN SITU TEM INVESTIGATION OF THE DEFORMATION AND FRACTURE MECHANISM IN NANOCRYSTALLINE METALS

Zhiwei Shan, PhD

University of Pittsburgh, 2005

The strength of a material is known to increase with the decreasing grain size and will reach its peak strength at certain critical grain size. It was proposed and has been widely accepted that this results from the deformation mechanism crossover, i.e. a continuous transition from dislocation nucleation and motion to grain boundary mediated plasticity. Evidence for this has been sought for many years, however, to date, direct experimental confirmation remains elusive.

By solving the challenging problems encountered in previous studies, in situ dynamic dark field transmission electron microscope (TEM) investigations combined with in situ high resolution TEM observations have been performed successfully on high purity nanocrystalline nickel samples with an average grain size about 10nm, which show: 1) grain agglomerates formed very frequently and rapidly in many locations apparently independently of one another under influence of the applied stress, 2) both inter- and intra-grain agglomerate fractures are observed in response to the deformation, 3) trapped dislocations are frequently observed in grains which may be still in a strained state and no deformation twinning was detected, 4) trapped lattice dislocations were observed to move and annihilate during the stress relaxation. These TEM observations i) for the first time provide conclusive experimental evidence that grain boundary mediated plasticity, such as grain boundary sliding and grain rotation, has become a

prominent deformation mode for as deposited Ni. Theoretical analysis suggested that the deformation mechanism crossover resulted from the competition between the deformation controlled by nucleation and motion of dislocations and the deformation controlled by grain boundary related deformation accommodated mainly by grain boundary diffusion with decreasing grain size, ii) confirmed the speculation that dislocations are most probably observed in stressed grains, iii) suggested that the dimpled fracture surface of nanocrystalline materials may result from those newly formed grain agglomerates. Additionally, direct measurement of lattice distortions during straining revealed that grain interiors may experience ultra-high elastic distortions during tensile deformation.

TABLE OF CONTENTS

ACKNOWLEDGEMENTS.....	xii
1.0 GENERAL INTRODUCITON.....	1
2.0 BACKGROUND.....	5
2.1 INTRODUCTION.....	5
2.2 LITERATURE REVIEW AND RESEARCH OBJECTIVES.....	7
2.2.1 Processing of nanocrystalline materials.....	7
2.2.2 Mechanical properties of fcc nanocrystalline metals.....	9
2.2.3 Atomistic simulation.....	11
2.2.4 Transmission electron microscopy observations.....	13
2.2.5 Motivation and objective.....	16
3.0 EXPERIMENTAL PROCEDURES.....	18
3.1 MATERIALS.....	18
3.2 EXPERIMENT PRICIMPLE.....	19
3.2.1 Transmission electron microscope.....	19
3.2.2 Selected area electron diffraction patterns.....	21
3.2.3 Nano beam electron diffraction (NBED).....	22
3.2.4 Principles of TEM image contrast.....	23
3.2.5 Bright field and Dark field observation.....	24
3.3 EXPERIMENT EQUIPMENT AND METHODS.....	25

3.3.1	General observation	25
3.3.2	In situ dynamics BF TEM and NBED observations	26
3.3.3	In situ dynamics DF TEM and HREM observation.....	27
4.0	IN SITU BF TEM INVESTIGATION OF DEFORMATION IN NANOCRYSTALLINE NICKEL	28
4.1	INTRODUCTION	28
4.2	EXPERIMENT PROCEDURES	29
4.3	EXPERIMENT RESULTS.....	31
4.3.1	Microstructure of as deposited 60 nm Ni film	31
4.3.2	Dynamic bright field observation of microstructure evolution of 50nm Ni	33
4.4	DISCUSSION	36
4.5	CONCLUSIONS.....	37
5.0	IN SITU DF TEM INVESTIGATION OF THE DEDEFROMATION IN NANOCRYSTALLINE Ni	38
5.1	INTRODUCTION	38
5.2	EXPERIMENT PROCEDURE	39
5.3	EXPERIMENTAL OBSERVATIONS	40
5.3.1	Microstructure of as deposited 150 nm Ni film	40
5.3.2	Experimental observations.....	42
5.3.3	HRTEM observation.....	46
5.3.4	Discussion	47
5.4	CONCLUSIONS.....	49
6.0	IN SITU DYNAMICS HREM OBSERVATION	50
6.1	INTRODUCTION	50
6.2	EXPERIMENT PROCEDURE	51
6.3	EXPERIMETNAL RESULTS AND DISCUSSIONS	52

6.4	CONCLUSIONS.....	60
7.0	IN SITU NANO BEAM DIFFRACTION OBSERVATION.....	62
7.1	INTRODUCTION	62
7.2	EXPERIMENT PROCEDURE	63
7.3	EXPERIMENTAL OBSERVATIONS	63
7.4	DISCUSSION.....	69
7.5	CONCLUSIONS.....	75
8.0	FORMATION MECHANISM OF THE DIMPLED FRACTURE SURFACE	76
8.1	INTRODUCTION	76
8.2	MATERIALS AND EXPERIMENTAL METHODS	78
8.3	RESULTS AND DISCUSSION.....	80
8.4	DISCUSSION.....	89
8.5	CONCLUSION.....	92
9.0	SUMMARY AND CONCLUSIONS	94
10.0	OUTLOOK-QUANTITATIVE INVESTIGATION OF NANOCRYSTALLINE DEFORMATION	97
10.1	MOTIVATION.....	97
10.2	EXPERIMENTAL FEASIBILITY.....	99
	APPENDIX A.....	105
	APPENDIX B.....	110
	BIBLIOGRAPHY.....	119

LIST OF TABLES

Table 7.1: Summary of measured results of 8 NBED patterns.....	66
Table 7.2: Strength of whiskers ¹¹⁴	70

LIST OF FIGURES

Figure 3-1: Diagram of the main elements of TEM.	20
Figure 3-2: Selected area diffraction patterns from (A) single crystalline Ni and (B) Nanocrystalline Ni.	21
Figure 3-3: Ray diagram showing NBED pattern formation. A convergent beam at the specimen results in the formation of disks in the back focal plane of the objective lens.	22
Figure 3-4: Comparison of the use of an objective aperture in TEM to select (A) the direct and (B) the scattered electrons forming BF and DF images, respectively.	24
Figure 3-5: The ion thinning room in NCEM, LBNL.	25
Figure 3-6: Model 654 single tile holder and tip detail.	26
Figure 4-1: Schematic of the straining specimen, in which the free standing Ni film was glued on the special designed copper substrate.	29
Figure 4-2: Typical BF TEM image (A) and typical HREM observation (B) of as deposited nanocrystalline nickel with its nominal thickness of 60nm.	32
Figure 4-3: Localized plastic deformation, giving rise to bands of thinning and further straining lead cracks to nucleate and propagate in those band-like thinning areas.	33
Figure 4-4: Bright field observation of contrast evolution of an area during straining.	35
Figure 5-1: (a) Schematic of the straining specimen construction and (b) TEM image of the starter crack prepared with FIB.	39
Figure 5-2: TEM observations of the typical microstructure in the as-deposited nanocrystalline nickel films. The bright field TEM micrograph (A) and the selected area diffraction pattern (inset in (A)) show roughly equiaxed grains with random orientations. The statistical distributions for grain size (B) were obtained from multiple TEM images of the same sample.	41
Figure 5-3: TEM micrographs showing the evolution of the Ni microstructure during in-situ straining.	44

- Figure 5-4: DFTEM observation of the rapid genesis of an agglomerate (e.g. white arrow) depicted by individual still frames extracted from a dynamic video-sequence. (A) $t=0$ s, no grains in strong diffraction condition near the white arrow; (B) $t=0.1$ s, a grain in strong diffraction condition with size about 6 nm is visible; (C) $t=0.2$ s, a group of grains in bright contrast, size about 28 nm, is visible; (D) $t=0.3$ s, now the group of grains has a nearly elliptical shape, dimensions 60 nm by 35 nm; (E) $t=0.4$ s and (f) $t=0.5$ s, the size of the group of grains increases to maximum dimensions of about 80 nm by 60 nm. 45
- Figure 5-5: A typical HREM image of a thin area newly formed by deformation. A dislocation is trapped inside a grain close to the grain boundary (delineated by dark dash line). The inverse Fourier-filtered image (inset at upper right corner) from inside the white box shows the dislocation with more clarity..... 46
- Figure 6-1: (a) HREM micrograph of a thin area freshly formed by deformation. The Ts and arrowheads indicate the position of a trapped lattice dislocation in the grain interior. Grain boundaries were delineated by dark lines. (b) IFFT of the area framed with the black box in figure 3a. The Fourier-transformed image shown as an inset indicates that the electron beam is close to the 110 zone axis of the grain. (c) IFFT of the area framed with the white box in (a). 53
- Figure 6-2: Determination of the Burgers vector of the trapped dislocation. (A) HREM showed a dislocation (indicated by white arrow head) was trapped inside a grain close to the grain boundary (delineated by dark dash line). (B) The inverse Fourier-filtered image from inside the dark box in figure 6.2 (A) showed the dislocation with more clarity. Burgers circuit used to determine the Burgers vectors of the trapped dislocation is also shown. 55
- Figure 6-3: Dynamical HREM observations of the microstructure evolution of a grain during the stress relief. The positions of the dislocation cores have been indicated by T. (A) $t=0$ (B) $t=89$ s (C) IFFT of Figure A and (D) IFFT of Figure B 57
- Figure 7-1: Bright-field contrast (A, C, E) and its corresponding NBED pattern (B, D, F) evolution of a grain (delineated by dash line) during straining of as-deposited Ni at room temperature. The diffraction patterns did not match any known f.c.c zone axis. The intensity change of the diffraction spots suggested that the rotation of the grain involves multiple rotation axes. A reference coordinate is shown in figure 2E with its X and Y axis horizontally and vertically, respectively. 64
- Figure 7-2: (A) Gives the measurements of the co-angle changes between 1, 2, 3 diffraction vectors and the reference X-axis. (B) Gives the measurements of the distances of 1, 2 and 3 diffracted beams from the zero-order beam. 67
- Figure 8-1: Microstructure of as deposited nanocrystalline nickel. (a) Bright field TEM micrograph of the nanocrystalline Ni, (b) Typical HREM image of as deposited Ni. 81
- Figure 8-2: DF TEM observation of the deformation and fracture process of as-deposited nanocrystalline Ni. 82

Figure 8-3: DFTEM observation of the intra-agglomerate deformation depicted by individual still frames extracted from a dynamic video-sequence. 84

Figure 8-4: DFTEM observation of intra-agglomerate fracture depicted by individual still frames extracted from a dynamic video-sequence. (a) $t=0s$, a agglomerate with dimension of about 60nm by 90nm is indicated by the white arrow. (b) The agglomerate split at $t=0.13s$ (c) $t=0.23s$, the crack propagated across the agglomerate; the residual parts located at the crack edges are indicted by the white arrows. 86

Figure 8-5: Typical HREM image taken from the areas around the propagating crack tip. All the grains identified are divided by low angle grain boundaries and the lattice fringes are belong to $\{200\}$ type. 87

Figure 10-1: (a) Scanning electron micrograph of the microstage showing the freestanding aluminum thin-film specimen being attached to the force sensor beam at one end and to supporting beams at the other. Markers D and F, read displacements at both ends of the specimen. The left end of the microstage is pulled by a piezo actuator of a TEM straining stage. Deflection of the sensor beam (read by marker F), multiplied by its spring constant, gives the force on the specimen. The difference between the two markers' (D and F) gaps gives the elongation of the specimen. The gap XX' prevents accidental straining of the sample during mounting of the microstage on to the TEM straining stage. The TEM straining stage has to move and deform the microstage to close the gap XX' before loading the sample. (b) Microtensile test stage on a TEM straining stage. (c) Zoomed view of the specimen and the two displacement sensors D and F. There is no substrate under the specimen so that the TEM beam can go through the sample for microstructural inspection¹²⁷. 99

Figure 10-2: Schematic of original in situ nanoindentation holder for the high-voltage electron microscope¹³². 101

Figure 10-3: Schematic of in situ NI-II holder developed in NCEM, LBNL¹³³. 102

Figure 10-4: New quantitative in situ nanoindentation stage (NI-III), NCEM, LBL. 102

Figure 10-5: Preliminary results of the NI-III quantitative device. 103

ACKNOWLEDGEMENTS

First, from the depths of my heart, I would like to express my sincere gratitude and appreciation to Dr. Scott Mao, my major advisor, for his inspiration, encouragement and trust; to my unofficial co-advisor Jörg M. K. Wiezorek for his encouragement and endless support; to Dr. David Follstaedt and Dr. James Knapp, who are in Sandia National Laboratory, for their generous help in sample preparation; to Dr. Eric Stach, who is now a professor in Purdue University, for his assistance in the use of the facility in NCEM. I also would like to thank other members of my committee, Dr. Judith Yang, Dr. Minking Chyu, and Dr. William Slaughter, who have always been there for me. What I learn from all of them not only the academic excellence, but also the character nobleness.

My special thanks go to the National Center Electron Microscopy, Lawrence Berkeley National Laboratory, where most of the experimental work in this thesis was carried out. I would like to thank C. Y. Song, J. Cavlina, C. Nelson, J. Turner, D. Owen for their generous technical assistance; thank all my friends there for their kindly help.

I also owe gratitude to the faculty, staff, and student in Department of Mechanical Engineering and Department of Materials Sciences at the School of Engineering, University of Pittsburgh, for their help and encouragement, especially Dr. Zheng Chen, Dr. Long Li, and Dr. Huiping Xu, Dr.

Mingjina Hua for their guidance both professionally and personally. I am grateful to my colleagues and friends, M. Zhao, H. Wang, D. Li, H. Li, F. Xu, Q. Wang, Y. Lu, Z. Yang, T. Zhang, P. Yuan, for their assistance on countless occasions.

My final, and most heartfelt, acknowledgment must go to my wife, Xiaowen Zhu, My son, Benjamin and my family in China. Their understanding, motivation, encouragement, patience and love were as the foundation for me to go through this challenging endeavor.

1.0 GENERAL INTRODUCTON

The Hall-Petch relationship, i.e. the strength and hardness of materials is inversely proportional to the square root of the grain size, has been well established experimentally from millimeter-sized grains down to the submicron regime ¹. However, as grain size of the material is reduced to nano range (i.e. the grain size typically less than 100nm), a character length scale, d_c is observed, at which the material reaches its peak strength ². For the material with grain size greater than the d_c , a Hall-Petch relation roughly holds, but deviates form the classical $-1/2$ exponent to a value near zero. As grain size is reduced to less than d_c , a negative Hall-Petch slope, i.e., an inverse Hall-Petch behavior (softening) begins to emerge.

In order to uncover the underlying physical mechanism, numerous models have been proposed ^{3,4} and molecular dynamics simulations (MDS) ^{5,6} have been carried out. So far, it has been more or less accepted that the deformation mechanisms of a nanocrystalline material can be classified into three regimes, based on grain size. At the finest grain sizes (typically less than 10nm), it is believed that the only plastic deformation mechanisms possible are grain boundary (GB) processes. In the largest grain size regime (typically 30nm~100nm), the dominant deformation mode has been proven experimentally to be dislocation-mediated plasticity ⁷. Between them lies a crossover regime, where a continuous transition from dislocation nucleation and motion to GB mediated plasticity, i.e. from an intragranular process to an intergranular one, is expected.

The above proposed mechanism offers a reasonable explanation for the existence of peak strength of a material. However, they are mostly based on indirect experimental evidence ¹ as well as MDS ⁵. The latter, as suggested in a recent review ⁸, should be regarded only as a source of inspiration and qualitative guidance and not as a means to validate or disprove the existence of mechanism. Therefore, to find direct evidence that shows the operation of deformation mechanism transition has become critical to evaluate the above proposed mechanisms.

In-situ TEM investigation has been proven to be the powerful tool for revealing the underlying physical mechanism that dominates the macro behavior of the materials and it has been employed to find such direct evidence for many years. However, to date, experiments ^{7,9,10} failed to detect conclusive direct evidence for the operation of non-dislocation based plasticity mechanism. This naturally led to two questions: 1) Does a deformation mechanism crossover regime really exist? 2) If “yes”, where is it and how can we probe it experimentally? The paucity of such direct evidence severely limits our further understanding on this topic.

Backed by the abundant indirect evidence and the resounding physical insight from MDS, the existence of a crossover regime seems unchallenged. Therefore the failure to detect grain boundary mediated plasticity is most probably due to the inappropriate experimental means that have been employed. A detailed review of previous works readily shows that the materials used usually suffered from contamination, texture, porosity and other artifacts, and that the grain size is often at the upper limit or larger than the predicted crossover grain size regime. This means that high quality sample is necessary. After a comprehensive literature investigation, it was found the Ni prepared by pulsed laser deposition may be the best candidate material for our research objective due to its high purity, fully dense, very small grain size and narrow grain size distribution. The detail of the sample preparation procedure will be described in Chapter 3.

As for the technique, it has been proven that TEM provides the best means to reveal the underlying physical mechanism of nanocrystalline materials deformation and fracture due to its in situ, dynamics, atomic resolution and direct observation capability. Chapter 3 also gives the basic background for TEM. Due to the limitation of the sample design, all previous TEM investigations were performed only in bright field TEM mode, which makes it difficult to differentiate between the contrast changes resulting from dislocation activity and those from grain boundary activities. Therefore, in order to reveal the existence of the crossover regime, improved sample design and selective TEM observation techniques are required. Based on above consideration, in situ bright field TEM investigation under low strain rate (Chapter 4), in situ dark field TEM investigation (Chapter 5), in situ high resolution TEM observation (Chapter 6) and in situ nano beam diffraction observations (Chapter 7) with improved sample designs have been performed, respectively. For the first time, direct and compelling conclusive evidence of the deformation mechanism crossover was provided (Chapter 5). In addition, unexpected dislocation activities were also observed in grains as small as 5 nm (Chapter 6). Nano beam diffraction observations revealed that a nanocrystalline grain with a size of about 20 nm may experience ultrahigh elastic strain during deformation and the implication of this finding will be discussed in Chapter 7.

Dimpled structures are always observed on the fracture surface of nanocrystalline materials. In order to explain the observed phenomenon, several grain sizes related mechanisms have been proposed. However, none of them can give a reasonable explanation for the entire grain size regime. In Chapter 8, a new mechanism inspired by in situ TEM results was proposed which provides a rational for the formation mechanism of dimpled fracture surface for the entire grain size regime.

To date, most of the TEM works have been done qualitatively. However, in order to approach the truth of this tiny world, quantitative characterization is necessary. In chapter 9, I give the outline of possible future works.

2.0 BACKGROUND

2.1 INTRODUCTION

Nanocrystalline (nc) metals (characterized by a grain size less than 100nm) exhibit ultra-high yield and fracture strength and hardness^{1,11-14}, superior wear resistance^{15,16}, enhanced superplastic formability at lower temperature^{17,18} and faster strain rates relative to their coarse-grained counterparts^{19,20}. These appealing characteristics with potential significance for engineering applications have generated considerable interest both in the processing and in the characterizing of nc metals. The various methods invented to produce nc metals can be classified into two categories. One involves producing atom clusters or nano-scaled particles as precursor to form nanocrystalline materials with relatively large dimension by further consolidation process, e.g. physical vapor deposition, pulsed laser deposition^{21,22}, inert gas consolidation²³, chemical vapor deposition²⁴, electron deposition^{25,26}, amorphous crystallization²⁷⁻²⁹ etc. The other is to produce nanocrystalline materials from bulk coarse-grained materials. This approach includes processes like mechanical milling^{30,31}, shot peening³²⁻³⁵, severe plastic deformation^{36,37}, equal channel angular pressing³⁸, high pressure torsion^{39,40} etc.

How the grains deform in nc metals under stress is directly responsible for the observed unique mechanical properties. Among the important variables (such as grain shape, grain size, grain boundary structure, etc) that characterize the microstructure of nc metals, grain size plays

an important role in deciding the dominant mechanism of plastic deformation for crystalline materials. In coarse grained (cg, grain size larger than 1000nm) and ultra-fine crystalline (ufc, grain size ranged from 100-1000nm) metals, plastic deformation is mainly carried by the nucleation and motion of dislocations within the individual grains. Dislocations can move through the crystal grains and can interact with each other. Grain boundaries often act as barriers for dislocations transmission. It is the dislocation pile up at the boundary and the tangle of the dislocations in the grain interior that make the material harder to deform. Based on dislocation pile up, the strengthening with grain refinement has traditionally been rationalized by so-called Hall-Petch mechanism, i.e., the increase in yield stress is inversely proportional to the square root of the grain size. However, as grain sizes are reduced to the nanometer scale (less than 100nm), this process invariably breaks down and the yield stress versus grain size relationship departs markedly from that seen at cg and ufg metals⁴¹⁻⁴³. With further grain refinement, the yield stress of the nc metals peaks in many cases at an average grain size value on the order of 10~15nm or so and weakens with further decrease in grain size^{1,44}. Despite the large number of investigations devoted to the examination of their mechanical response and underlying reasons, the picture of the deformation mechanism in nc metals is far from being understood. Consequently, there is a concerted global effort underway using a combination of novel processing routes, experiments as well as large-scale computations^{5,45-48} to develop deeper insights into the various aspects of these phenomena.

2.2 LITERATURE REVIEW AND RESEARCH OBJECTIVES

2.2.1 Processing of nanocrystalline materials

The past two decades have witnessed remarkable advances in processing and characterization of materials with nanometer range. The motivation of these improvements is to get what so called high purity, fully dense, bulk, uniform, narrow grain size distribution, free of texture, and with an as small as possible average grain size value nanocrystalline materials. Gas phase condensation followed by consolidation (GPCC) is the earliest one employed. This technique was pioneered by Gleiter¹¹ and only produces nano structured materials in powder form. Subsequent compaction and densification to full density have been proven to be a great challenge. The major stumbling block is grain growth during consolidation of the nanometer-sized powder, diminishing the unique characteristics of the nanostructure. Another problem associated with powder metallurgy is the introduction of impurities during the course of processing. It has been shown recently that the density of the specimens can be increased by cold rolling, while retaining the equiaxed, texture free microstructure without a change in grain size⁴⁹; So far, contamination, imperfect particle bonding and volume flaws such as porosity have been the major artifacts that adversely influence the properties of nano-structured (ns) metals. They are also the origin of controversies in the interpretation of various experimental observations of the mechanical properties. As pointed out by some previous work, the use of a two step⁵⁰ (powder production and consolidation) process to obtain bulk samples can be both expensive and problematic.

Electrodeposition⁵¹ (ED) (direct current and pulsed) has been proposed to be able to prepare fully dense nanocrystalline materials^{41,51,52}. It has been used to produce sheets (with

thickness of 100µm or more) of nc metals such as Ni⁵³, Co^{54,55}, Cu^{52,56}. Grain size of 20-40nm are routinely produced by controlling the component of the plating bath and other parameters. However, possible roles of texture, pre-existing voids, columnar grain structure, and hydrogen, carbon and sulfur either in solid solution or segregated to grain boundaries influencing the mechanical response are intrinsic problem of this popular method. Therefore, reports on mechanical properties have to be accompanied by an accurate microstructure investigation.

Equal channel angular extrusion (ECAE) is a technique invented and pioneered by Segal⁵⁷ by subjecting a metal to severe plastic deformation through a simple shear processes with little, if any change in the cross sectional area of the work piece. The technique is announced to be able to produce truly bulk, fully dense and contamination-free metals with sub-micron to nanoscale grain sizes and therefore attracted the growing interest of specialists in materials science (for detail, see review by Valiev R.Z et al,⁵⁸). However, this method has limited ability to refine the grain size of metals into tens nanometer or smaller as well as to get expected high angle grain boundaries.

Surface mechanical attrition treatment (SMAT) was asserted⁵⁹⁻⁶² to be a “one-step processing” technique compared with GPCC and can prepare nc microstructures with predominantly high-angle grain boundaries in a sample that is sufficiently thick to represent bulk behavior, yet without introducing contaminations or porosity. However, as prepared samples are far from uniform. The grain sizes are usually a function of depth from the surface.

Recently, Hugo R.C et al⁹ have studied the nanocrystalline Ni thin films prepared by DC Magnetron sputtered and pulsed laser deposition, respectively with in-situ TEM. It was found the material processed by DC magnetron sputtered deposition behave in a brittle manner, with failure occurring via rapid coalescence of intergranular cracks. Conversely, the laser deposited

film behaved in a ductile manner, with failure occurring by slow ductile crack growth. The difference was attributed to the high porosity found at the grain boundaries in the sputtered film. Further TEM and indentation studies²² show that the Ni films prepared by pulsed laser deposition are especially defect free, high purity nanocrystalline material with a narrow grain size distribution. In addition, the grain size is controllable. It is evident from the foregoing discussion that the nanocrystalline materials prepared with pulsed laser deposition (PLD) may be the best candidate material for the objective of our study.

2.2.2 Mechanical properties of fcc nanocrystalline metals

The grain size dependence of yield stress in metals has been represented as a $d^{-1/2}$ relationship since the pioneering work of Hall⁶³ and Petch⁶⁴. The term Hall-Petch was introduced by Conrad⁶⁵ as a tribute to these researchers. The classic Hall-Petch relationship has been used for several decades to describe the relationship between yield stress and grain size, namely

$$\tau = \tau_0 + kd^{-\frac{1}{2}} \quad (1)$$

where τ is the yield stress, τ_0 is the friction stress needed to move individual dislocations, k is a constant (often referred to as the Hall-Petch slope and is material dependent), and d is the average grain size. The original explanation for this effect, envisaged by Hall and Petch⁶⁶, was that pile-ups formed at grain boundaries, and required a critical stress to break through them. However, this relation has been the subject of intensive research in recent years due to the complex behavior observed in nanophase materials^{22,44,67-69}. Most of the results confirm the validity of the classical H-P relation down to the grain sizes of the order of a few tens of nanometers, eventually with a different slope in the sub-micro range but keeping the classical

exponent $-1/2$. Masumura et al¹ plotted a Hall-Petch plot based on the published data. According their plot, the reported data show three different regions: (1) a region from single crystal to a grain size of about $1\mu\text{m}$. There is universal agreement of effectiveness of Hall-Petch relation in this grain size region. (2) A region for grain sizes ranging from $1\mu\text{m}$ to about 30nm . Hall-Petch relation roughly holds, but deviates from the classical $-1/2$ exponent to a value near zero. Although some of the deviation from Hall-Petch strengthening could be simply be due to the artifacts of the samples, such as pores, impurities at the grain boundary and trapped in the interior of the grains, if the totality of the data is taken into consideration, it is fairly safe to conclude that the increase in strength on grain refinement in this region is somewhat less than predicted by the Hall-Petch relation. (3) A region for grain sizes less than 30nm . Much more controversial observations have been reported in this grain size region. The inaccurate measurement of grain size, uncertainties about the nature of the grain boundary, as well as different measuring methods can all be responsible for the diversity of the results. However, if all available evidence in taken into consideration, a negative Hall-Petch slope of softening with further reduced grain size, i.e., an inverse Hal-Petch relation appears to be visible at least in some systems.

Based on the idea that dislocation pile-ups can not be supported at the very small grain sizes⁷⁰, Various models have been proposed to offer an explanation for the apparent controversy^{1,44,68,70-73}. These frequently predict a deformation mechanism transition from one mainly controlled by dislocation mediated plasticity to one mainly controlled by grain boundary activities along with the decrease of the grain size. However, except for indirect evidence, to date, direct experimental confirmation of deformation mechanism crossover remains elusive⁷⁴.

2.2.3 Atomistic simulation

The use of large scale molecular dynamics (MD) simulations has provided insight into the atomic scale processes that may occur during plastic deformation. Such computer simulations are usually performed in uniaxial tension, with high loads chosen to produce a measurable strain within the sub-nanosecond MD time scale. Two loading models have been taken in the simulation of deformation: the first is to keep the load constant and evolution of deformation over time is followed⁷⁵⁻⁸⁵. The second is to apply a strain step by step, followed by a short relaxation time during the interval^{5,45}. This is similar to the constant strain rate deformation. Both room temperature deformation and high temperature deformation^{47,80} have been performed with MD simulations.

At room temperature and in fully 3D grain boundary networks with an average grain size value below 30nm in Ni and Cu, the simulation demonstrates the ability of the nano-sized grain boundary network to accommodate an external applied stress by means of GB sliding and emission of partial dislocations involving local structure changes in the network^{5,45,79-82}. When a constant strain rate is applied to nc Cu, the yield stress is found to decrease with decreasing grain size, thereby suggesting a reverse Hall-Petch type relationship^{5,45}. This softening has been ascribed to the increased content in grain boundary atoms that facilitate sliding and no direct link with dislocation activity.

Simulations of tensile deformation have also been performed at room temperature on Al with 2-D-columnar GB networks^{76,77,86}. The four columnar grains have special orientations, so

that only three types of grain boundaries are represented. For a 20nm columnar diameter sample, it was shown that by increasing the load from 2 to 2.3 GPa, the strain rate increases by more than two orders of magnitude resulting in strain rates of $\sim 10^8$ - 10^9 /s, and that the deformation process changes from one involving grain boundary processes to one dominated by partial dislocations with a strain rate that depends inversely on the grain size. The presence of two length scales, one the grain size and the other represented by the dislocations splitting distance under stress, was recognized as being important to the onset of slip-deformation processes in nc Al. The analysis led to the generation of a deformation map that captured the interplay between these two length scales. Twinning was shown to occur after approximately 12% plastic strain and a stress level of 2.5 GPa for a grain size of 45nm, with twins originating at grain boundaries as well as in the grain interior from the interactions of stacking faults⁸⁶. Further, the authors predicted that the plastic deformation is predominantly carried by deformation twinning. However, by repeating the simulation for a 2D columnar sample using the same potential as for their 3D samples, Frøseth et al⁸⁷] found that the dominant deformation mechanism in defect-free samples is full dislocation activity instead of partial dislocations as reported earlier and twinning cannot be a predominant deformation mechanism in defect-free samples. The apparent discrepancy between different simulations shows that except the intrinsic limitation, such as restricted time-scale (only last for picoseconds) or strain rate (be 10^9 /s), unrealistic perfect samples as well as all kinds of unproven assumptions, the simulation itself is far from a self-consistent system. Therefore, as asserted in a recent review by Kumar et al⁸, the simulation should be regarded only as a source of inspiration and quantitative guidance and not as a means to validate or disprove the existence of a mechanism

2.2.4 Transmission electron microscopy observations

From the foregoing literature review, it is clear that a deformation mechanism crossover at a given critical grain size regime has been suggested by both the MD simulations and indirect evidence (mainly the indentation, tensile or compression experiment). But how, and at what grain size will the deformation mechanism crossover occur is still under discussion. Transmission electron microscopy (TEM) has been proven to be a powerful tool that may disclose the secret of this black box because of its ability to examine the postmortem deformation microstructure at atomic scale and/or the deformation processes directly. By checking the microstructure with the help of post-mortem TEM investigation, Legros et al.⁴ failed to detect any dislocation debris or trapped lattice dislocations in their tensile deformed nanocrystalline Ni with its initial average grain size about 28nm. By assuming that grain boundary acts as dislocation source and based on the yield stress measured in their experimental, the authors⁴ further predicted that the critical grain size below which dislocations stopped to contribute to deformation is about 20~30nm for Ni. However, this estimate for the critical grain size at which dislocation source activation stops contradicts the results from MD simulation and the models based on the mechanical test, both of which showed that dislocations will remain active to grain size as small as about 10nm.

With the objective of observing activated deformation mechanism, dislocation motion, and/or grain boundary related deformation as they occurred, a few pioneering in situ deformation studies have been conducted in the TEM^{7,9,10,88}. The first of these observations was performed on a nanostructured gold thin film with grain diameters of 10nm and a film thickness of 10~20nm by Ming Ke et al⁸⁸. The gold thin films were produced by ion beam sputter deposition

on a layer of 50nm amorphous polyvinylalformal film, which was supported by a 200 mesh copper grid and then strained the copper grid in JEOL 4000FXS TEM with a Gatan single tilt heating/straining stage equipped with displacement control and measurement capabilities. By measuring the changes in the angular relationships between the lattice fringes of different grains during deformation, grain rotation was asserted to be observed. In addition, no evidence of dislocation activity was detected during or after staining. However, the authors did not give comments on the possible effect of the substrate, which can definitely affect the arrangement of the grains on its top and therefore any results gained may be much different from that expected for free standing thin film. In addition, the thickness of the gold film is only one to two times of grain size, which means the films are far from a continuous solid, but may include many pores (as indicated by authors) and cracks. What is more, the extremely low pore growth rate ($10^{-12}\sim 10^{-13}$ m/s) makes the experiment much more like a traditional creep test instead of an in situ tensile deformation test. All of the above reasons seriously weaken the reliability of the conclusion gained in this experiment.

The second of these studies was recently accomplished by Youngdahl et al¹⁰. The copper specimens used in this study were produced by inert gas condensation followed by compaction with a reported dense of 97%. Although the nominal grain size measured by X-ray diffraction data was 30nm, the TEM observation shows the samples have a much wider grain size distribution ranging from 20-500nm and with the majority lying between 50-80nm. (This indicated the measurement of the grain size based on indirect method such as X-Ray may deviate much from the truth and therefore one has to be very careful of the value gained.) The samples were strained and viewed in a Philips CM30 TEM operating at 300kv in the bright field mode. Parallel arrays of dislocations are claimed to be observed in grains as small as 50nm in size. Rapid

and repeated contrast changes in individual grains with their size down to 30nm during straining are observed and ascribed to be the result of dislocation motion. However, for the grains with their size less than 30nm, the visualization is not available due to the size overlap problem. Further, it was noted that no evidence for grain boundary related deformation has been detected in their experiment.

Kumar et al.⁷ reported observations of an in-situ deformation study on a so called electrodeposited, fully dense, nanocrystalline Ni with an average grain size of ~30nm and a narrow grain size distribution. They found extensive dislocation activity within several grains ahead of the crack tip, emission and absorption of dislocations at grain boundaries. Further, the authors concluded that dislocation-mediated plasticity plays a dominant role in the deformation of nanocrystalline Ni examined. Although the authors mentioned that grain boundary sliding facilitated the nucleation of voids (which are thought as nucleation sites for dimples formed on the fracture surface) in their proposed deformation mechanism, no evidence of grain boundary related deformation have been reported.

Hugo et al.⁹ reported in-situ TEM tensile testing on two nanocrystalline Ni thin films, one prepared via DC magnetron sputtering and the other prepared via pulsed laser deposition. The former had a grain size of 19nm and latter has a grain size of 17nm. Both films had a nominal thickness of 100nm. Because of the presence of grain boundary porosity, the sputtered material was found to behave in a brittle manner, with failure occurring via rapid coalescence of intergranular cracks. However, the laser deposited film behaved in a ductile manner, with failure occurring by slow ductile crack growth. Because of what so called global and local tilting of the samples, all of the experiments reported in this work were performed in bright-field imaging

mode. Again, the authors reported that both films exhibited pervasive dislocation motion before failure, and showed no conclusive evidence of grain boundary related deformation.

2.2.5 Motivation and objective

It is evident from the foregoing discussion that very limited fundamental understanding exists of the deformation in nanocrystalline metals. The key point is whether or not grain boundary related deformation will submit traditional dislocation mechanism as the dominant deformation mechanism when grain size is reduced down to some critical value. No doubt, in situ dynamics TEM tensile test are the best choice for the direct study and possible verification of this mechanism.

It has been argued by MD simulation that grain boundary related deformation, grain rotation and/or grain boundary sliding will be facilitated by the thin film geometry and the accelerated diffusive events near the surface under the electron beam flux. If this is true, the absence of the grain boundary mediated deformation in thin film means this phenomenon is less likely present in bulk materials. Then all the theories based on grain boundary mediated deformation have to be reconsidered. However, the numerous indirect evidences as well as the theoretical analysis indicated this is not likely to be the case. Another possibility is that what so called artifacts of film geometry and/or the effect of beam flux are not important to the observed deformation mechanism. In a recent review ⁸, it has been pointed out that the simulation should be regarded only as a source of inspiration and qualitative guidance and not as a means to validate or disprove the existence of a mechanism. By carefully examining the existing theoretical analysis as well as the reported experiments, the absence of the grain boundary related deformation may be due to the following reasons: First, the average grain size used in the

in situ TEM tests are not small enough. As mentioned in the foregoing discussion, the peak value of the strength or the softening occurred when the average grain size is in the range of 10~20nm. This means the obvious deformation mechanism transition are most likely to be observed in the samples with the average grain size in this regime. Therefore, good sample, i.e. one that is full dense, with narrow grain size distribution, a lower average grain size value (10~20nm), free of contamination and texture is necessary for the further experiment. Second, the TEM technique employed to identify the possible activated deformation mechanism has not been appropriate. To date, all the observations reported are obtained with the bright field mode, which makes it difficult to differentiate the contrast changes resulting from grain boundary related deformation and those resulting from the motion of lattice dislocations in such small grain size system under normal straining conditions. Therefore, it is necessary to explore other effective TEM techniques, for instance, such as low strain rate observations, dark field observation, as well as micro beam diffraction.

The present study was, therefore, initiated with the specific objective of observing, both during and after deformation by TEM experiments, the mechanisms of the deformation and fracture using state of the art experimental tools in high purity, fully dense nanocrystalline metals with a narrow range of grain sizes.

3.0 EXPERIMENTAL PROCEDURES

3.1 MATERIALS

In this work, we chose to use the nanocrystalline nickel film prepared by pulsed laser deposited (PLD). The Ni films were deposited in vacuum using a KrF excimer laser, with a wavelength of 248nm, a 34ns full width at half maximum (FWHM) pulse width, and operated at a pulse rate of 35HZ. The pure Ni ablation target and sample substrates were mounted in an all-metal vacuum chamber with a base pressure of 2×10^{-7} Torr. The laser light was directed through a UV-transparent window to a fixed position in the plane of the Ni target. The target was continuously rastered in that plane over several square centimeters during deposition. The laser power density at the target was typically $1-2\text{J}/\text{cm}^2$, such that $\sim 0.007\text{nm}$ of material was deposited with each shot, yielding a $\sim 0.25\text{nm}/\text{sec}$ growth rate.

A particle filter is mounted between the targets and the sample to eliminate the slow, non-plasma components of the laser ablation plume, which would otherwise lead to a rough, nonideal film. The interposed velocity filter consists of a 15cm diameter wheel with two 5cm wide slots around the periphery; it is spun at high speed during the deposition, with the laser synchronized to the wheel position. The laser is fired when one of the openings is positioned between the target and sample substrate, allowing the fast ($\sim 10^3\text{m}/\text{s}$) plasma component of the plume to pass though to the substrate, while blocking the slower moving ($\sim 10\text{m}/\text{s}$) particle component. The

velocity filter is spun at 2100 rpm with a wheel to target spacing of 2cm, producing an area on the substrate ~1cm wide with a smooth, uniform film incorporating very few large particles²². The substrate used in our study is [001] NaCl.

3.2 EXPERIMENT PRICIMPLE

3.2.1 Transmission electron microscope

TEM is a unique tool in characterization of materials crystal structure and microstructure simultaneously by diffraction and imaging techniques. A projector shines a beam of light through (transmits) the slide, as the light passes through it is affected by the structures and objects on the slide. These effects result in only certain parts of the light beam being transmitted through certain parts of the slide. This transmitted beam is then projected onto the viewing screen, forming an enlarged image of the slide. TEM work the same way except that it shines a beam of electrons through the specimen.

Figure 3.1 shows briefly the principle of TEM. The electron gun produces a stream of monochromatic electrons. This stream is focused to a small, thin, coherent beam by the use of condenser lenses 1 and 2. The first lens which is usually controlled by the "spot size knob" largely determines the "spot size", i.e. the general size range of the final spot that strikes the sample. The second lens which are usually controlled by the "intensity or brightness knob" actually changes the size of the spot on the sample; changing it from a wide dispersed spot to a pinpoint beam. The beam is restricted by the condenser aperture, knocking out high angle electrons (those far from the optic axis, the dotted line down the center). The transmitted portion

is focused by the objective lens into an image. Optional Objective and Selected Area metal apertures can further restrict the beam; the Objective aperture enhancing contrast by blocking out high-angle diffracted electrons, the Selected Area aperture enabling the user to examine the periodic diffraction of electrons by ordered arrangements of atoms in the sample. The image is passed down the column through the intermediate and projector lenses, being enlarged all the way. Finally, the electrons strike the phosphor image screen and light is generated, allowing the user to see the image.

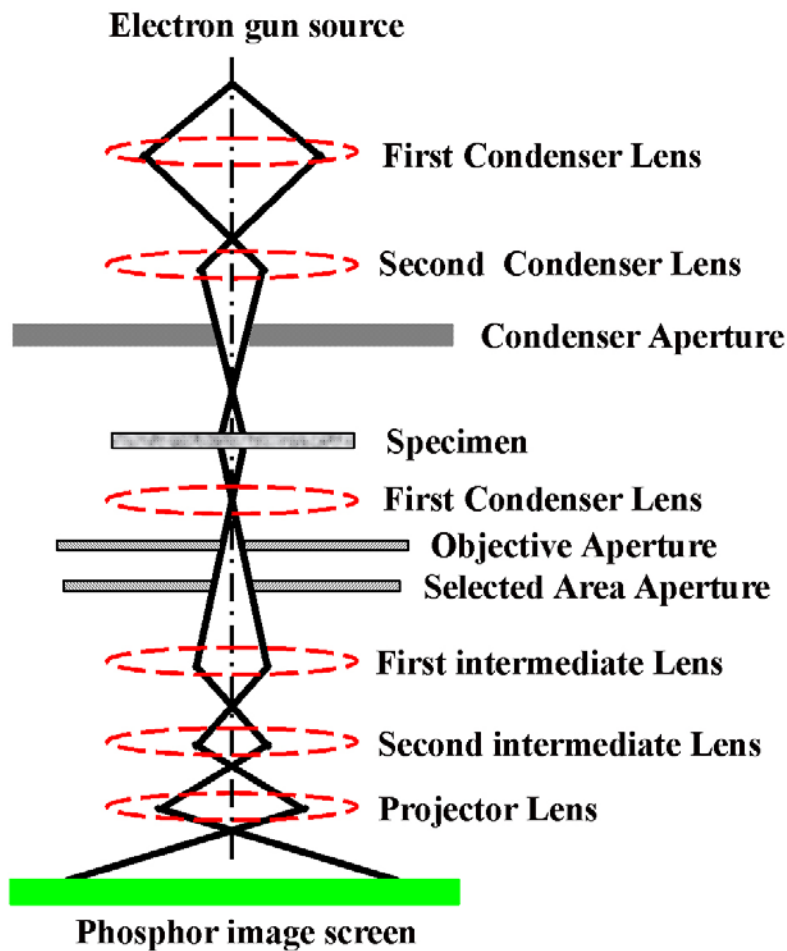


Figure 3-1: Diagram of the main elements of TEM.

3.2.2 Selected area electron diffraction patterns

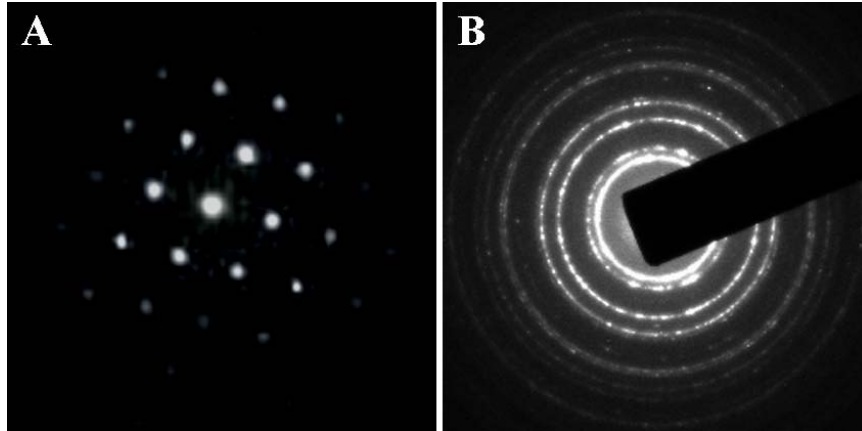


Figure 3-2: Selected area diffraction patterns from (A) single crystalline Ni and (B) Nanocrystalline Ni.

Selected area electron diffraction (SAED) is a method in which the selected area diffraction pattern (SADP) was produced on the display screen of the microscope when parallel electrons which are excited from gun under high voltage (80~1000 kV) transmitted through a small area (usually $\sim 1\text{-}10\mu\text{m}$ in diameter, determined by intermediated lens aperture size) of the thin foil specimen and are diffracted according to Bragg's law. For single crystal material, SADP consists of a transmitted beam (or direct beam) spots and many other periodic distributed diffracted beam spots (figure 3.3 A). But for poly- or nanocrystalline materials, the SADP consists of a transmitted beam and a number of rings (figure3.3 B). Although the real diffraction phenomena is due to complex interactions of charged electrons with the periodic potential field of the lattice, Bragg's Law or Laue Conditions are sufficient approximations for usual practical applications. A SADP is, in the simplest sense, a Fourier transform of the periodic crystal lattice, giving us information on the periodicities in the lattice, and hence the atomic positions. With the help of

SADP, one can obtain the following information of the sample from which the EDP was taken: crystalline or amorphous; if crystalline, the crystallographic characteristics, such as lattice parameter, symmetry, etc; orientation of the individual grains with respect to the electron beam; any special grain boundaries, such as twin boundary, single phase or multi phase boundaries, etc.

3.2.3 Nano beam electron diffraction (NBED)

Unlike conventional SAED in which the electron beam incident on the specimen is parallel, nano beam electron diffraction (NBED) is a method in which a diffraction pattern is formed on the display screen by finely converged electron beam illuminating only a very small area (usually ~10~100nm in diameter, depend on the type of equipments used) on the specimen.

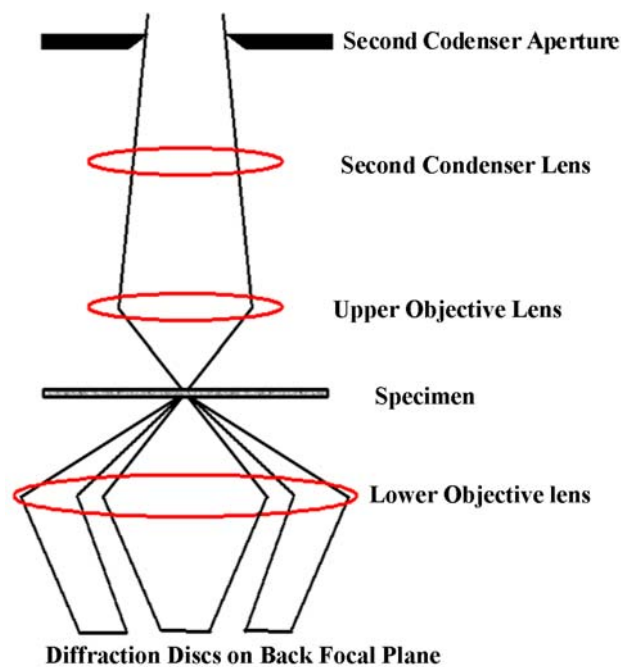


Figure 3-3: Ray diagram showing NBED pattern formation. A convergent beam at the specimen results in the formation of disks in the back focal plane of the objective lens.

3.2.4 Principles of TEM image contrast

Quantitatively, contrast can be defined as the difference in intensity (ΔI) between two adjacent areas

$$C = \frac{I_2 - I_1}{I_1} = \frac{\Delta I}{I_1} \quad (3.1)$$

Generally speaking, TEM image contrast arises because of the scattering of the incident beam by the specimen. The electron wave can change both its amplitude and its phase as it traverses the specimen and both these kinds of change can give rise to image contrast. Thus a fundamental distinction we make in the TEM is between amplitude contrast and phase contrast. In most cases, both types of contrast actually contribute to an image, although one will tend to dominate. Amplitude contrast includes two principle types, namely mass-thickness contrast and diffraction contrast.

Mass-thickness contrast arises from incoherent (Rutherford) elastic scatter of electrons. It was found the cross section for incoherent scatter is a strong function of the atomic number as well as the thickness of the specimen⁸⁹. Generally speaking, a region with high atomic number element is expected to scatter more electrons than low atomic number region of the same thickness; thick regions scatter more electrons than thin region of the same elements. As a consequence, for the case of a bright field image, thicker and/or higher mass areas will appear darker than thinner and/or lower mass areas. The reverse will be true for a dark field image.

Diffraction contrast is simply a special form of amplitude contrast because the scattering occurs at special angles (Bragg diffraction) which are controlled by the crystal structure and orientation of the specimen.

3.2.5 Bright field and Dark field observation

Bright field (BF) and dark field (DF) are two basic TEM modes to form amplitude-contrast images. When only the direct beam is selected by objective lens, a BF image will be formed in the image plane of the lens, as shown in Figure 3.4 A. The arrangement will produce amplitude contrast whether the specimen is crystalline or amorphous. If we tilt the incident beam such that one of the diffraction beams remain on axis (Figure 3.4 B), then a centered dark-field (CDF) image will be formed. In this work, I assume CDF is the operational mode in DF imaging.

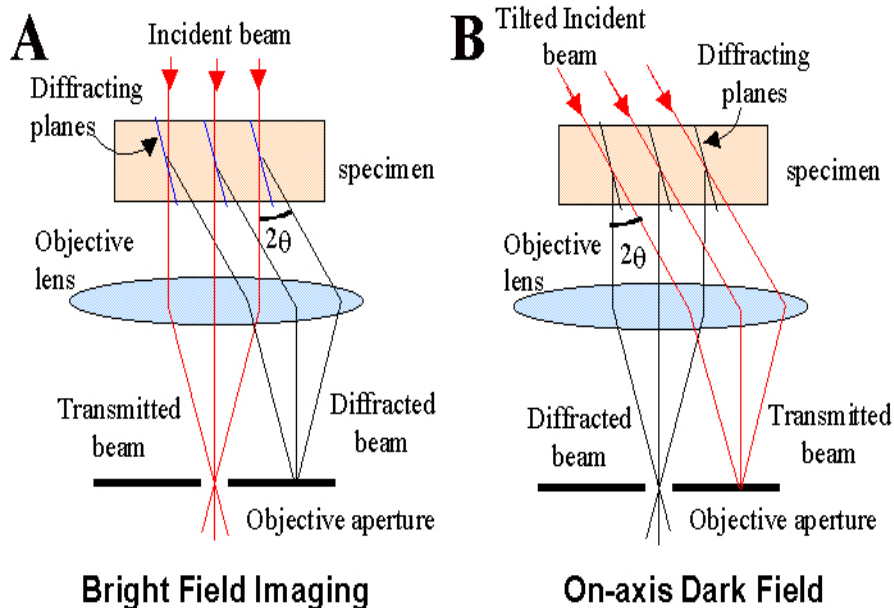


Figure 3-4: Comparison of the use of an objective aperture in TEM to select (A) the direct and (B) the scattered electrons forming BF and DF images, respectively.

3.3 EXPERIMENT EQUIPMENT AND METHODS

3.3.1 General observation



Figure 3-5: The ion thinning room in NCEM, LBNL.

For general observations, the Ni films which have been trimmed into 2 by 3 mm along with its salt substrate were first carefully put into a cup of deionized water to get the free standing films. Then 200 mesh copper grids (TED Pella) were used to take the Ni films out with the help of tweezers. Great patience has to be paid in this step to make sure the Ni films were filtered out as a flat patch. After drying with clean filter papers, the Ni film was transferred into the chamber of a Fischione ion thinning machine (as shown in the middle of Figure 3.5) with the copper grid

down. The specimen was then ion-thinned to perforation from the upside by means of single-gun milling with the aid of liquid nitrogen cooling. The operating voltage was 5 kv and the tilt angle was about 10 degree. Finally, in order to remove possible deposited contamination on the specimen surface, a cleaning process was performed under a voltage of 2 kv with double-gun milling for 10 min. The resulting thinned specimen was examined in an atomic resolution microscopy (ARM) with a point to point resolution of 0.15nm to characterize the micro structures of as-prepared Ni.

3.3.2 In situ dynamics BF TEM and NBED observations

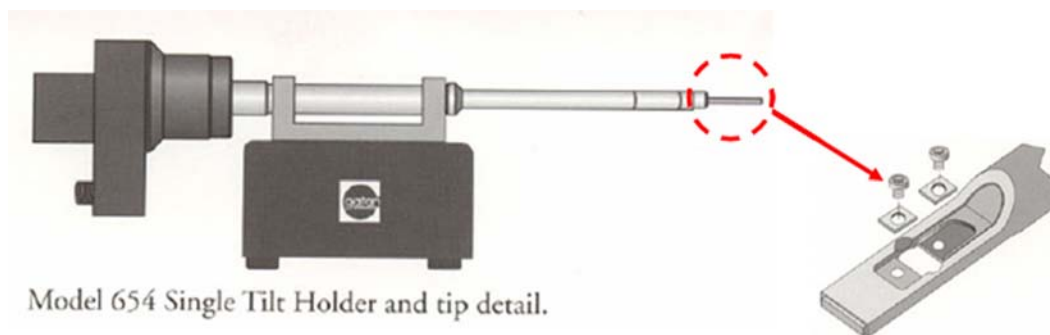


Figure 3-6: Model 654 single tile holder and tip detail.

Both the in situ dynamics BF and nano beam electron diffraction (NBED) were performed within a JEOL 2000 STEM which is located in electron microscopy center, Department of Materials Science, University of Pittsburgh. The operative voltage is 200kV. The room temperature tensile loading during in-situ TEM experiments was applied incrementally in discrete steps with a Gatan 654 single tile straining holder (as shown in Figure 3.6). The use of the thermal-emission electron gun of the JEOL 2000FX limited the minimum workable probe size for NBED to a

diameter of about 20nm. Hence, here only the larger grains in the Ni film could be probed during the tensile loading in the TEM. All the images were taken with a Gatan CCD camera.

3.3.3 In situ dynamics DF TEM and HREM observation

Both in situ dynamics dark field TEM observation and in situ dynamics HREM observation were done by employing a JEOL 3010 instrument operating at 300kV with a point-to-point resolution of 1.9 Å. Still images were obtained with a Gatan 754 Digital CCD camera and videotape images were obtained with a Gatan 622 TV-rate video-intensified camera and recorded with a VCR. The regions immediately ahead of the crack tips were monitored during in-situ straining to identify the active deformation mechanisms. Part of the {111} and {200} diffraction rings were selected as the image forming diffraction vectors. As an upper limit of deviation in tilt away from the exact Bragg orientation one may assume about two Bragg angles, 2θ , which for 300kV electrons and Ni with a lattice parameter of 0.3512nm is on the order of only $2\theta \approx 0.6$ degrees. Thus, the diffracting (200) and (111) type planes in the grains that constitute the strongly diffracting bright regions in the DF images of the Ni-film are essentially in an edge-on orientation with respect to the plane of the image.

In order to address the challenging problem of observing the microstructure of nanocrystalline Ni in the stressed state, I adopt a loading to deformation, holding to stable, and imaging with *in situ* HREM method. For the first time, the microstructure of nanocrystalline material Ni at atomic scale was investigated successfully in the stressed state.

4.0 IN SITU BF TEM INVESTIGATION OF DEFORMATION IN NANOCRYSTALLINE NICKEL

4.1 INTRODUCTION

Due to the tiny size of the nano grains, all TEM observation has to be performed at high magnification in order to get useful deformation information. As a consequence, the observation has to be focused in a very small area of the whole sample. What is more, in order to catch the deformation information efficiently, the deformation process in the monitored area is highly expected to occur continuously in response to the discrete external loading steps. Based on above consideration, almost all in situ TEM researchers^{7,10,21} chose to monitor the areas ahead of a propagating crack. However, the local strain rates of these areas are expected to be quite high upon the loading. As a result, rapid changes in contrast occurring continuously in many different grains were frequently observed under BF TEM observation mode. This type of TEM contrast change phenomenon has usually been identified as dislocation activity⁹ although the contrast changes may also result from other factors, such as grain rotation and/or grain boundary sliding and moving bend contours, grain boundary fringes, moiré fringes et al. As a consequence, it is hard to get convincing evidence for the identification of those activated deformation mechanism.

During dynamic deformation process, dislocations are expected to move in discrete steps with an abrupt and asynchronous manner, dislocations in arrays are expected to move

individually while grain boundary mediated deformation and other features are expected to move smoothly and continuously. Therefore, if the effects from global rotation and/or local bending can be minimized or even eliminated and at the same time make the deformation occur in a relatively slower manner, then it is possible for TEM researchers to identify those activated deformation mechanism of nanocrystalline materials, such as dislocation nucleation and/or grain boundary mediated plasticity.

4.2 EXPERIMENT PROCEDURES

For in situ TEM tensile testing, one critical requirement is of to minimize the effect from global rotation (the entire rotation of the specimen) and those so called local bending. This is because all TEM work is based on the contrast change of the image. Just like deformation can induce grain contrast change, global rotation and local bending can also lead to changes in image contrast of a grain. Therefore, these non-deformation effects have to be eliminated or at least minimized for a successful TEM investigation on identifying the activated deformation mechanism. For this purpose, a special substrate was designed, as shown in Figure 4.1.

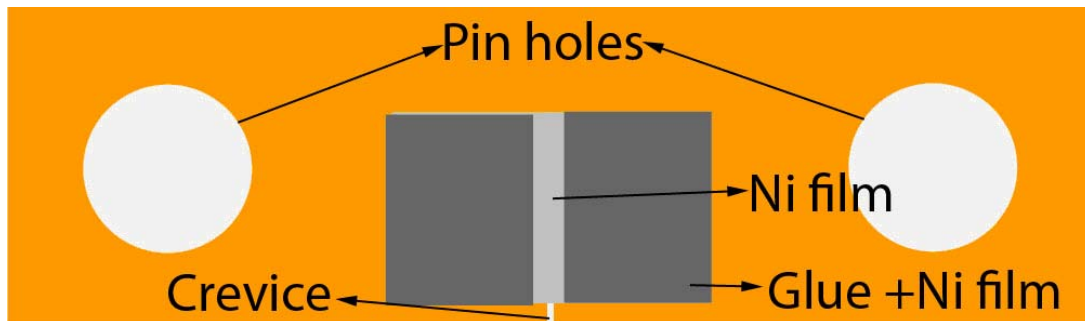


Figure 4-1: Schematic of the straining specimen, in which the free standing Ni film was glued on the special designed copper substrate.

The substrates were prepared from a commercially available Cu film with its thickness of 50 μ m. The film was trimmed into oblong substrates with their size about 2.5mm \times 11.5mm. Two holes, 1.32mm in diameter and with a center to center distance of 9mm were drilled into each substrate for purposes of pin loading. As shown in Figure 3.1, one narrow crevice about 0.2mm wide was also created with a sharp knife in one side of the substrate at its middle part to allow the electron transmission. The narrow width of the crevice is designed to ensure that the film deformed in a single axis tensile manner while at the same time minimize entire rotation of the sample (global rotation). The length of the crevice is experimentally decided so that the residual part of the substrate is enough to keep the shape of the substrate whereas small enough to be deformed by the in situ tensile stage. After flattening, the substrate was cleaned with acetone in an ultrasonic cleaner for ten minutes to remove any possible pollution induced during the handling procedure.

The PLD Ni films used in this part of the work has a nominal thickness of 60 nm. First, a thin layer of super-glue was painted around the crevice of the copper substrate, and then the nanocrystalline Ni film, which has been trimmed into 2 mm \times 1.5 mm piece along with the sodium chloride (NaCl) substrate was pressed down to the copper substrate. After curing, the salt substrate was removed by dissolving it in deionized water. To ensure the best conditions for TEM observations, only samples that were well attached to the Cu-substrate and free of other contamination from the sample preparation procedure were selected for TEM investigations.

4.3 EXPERIMENT RESULTS

4.3.1 Microstructure of as deposited 60 nm Ni film

Figure 4.2 A is typical BF TEM image of as-deposited nc-Ni films with nominal thickness of 60nm. The measurements of dark field electron microscopy reveal a fairly narrow grain size distribution and a narrow grain size distribution with a mean grain size of approximately 10nm. Twins are occasionally seen in some grains. The prevalence of the Moirè fringes is due to the superposition of grains lying on the top of each other. No pores are detected. The selected area diffraction pattern (SADP) shown as an inset indicates that no apparent preferred orientation or ‘texture’ of the grains although the substrate surface is (001) single crystal NaCl. This may be due to the large lattice mismatch between substrate and Ni as well as the small thickness. Moiré fringes are due to the super position of the grains lying on the top of each other.

Microstructure characterization by means of HREM observation confirmed that the as deposited sample consists of nanocrystalline grains with an average grain size of about 10nm. Most of the nanometer sized grains are equiaxed and separated by high angle grain boundaries (Figure 4.2 B). For example, five grains are identified in Figure 4.2 B and indicated as G1, G2, G3, G4 and G5, respectively. The orientation difference angle of the edge-on plane between G2 and G3 is about 53° , and that between G3 and G4 is about 9.5° . No grain boundary phases were revealed in these samples. Some distortion areas with size about 1~2 nm are often detected at the position of grain boundary junctions. It is worth to point out that most of the grain boundaries are curved and therefore maybe in strained state.

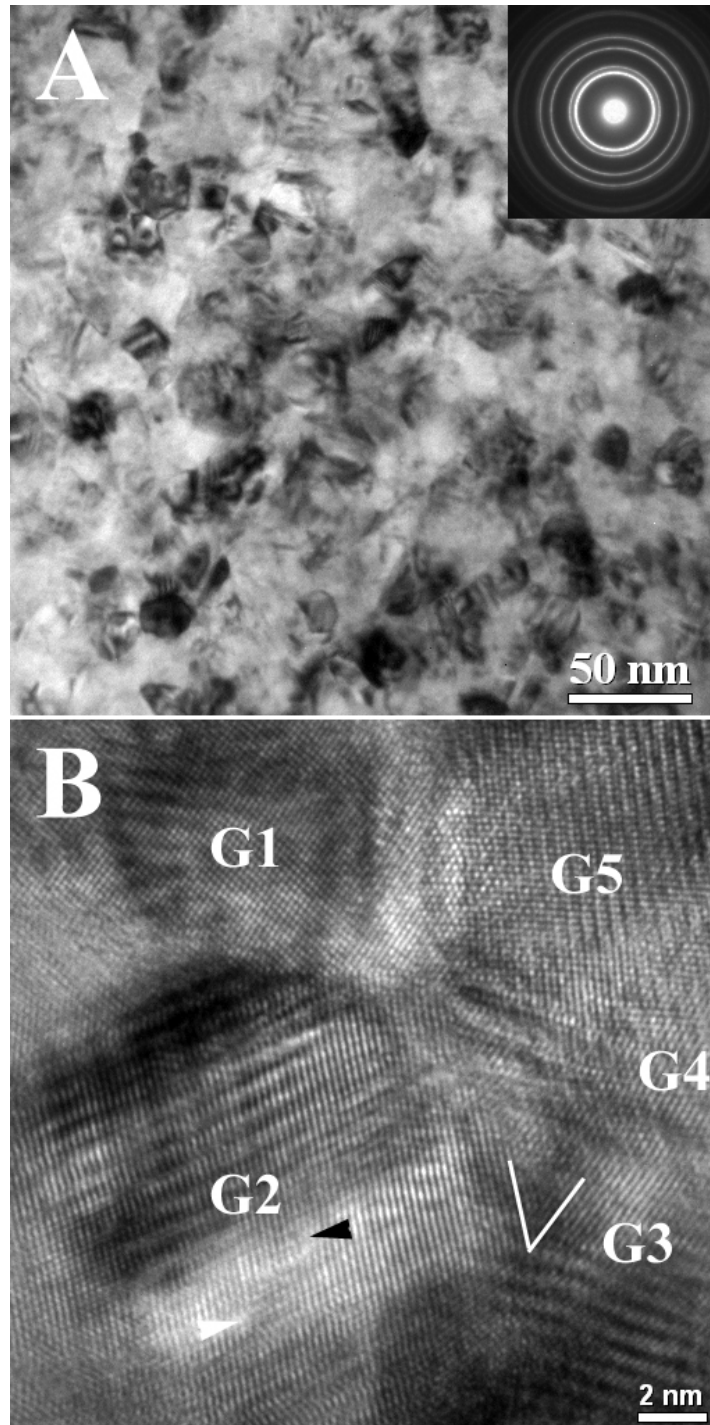


Figure 4-2: Typical BF TEM image (A) and typical HREM observation (B) of as deposited nanocrystalline nickel with its nominal thickness of 60nm.

4.3.2 Dynamic bright field observation of microstructure evolution of 50nm Ni

When the 60nm Ni films are in-situ deformed on the special designed substrate by tensile loading steps in TEM, many localized band-like thinning areas are first observed to form at favorite sites and further straining leads cracks to nucleate and propagate in those band-like thinning areas, as shown in Figure 4.3.

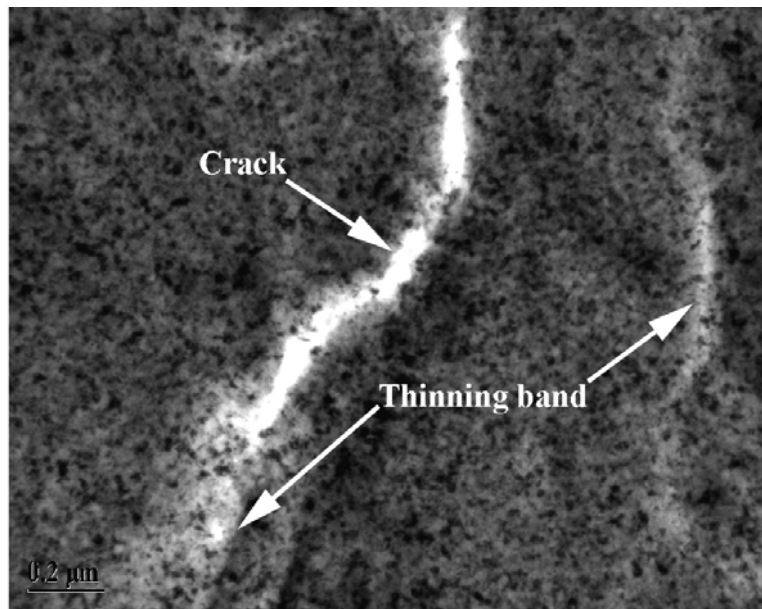


Figure 4-3: Localized plastic deformation, giving rise to bands of thinning and further straining lead cracks to nucleate and propagate in those band-like thinning areas.

After the initial few loading pulses, a main crack will finally be formed through the coalescence of some dispersed cracks. As reported in previous studies^{10,21}, the materials ahead of the main crack always experience fast deformation upon the loading and therefore make it difficult to identify those activated deformation mechanism. However, it is interesting to note that besides the main crack, there existed quite a few branch cracks. These branch cracks can be

classified into two types based on their relationship to the main crack. The first type is the branch cracks that are connected to the main crack. Because the main crack bears the major part of the strain upon loading, the local strain rate ahead of this type of branch cracks are relative low. Moreover, because the crack tip area is always in tensile state, local bends can be eliminated in maximum extent during the observation. The second type is of the branch cracks that are independent of the main cracks. Because the main cracks and those first type cracks have born almost all the applied external strain, the local strain rate of those areas adjacent to this type of cracks is almost indiscernible upon the further straining. Taking all the factors in consideration, I chose to study the deformation of the materials that located in areas ahead of the first type branch cracks.

Figure 4.4 shows a series of images extracted from the dynamic BFTEM observation. The studied grain-like dark area (as indicated by the black arrow, here we call it grain-like dark area instead of a grain, because it is difficult to confirm that the area with same contrast resulted from a grain or a grain group with close crystalline directions simply by contrast) is located ahead of a branch crack. Due to the relaxation of other areas, the local strain rate is low enough to allow observation of the detail evolution of the grain-like dark area. By measurement, it was found that the grain-like dark area located about 170nm ahead of a crack tip and its size is about 20nm at the initial state. The direction of the tensile axis is approximately perpendicular to the narrow thinning band formed ahead of the crack.

At the start of straining, the grain-like dark area is approximately equiaxed with its lower part in dark contrast. The boundary of these two parts is almost parallel to the thinning band, as shown in Figure 4.4 a. The contrast of the studied grain-like dark area is sensitive to every displacement pulse. Upon application of a displacement step, the contrast of the whole grain-like

area changes immediately into dark contrast in an abrupt manner. After that, some relaxation occurs and the contrast boundary of the dark area goes back somewhat toward its initial position. About 3 step displacements later, the contrast of the dark area becomes uniformly dark and stable, as shown in Figure 4.4 b. The above procedure indicates that both elastic and plastic deformation occurred on every staining pulse. The elastic part relaxes immediately after the displacement pulse.

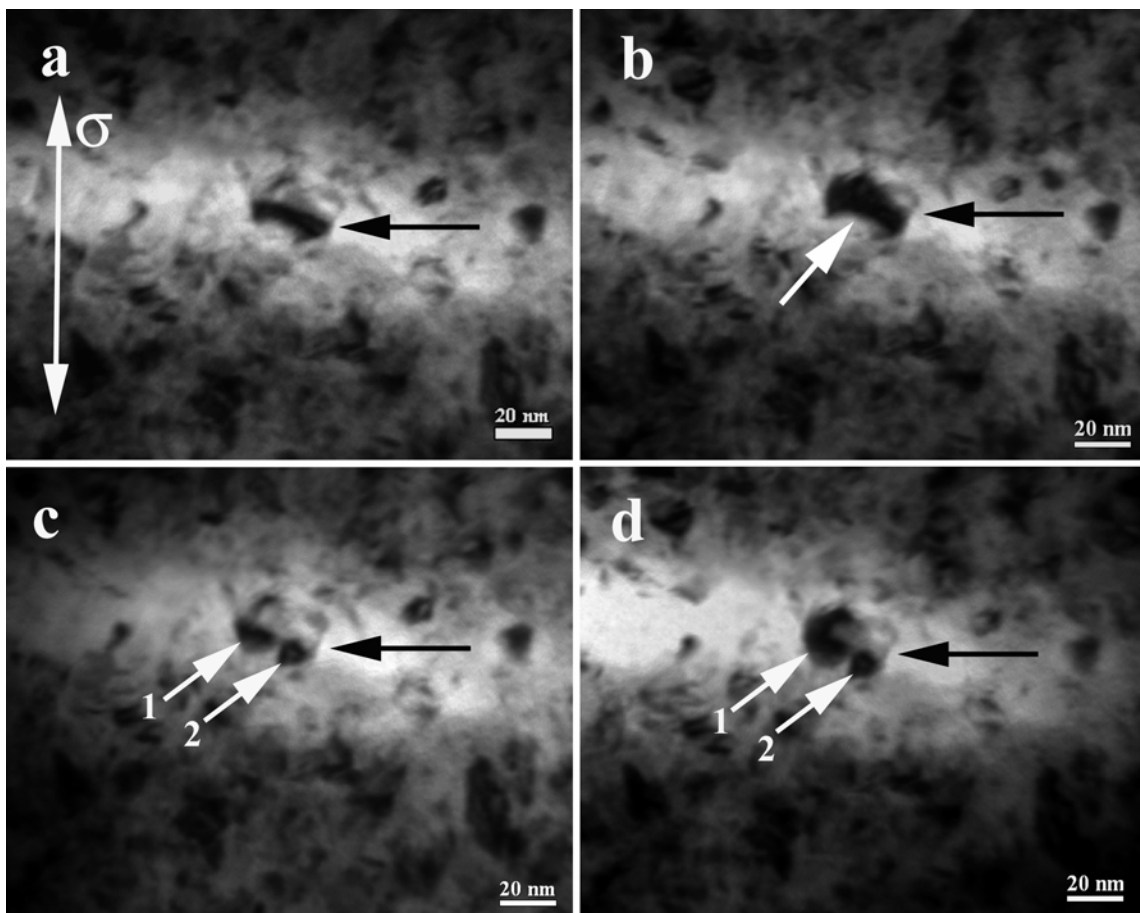


Figure 4-4: Bright field observation of contrast evolution of an area during straining.

It is interesting to note as loading progresses, a notch beginning to emerge at the position indicated by the white arrow in Figure 4.4 b. At the same time, the contrast boundary moves

back to the middle of the area again. This can be explained as stored strain energy being released through the formation of the notch. The notch grows with each additional loading step and shrinks a little during two loading step intervals. Step by step, the original grain-like dark area is separated by the growing notch. After another 4 loading steps beyond those of Figure 4.4 b, the rudiments of two grains 1 and 2 are clearly seen, as indicated by the two white arrows in Figure 4.4 c. Since a high energy would be necessary for the splitting of a single grain, the grain-like dark area presumably corresponds to two or more grains with their crystalline direction closely aligned to each other. In fact, we will in our following study that such agglomerates of nearly aligned grains form early during tensile deformation of this material⁹⁰. Note now that the direction of the contrast boundary line is tilted from the original one which indicates some inner structural change has occurred. Further loading steps lead the contrast of ‘new born’ grains 1 and 2 to become darker and uniform, as shown in Figure 2D. The sizes of grains 1 and 2 are about 18nm and 8nm, respectively.

4.4 DISCUSSION

While it is possible that the contrast change of the studied grains resulted from global rotation of the whole film, this is not consistent with the fact that other nearby grains did not rotate out of their initial contrast during this sequence. It is also unlikely that the contrast change resulted from local bending in such a small area or from complex local elastic strain change. A characteristic of elastic strain is that it will diminish through the release of external applied stress. Although the force exerted on the studied grains by those around them can be very complex due to the non-uniform grain size (from several nm to 28nm), the fact all the other

grains in view show essentially no contrast change indicates that elastic strain induced contrast change can account at most part of the contrast change. A more likely explanation is that the contrast evolution was induced by grain rotation and/or grain boundary sliding in response to the tensile deformation process.

4.5 CONCLUSIONS

The microstructure of the PLD Ni film with its nominal thickness of 60 nm has been characterized by TEM. It was found this high quality Ni sample is essentially fully-dense, artifact-free thin film with its average grain size about 10nm and narrow grain size distribution. The deformation process has been studied by using in situ BF TEM observation under low local strain rates. The observation suggested that grain boundary mediated plasticity, such as grain rotation and grain boundary sliding is very likely to contribute prominently to entire plastic deformation.

5.0 IN SITU DF TEM INVESTIGATION OF THE DEDEFROMATION IN NANOCRYSTALLINE Ni

5.1 INTRODUCTION

In previous study, it has been shown that the Ni film prepared by PLD has a very high quality and grain boundary mediated plasticity very likely contributed prominently to the entire plastic deformation. However, more convincing evidence is necessary. Considered that grain boundary processes, such as grain boundary sliding and grain rotation, if existed, will inevitably lead to the reorientation of those involved grains, therefore, DF TEM observation would be the best choice for us to reveal these activated mechanisms. Unlike the BF TEM observation, which may include all the contrast information, such as mass-thickness contrast, diffraction contrast and phase contrast, the DF TEM observation mainly reflect the information of diffraction contrast and therefore is very sensitive to grains' orientation changes. However, at mentioned earlier, global rotation and local bending can also introduce grain orientation changes. Therefore, in order to take the advantage of DF TEM observation, we have to eliminate or at least minimize the effects from global rotation and local bending.

5.2 EXPERIMENT PROCEDURE

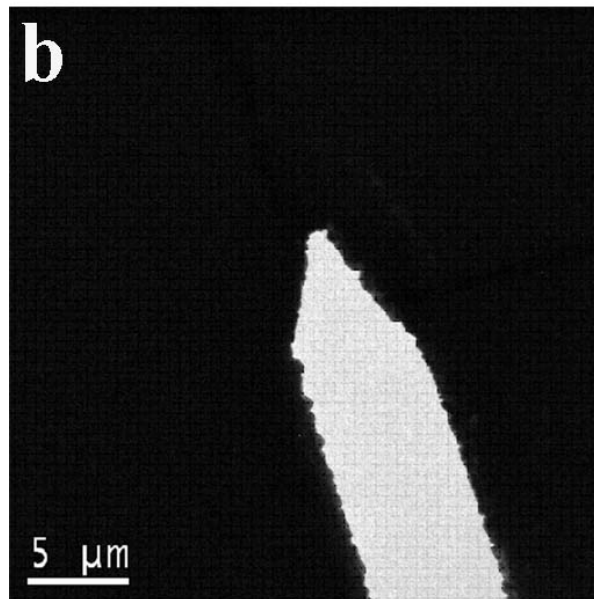
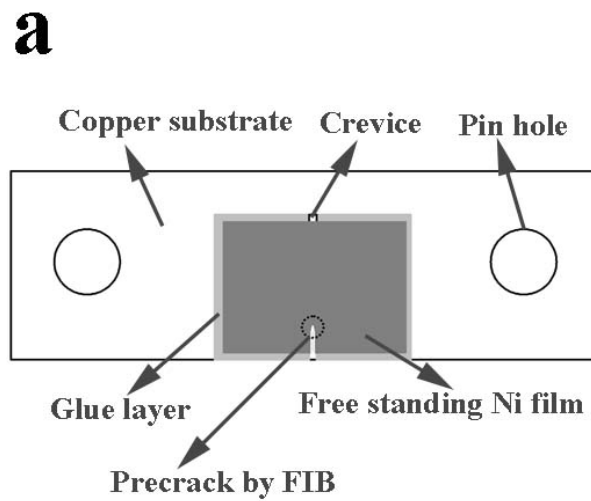


Figure 5-1: (a) Schematic of the straining specimen construction and (b) TEM image of the starter crack prepared with FIB.

The samples used in this part of work were PLD Ni films with its nominal thickness of 150 nm. The sample preparation introduced in section 4.2 was adopted because it has been experimentally proven that such a design can minimize the effects from global rotation and local bending and ensure the Ni film deformed under a stress state that is close to single axis tensile conditions. To allow the deforming region of the film to be easily located, a starter crack with a size about 5 μm wide and 1 mm long was fabricated with a focused ion beam (FIB) from the open edge of the free standing Ni film, as shown in Figure 5. 1. Such a design ensured that the cracks would advance perpendicular to the tensile loading direction.

The room tensile loading and imaging were performed with a JEOL 3010. (For detail see section 3.3). The regions immediately ahead of the crack tips were monitored during in situ straining to identify the active deformation mechanism. High resolution TEM (HRTEM) observations were done both in ARM (section 3.3) and in JEOL 3010.

5.3 EXPERIMENTAL OBSERVATIONS

5.3.1 Microstructure of as deposited 150 nm Ni film

TEM observations (Figure 5.2 A) indicate that the as-deposited Ni consists of roughly equiaxed grains with random orientations (see inset in Figure 5.2 A). Statistical measurements of DF TEM images reveal a narrow, log-normal grain size distribution, ranging from several nanometers to 23 nm with an average value of 9.7 ± 3.9 nm (Figure 5.2 B). HRTEM shows that most grains are separated by large-angle grain boundaries.

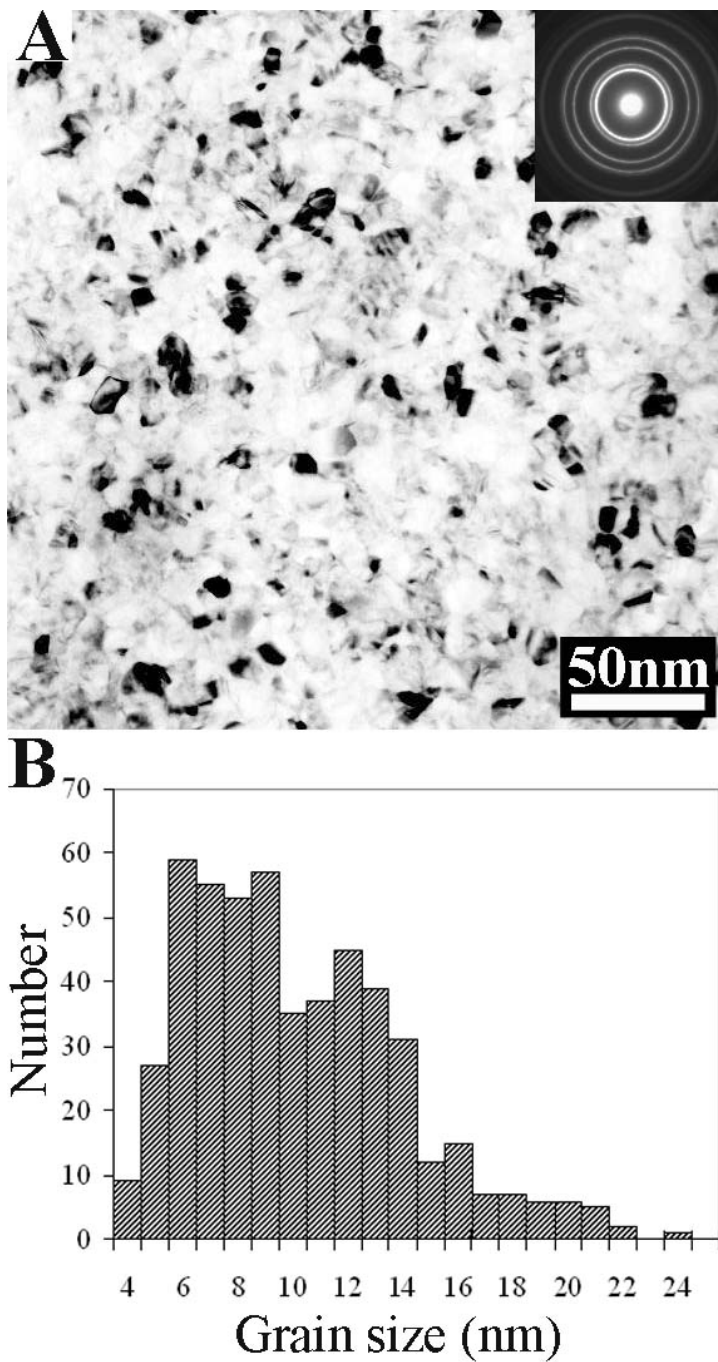


Figure 5-2: TEM observations of the typical microstructure in the as-deposited nanocrystalline nickel films. The bright field TEM micrograph (A) and the selected area diffraction pattern (inset in (A)) show roughly equiaxed grains with random orientations. The statistical distributions for grain size (B) were obtained from multiple TEM images of the same sample.

5.3.2 Experimental observations

Figure 5.3 A is a typical DFTEM image of a Ni sample taken from an area which has been pre-thinned by recourse to low temperature ion milling in the undeformed state. Figure 5.3 B is the selected area diffraction pattern (SADP) taken from an area of as-deposited Ni film prior to deformation. Upon straining, bright field TEM observations show rapid changes in contrast occurring continuously in many different grains. This has been identified as evidence of dislocation activity previously^{10,21}. However, the in situ DFTEM observations reveal that the deformation behavior is significantly more complex. It was found many strongly diffracting features that are much larger than the initial average grain size are formed immediately in the deformed zone upon straining (e.g. the feature marked by a white arrow is about 60 nm in diameter in Figure 5.3 C). The SADP from the deformed area (Figure 5.3 D, taken from the same region and with the same selected area aperture size as in Figure 5.3 B) exhibits fewer, asymmetrically distributed diffraction spots in each of the diffraction rings in comparison with the SADP obtained prior to deformation (Figure 5.3 B). The reduced background intensity and improved contrast in the SADP of the deformed area (Figure 5.3 D) indicate that the sample thinned locally during deformation. Higher magnification DFTEM micrographs revealed that the large bright features observed after deformation consist of a number of smaller grains (e.g. Figure 5.3 E) rather than a single large grain resulting from stress-assisted grain growth. Comparison of the undeformed state (Figure 5.3 A, B) and the post-deformation state (Figure 5.3 C, D and E) indicates that groups of neighboring grains have undergone an orientation change during straining and have formed numerous grain agglomerates. Because of the nature of the image formation mechanism of DFTEM images (section 3.3), we can conclude that the smaller grains in these agglomerates exhibit essentially edge-on orientations of their $\{111\}$ and/or $\{200\}$

lattice planes. The schematic in Figure 5.3 F depicts a possible crystallographic substructure associated with an agglomerated group of grains that would be consistent with the type of contrast observed in the DFTEM micrographs after straining (Figure 5.3 E).

To elucidate further the mechanism responsible for the formation of the agglomerated grain regions, real time observations were performed. Contrast changes in areas subject to high strain during in situ TEM straining experiments were recorded in the DF mode. The DF micrographs shown in Figure 5.4 are still frames extracted from a typical dynamic sequence of images taken during the application of a single displacement pulse. The times listed on each still frame are based on the video-acquisition rate of 30 frames per second. At the beginning of this sequence, there were no grains in a strongly diffracting condition in the area indicated by the white arrow (Figure 5.4 A). 1/30 of a second later, a bright spot emerges from a grain about 6 nm in diameter and remains well-defined in size as a single, approximately equiaxed grain until $t=0.1$ s (Figure 5.4 B). Over the next couple of frames a number of additional neighboring grains rotate into strongly diffracting conditions for either the $\{200\}$ or $\{111\}$ planes. The fact that other nearby grains, which are in a strong diffraction condition, do not rotate out of contrast confirms that there has been no global rotation of the specimen area and that the rotations observed at the arrowed location are internal changes of the sample structure. Additionally, note the small ‘notch’ discernible at the lower left corner of the agglomerate, in both Figure 5.4 D and E, which indicates that the growth in size of this agglomerated group of grains was not isotropic and involved sudden rotation of individual grains. At $t=0.5$ s, the group of grains has grown into an elongated equiaxed shape with an approximate size of 60 nm along the short axis and 80 nm along the long axis (Figure 5.4 F). After this very rapid morphological change the rate of growth of the grain agglomerate decreased significantly.

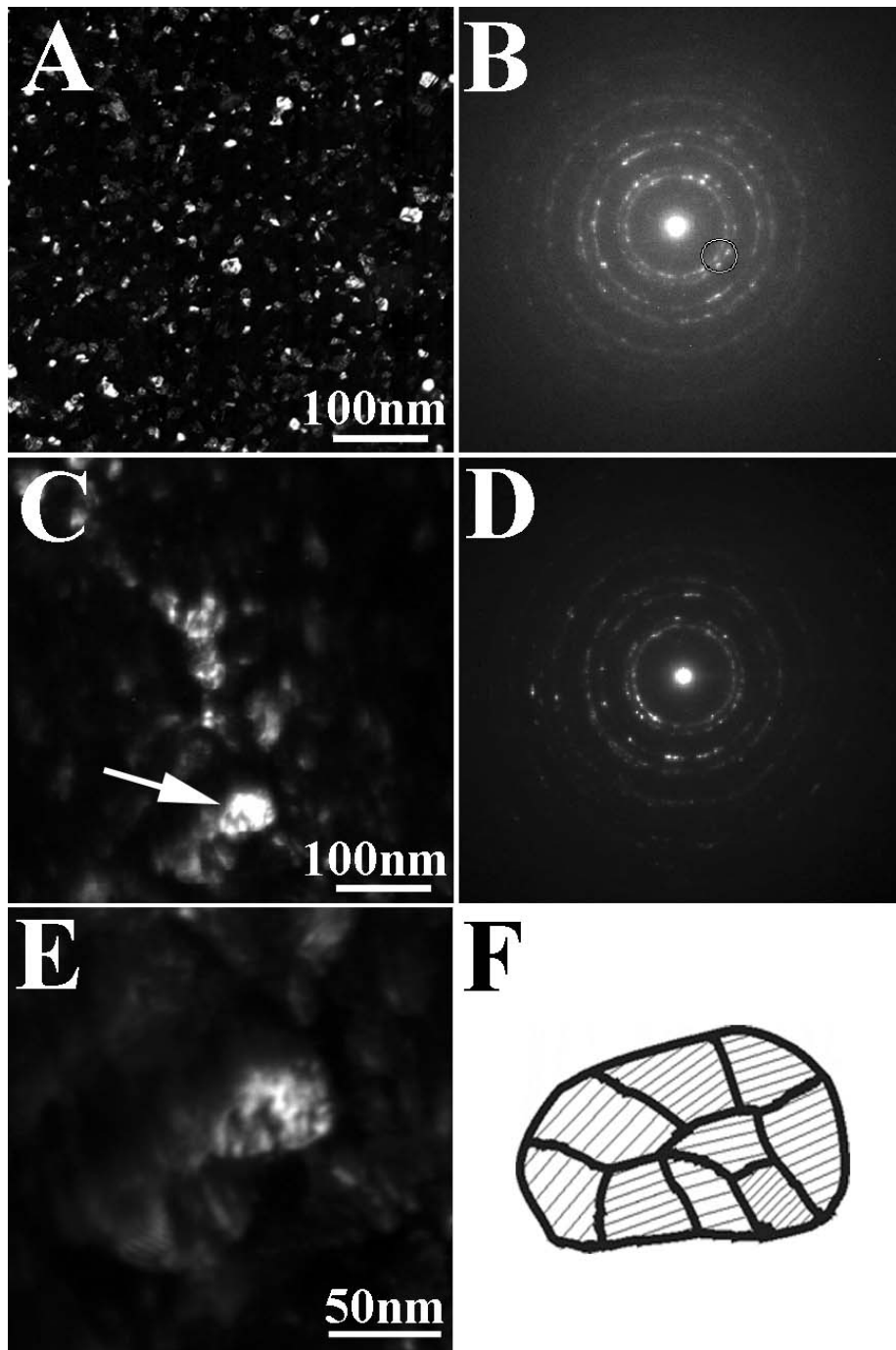


Figure 5-3: TEM micrographs showing the evolution of the Ni microstructure during in-situ straining.

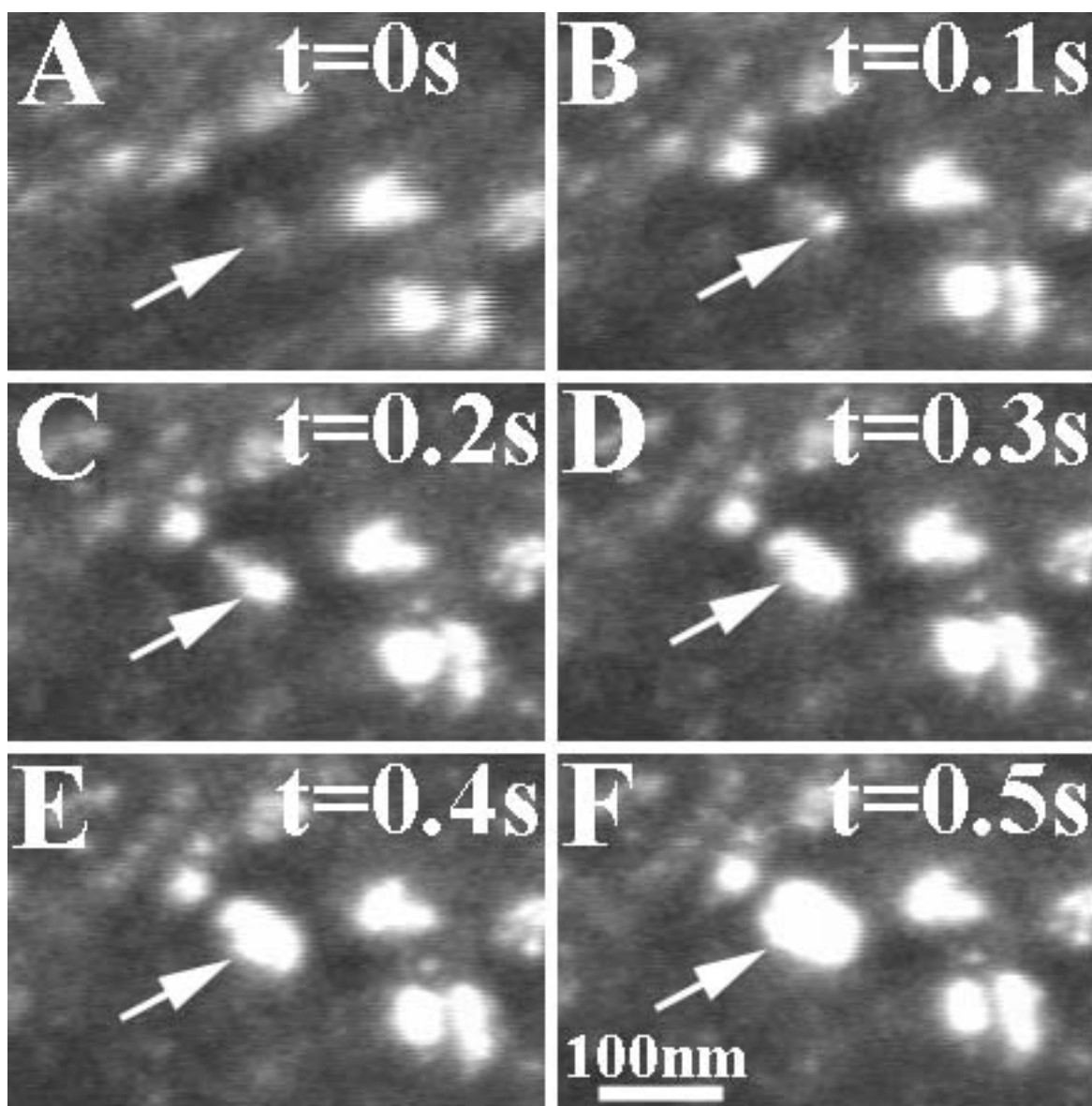


Figure 5-4: DFTEM observation of the rapid genesis of an agglomerate (e.g. white arrow) depicted by individual still frames extracted from a dynamic video-sequence. (A) $t=0$ s, no grains in strong diffraction condition near the white arrow; (B) $t=0.1$ s, a grain in strong diffraction condition with size about 6 nm is visible; (C) $t=0.2$ s, a group of grains in bright contrast, size about 28 nm, is visible; (D) $t=0.3$ s, now the group of grains has a nearly elliptical shape, dimensions 60 nm by 35 nm; (E) $t=0.4$ s and (f) $t=0.5$ s, the size of the group of grains increases to maximum dimensions of about 80 nm by 60 nm.

5.3.3 HRTEM observation

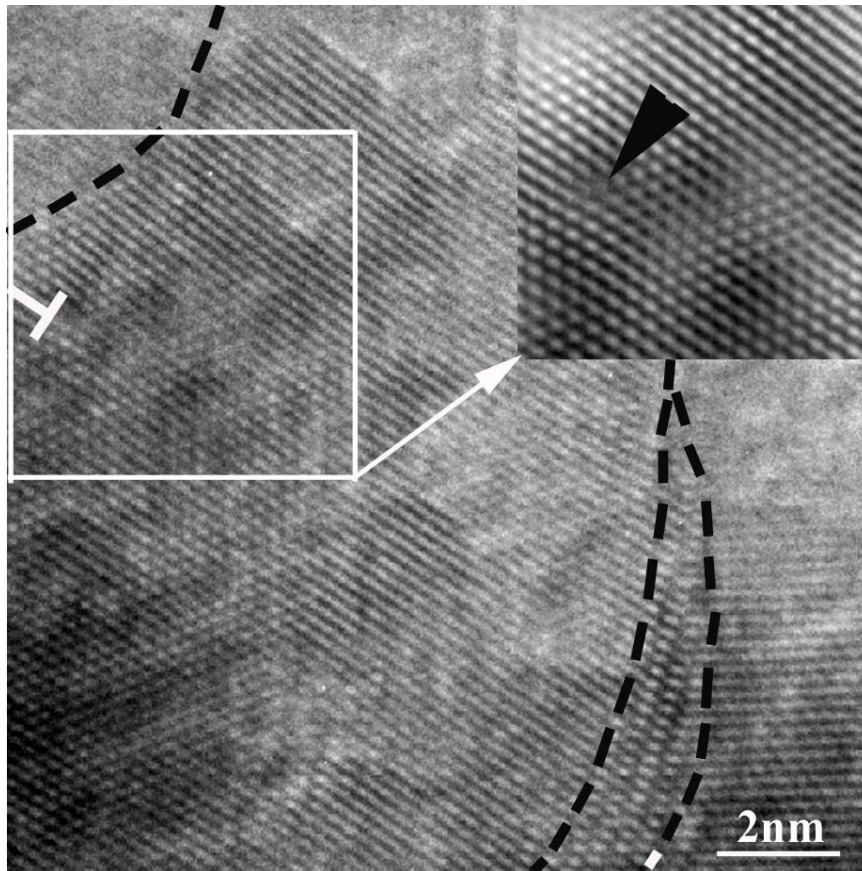


Figure 5-5: A typical HREM image of a thin area newly formed by deformation. A dislocation is trapped inside a grain close to the grain boundary (delineated by dark dash line). The inverse Fourier-filtered image (inset at upper right corner) from inside the white box shows the dislocation with more clarity.

During this part of work, HREM images of suitably oriented grains that were still under stress were also obtained in the thin area newly produced by the deformation. Trapped lattice dislocations were detected in some of the grains. An example HREM micrograph of one of these trapped dislocations is shown in Figure 5.5. A dislocation (white T) that is trapped in the vicinity of a grain boundary (delineated by dark dash line) can be seen. The inset at the upper right corner in Figure 5.5 is an inverse Fourier-filtered (FFT) image of the region framed by the

white box, which allows the dislocation to be displayed more clearly. The frequent observation of trapped lattice dislocations in the post-deformation state indicates that dislocation mediated deformation is still active even when the average grain size is about 10 nm. Two other very recent experiments also detect the presence of dislocations in nanocrystalline Ni while under stress^{91,92}, although for larger grains, 20 nm and 26 nm, respectively.

5.3.4 Discussion

The DFTEM observations confirm the prediction that grain boundary mediated deformation can become prominent when the average grain size of a material decreases below some critical value. Several theoretical studies have considered the operation of grain rotation and grain boundary sliding as possible deformation modes⁹³⁻⁹⁵. These studies assume that the driving force for grain rotation is the net torque on a grain, which results from the mis-orientation dependence of the energy of the GBs that delineate a given grain from its neighbors. Grain rotation is viewed as a sliding problem on the periphery of the grain; changes in the grain shape during rotation are assumed to be accommodated by diffusion, either through the grain boundaries or through the grain interiors. Assuming that grain boundary diffusion is dominant (reasonable in nanocrystalline metals with grain size below a certain value at room temperature) yields a d^4 dependence on the rotation rate, where d is the grain size. This is a striking dependence upon grain size. For example, for $d=60$ nm and 6 nm, respectively, and keeping all other factors identical, the grain rotation rate for the latter will be 10^4 higher than for the former. This qualitatively explains our observation of extremely rapid formation of the grain agglomerates by rotation during straining. The rate of the grain rotation processes will generally decrease with time, as a state of new equilibrium is approached locally.

However, the frequently observed trapped dislocation and the absence of deformation twinning are quite unexpected. It has been predicted that cut off grain size value for significant dislocation activities for Ni should lie between 20 to 40nm^{4,92} and twinning will be a preferred deformation mode when grain size drop down to certain value⁹⁶. The physics governing the observed deformation crossover can be understood by considering the effect of grain size on the different operative processes. A number of computational simulations have predicted that GBs can act as dislocation sources in nanocrystalline materials^{5,76,80}. Based on these simulations, Chen et al⁹⁶ proposed a dislocation-based model which suggests that the nucleation stress for both perfect and partial dislocations is inversely proportional to the grain size. Furthermore, this model predicts the existence of a critical size d_c , below which the deformation mechanism will change from one controlled by normal unit dislocation motion to one controlled by partial dislocation activity. If we take the dislocation core parameter $\alpha=1$, the shear modulus as $\mu_{Ni}=95$ GPa⁹⁷ and stacking fault energy of nickel as 0.128~0.24 J/m²^{98,99}, the critical size (d_c) for Ni then ranges from 11~22 nm. However, according to this theory, the lower bound of the nucleation stress for partial dislocations (for $d=23$ nm) in our sample is as high as 2.1~2.8 GPa. This indicates that very high local stress is necessary for the nucleation of partial dislocations in nanocrystalline Ni with an average grain size of 10 nm. In contrast, the rate of grain boundary mediated deformation, as mentioned above, increases rapidly with a scaling of d^{-4} . Thus, the deformation mechanism crossover is an inevitable result of the competition between the deformation controlled by nucleation and motion of dislocations (unit and partial) and the deformation controlled by grain boundary related deformation, accommodated mainly by grain boundary diffusion with decreasing grain size.

A critical part of this investigation was following the rapid sequence of initial grain realignments by closely examining successive video frames in dark-field TEM mode. The frequently observation of the GB mediated deformation observed here would not have been possible in bright field TEM conditions, because of the inherent difficulty with differentiating the contrast changes caused by grain boundary related deformations from those caused by the motion of lattice dislocations in small grains, e.g. less than 20 nm.

5.4 CONCLUSIONS

The plastic behavior of crystalline materials is mainly controlled by the nucleation and motion of lattice dislocations. However, in situ dynamic transmission electron microscopy observations of nanocrystalline nickel films with an average grain size of about 10 nanometers shows that grain boundary mediated processes have become a prominent deformation mode. Additionally, trapped lattice dislocations are observed in individual grains following deformation. This change in the deformation mode arises from the grain-size dependent competition between the deformation controlled by nucleation and motion of dislocations and the deformation controlled by diffusion assisted grain boundary processes.

6.0 IN SITU DYNAMICS HREM OBSERVATION

6.1 INTRODUCTION

Compared with their coarse-grained counterparts, nanocrystalline metals exhibit unique mechanical properties, including high strength, high hardness and an enhanced ability to deform superplastically^{17,100-102}, which currently represent a subject of intensive fundamental research. However, an experiment-based understanding of the fundamental physical mechanisms responsible for their unique mechanical properties remains elusive, especially for those metals with average grain size smaller than 30nm. Both experiments^{9,10,22,90} and atomistic simulations^{77,80,103} revealed that dislocation-mediated plasticity may still play a role in the deformation of nanocrystalline metals with grain sizes down to about 10nm. Hence, it may be expected that evidence of lattice dislocation glide activity during straining may exist in the microstructure of deformed nanostructured metals. However, providing experimental evidence of dislocation activity by post-mortem transmission electron microscopy (TEM) investigations, for instance in the form of dislocation debris or trapped lattice dislocations, has proven unsuccessful in previous studies⁴. Yamakov et al⁷⁷ suggested that extended dislocation can exist inside a nanoscale grain only under very high stress and that the removal of this stabilizing stress would lead to absorption of these dislocations at the grain boundary source from which they originally nucleated. Unfortunately, typical sample TEM sample preparation methods, e.g. mechanical thinning followed by ion thinning or twin-jet electropolishing, often inevitably result in

relaxation of some of the stresses associated with prior deformation. Hence, it is difficult to verify some of the intriguing predictions of computational and theoretical studies. The current paucity of experimental data on dislocation activities in nanocrystalline metals critically limits the development of a mechanistic understanding of the mechanical behavior and properties of these interesting materials.

In this Chapter, I reported the challenging experimental problem of observing the microstructure of nanocrystalline Ni in the stressed state. I employed an in-situ tensile deformation TEM technique in combination with dynamic in-situ high-resolution TEM (HREM) observations. Unlike previous studies, here trapped lattice dislocations are observed frequently in nanoscale grains that are still in a stressed state. Furthermore, during stress relaxation dislocation movement and even annihilation have been documented by dynamic HREM. Analyses of the TEM data indicate that some of the trapped dislocations have unit dislocations with Burgers vectors $\frac{1}{2}\langle 110 \rangle$.

6.2 EXPERIMENT PROCEDURE

The Ni film and the sample design used in this part of work is exactly same as those used in in-situ DF TEM observation (Chapter 5), i.e., PLD Ni film with its nominal thickness of 150nm. In order to address the challenging problem of observing the microstructure of nanocrystalline Ni in the stressed state, after initial incremental loading to induce deformation the samples were held under stress, while continuously imaging the deformed region using a JEOL 3010 instrument operating at 300kV with a point-to-point resolution of 1.9 Å. HREM images were obtained in

those newly formed thin areas which were still in the strained state after the samples became sufficiently stable.

6.3 EXPERIMENTAL RESULTS AND DISCUSSIONS

Because of the tiny grain size, the traditional contrast criterion⁸⁹ is no longer valid even for the identification of any trapped lattice dislocations. Therefore, the only possible means to detect any trapped lattice dislocations directly and to further determine the Burgers vector of those detected dislocations is through HREM. Trapped lattice dislocations were frequently detected in the grains after the samples became sufficiently stable.

An example HREM micrograph of two of these trapped dislocations is shown in Figure 6.1. For the lower grain, a dislocation that is trapped in the vicinity of grain boundary (delineated by dark dash line) can be seen clearly. The position of the dislocation is labeled by a white T. Figure 6.1 b depicts an inverse Fast Fourier-filtered (IFFT) image of the region framed by the dark box in Figure 6.1 a. The inset in Figure 6.1 b is the corresponding FFT, which confirms the approximate electron beam direction to be close to a $\langle 110 \rangle$ direction for the lower grain in Figure 6.1 a.

It is of interest to note a dislocation trapped in the middle of the upper grain shown in Figure 6.1 a, which has small dimensions of approximately $5\text{nm} \times 10\text{nm}$. Figure 6.1c is an IFFT image of the area marked by the dark square in Figure 6.1 a reconstructed using the spatial frequencies of the (200) planes and the trapped dislocation is labeled by a white T (Figure 6.1 a) and dark arrow (Figure 6.1c).

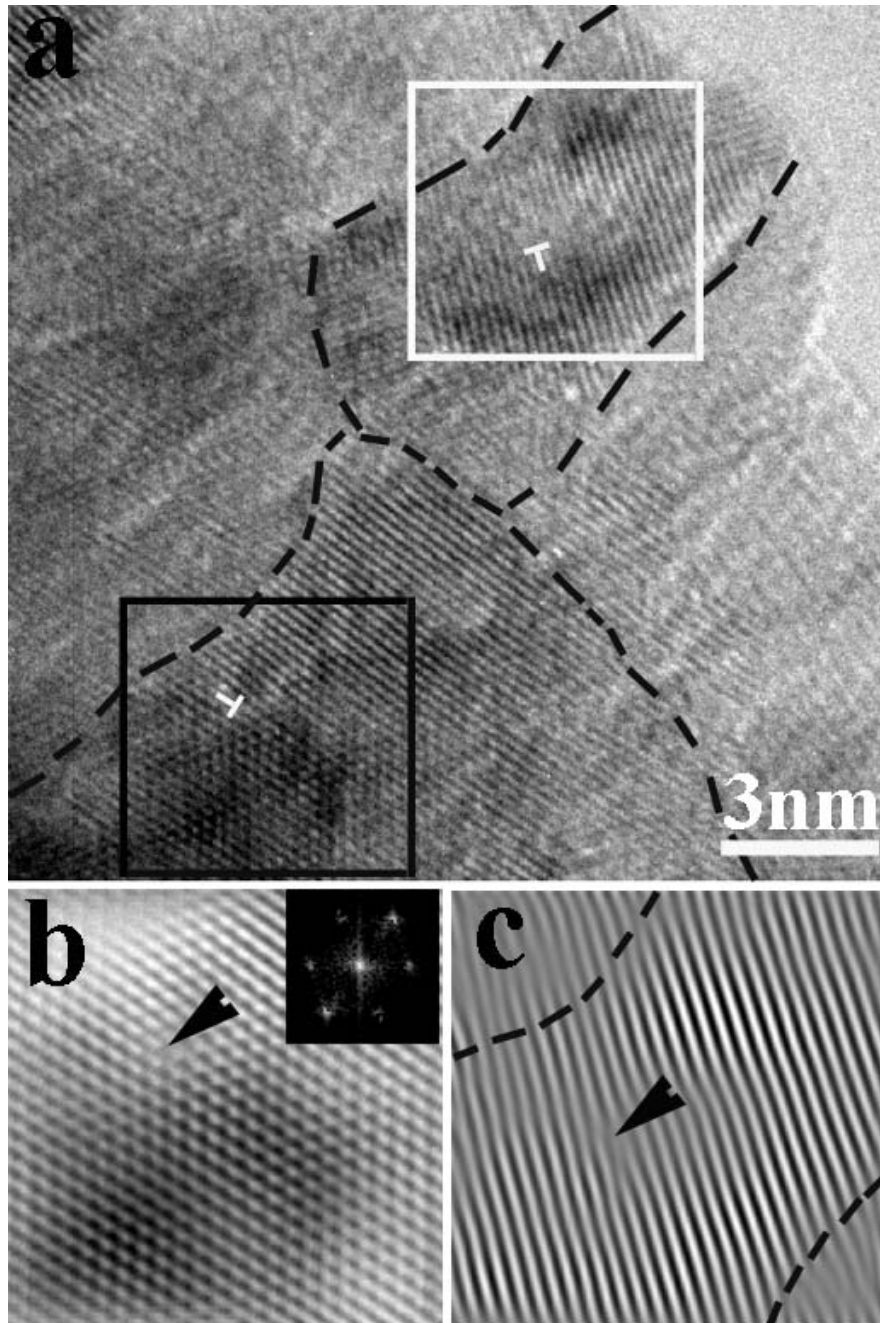


Figure 6-1: (a) HREM micrograph of a thin area freshly formed by deformation. The Ts and arrowheads indicate the position of a trapped lattice dislocation in the grain interior. Grain boundaries were delineated by dark lines. (b) IFFT of the area framed with the black box in figure 3a. The Fourier-transformed image shown as an inset indicates that the electron beam is close to the 110 zone axis of the grain. (c) IFFT of the area framed with the white box in (a).

Based on the idea that very small grains cannot sustain the stress necessary for the dislocation multiplication at the observed yield stresses and with an approximation of the source size equal to the grain size, Legros et al ⁴ evaluated a critical grain size below which a dislocation source can no longer operate to be about 20~40nm for face-centered cubic (fcc) metals, depending on the nature of the dislocations ^{4,92}. According to their model, the stress (τ) necessary for the nucleation of dislocation can be expressed as

$$\sigma = \frac{2\alpha\mu b}{d} \quad (6.1)$$

Here b is the magnitude of the Burgers vector; d is the grain size; μ is the shear modulus; α is the dislocation parameters [$\alpha=0.5$ and 1.5 for edge and screw dislocations, respectively]. Taking $\mu_{Ni}=95\text{GPa}$ and d equal to 7.5 nm , the estimated stress is approximately $3.2\sim 9.5\text{ GPa}$, depending on the type of the dislocations. This indicates that the yield strength of nanocrystalline Ni can be much higher than that measured by Legros et al (1.15 GPa) ⁴. Evidence for this is provided by recent reported experimental data from indentation tests which showed that the yield stress for these thin films of pulsed-laser deposited nanocrystalline Ni can be as high as $5.15\pm 0.86\text{ GPa}$ ²².

Quite unexpected, neither trapped partial dislocation nor deformation twinning was detected in our observations. Based on the lowest energy theory, atomistic simulations of 3D structures found only partial dislocations emission at grain boundaries for metals with grain size less than 30nm , followed by glide through the grain and absorption in the opposite side of the grain ^{77,80,103}. Inspired by the results from molecular dynamics simulations ⁸⁶ and the deformation twinning observed in aluminum, Chen et al ⁹⁶ proposed a dislocation model with the assumption that dislocation source size equal to the grain size. According this model, a critical grain size d_c

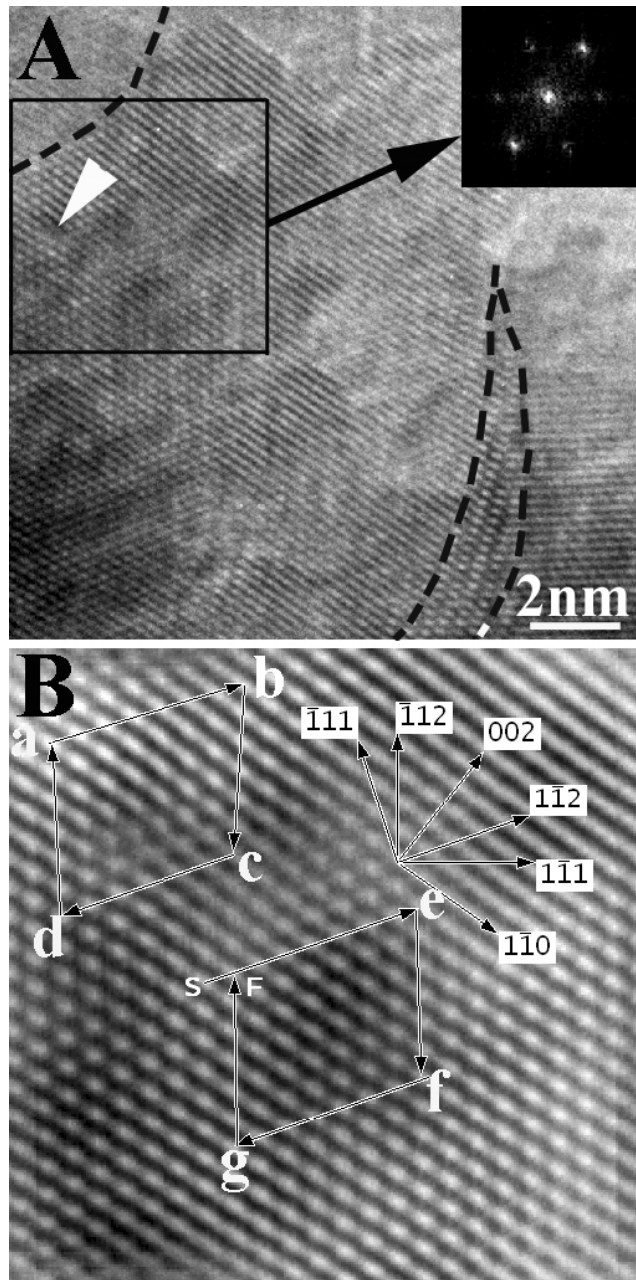


Figure 6-2: Determination of the Burgers vector of the trapped dislocation. (A) HREM showed a dislocation (indicated by white arrow head) was trapped inside a grain close to the grain boundary (delineated by dark dash line). (B) The inverse Fourier-filtered image from inside the dark box in figure 6.2 (A) showed the dislocation with more clarity. Burgers circuit used to determine the Burgers vectors of the trapped dislocation is also shown.

exists, below which the deformation mechanism will transit from those controlled by normal slip to those controlled by partial dislocations activity. Further, Chen et al ⁹⁶ predicted that that twinning will become a preferred deformation mode below this critical grain size. According to Chen et al's mode, the critical grain size for Ni was determined to lie between 11 nm ~22 nm. However, the failure to identify any partial dislocation and/or deformation twinning in deformed as-deposited Ni indicated deformation twinning is not in general possible and only restricted to peculiarities of high-pressure loading techniques, such as indentation, rolling or high-pressure torsion ^{87,96,104,105}.

All previous HREM observations have been performed near static state. Therefore it may be argued that the observed trapped dislocations are resulted from the pinned effect of surface contamination, such as surface oxidation rather than from the effect of residual stress. In order to clarify this, a series of HREM images of a given stressed area that contained trapped dislocations were collected after a displacement pulse had been applied. If the observed trapped dislocations are resulted from surface pinned effect, they are not expected to move or rearrange themselves along with stress relaxation process. On the contrary, if the observed dislocations are due to the effect of residual stress, then it is conceivable that stress relaxation should lead to the rearrangement or even annihilation of these trapped dislocations in nanocrystalline grains.

The example HREM images extracted from such a dynamic sequence, shown in Figure 6.3 A and 3 B, were obtained over a relaxation period of about 90 seconds. The strong ripple contrast in Figure 3 A and 3 B may be taken as an indication that the area is experiencing substantial strain¹⁰⁶. In contrast to the as-deposited state where most of grains are found to be divided by high angle grain boundaries, the grains after deformation appear to be divided mainly by low-angle grain boundary.

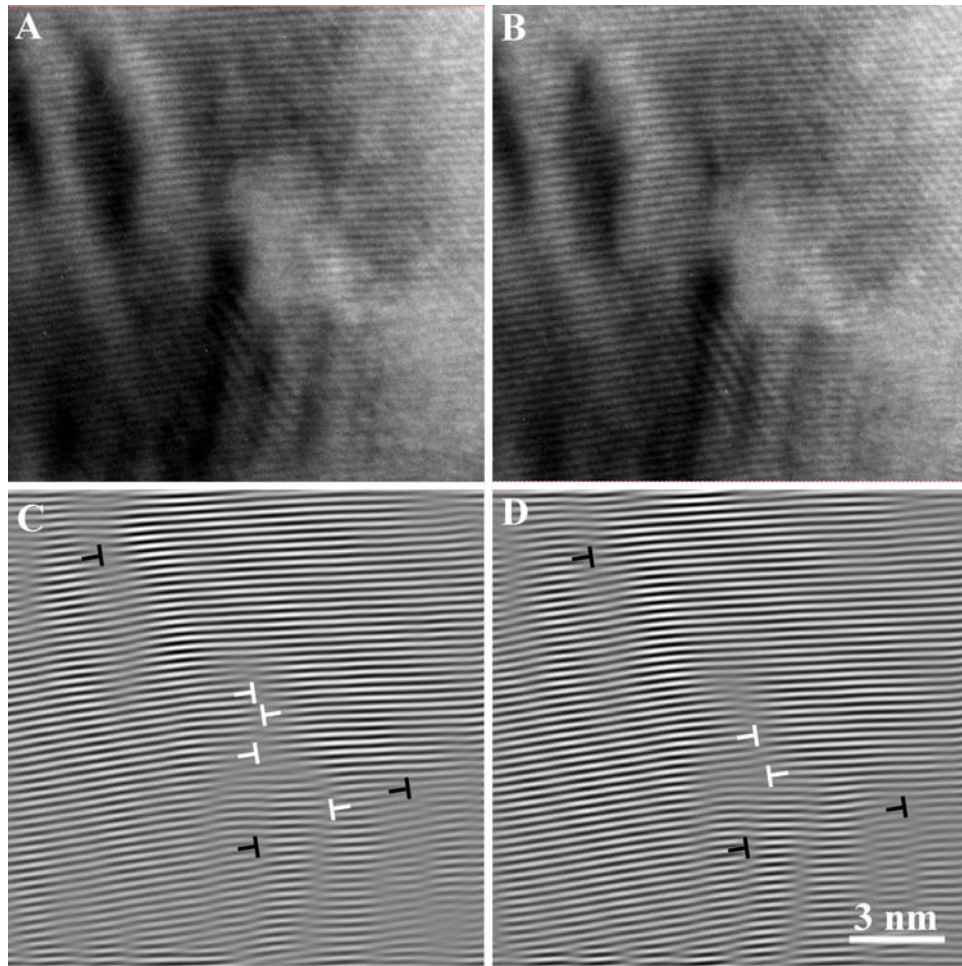


Figure 6-3: Dynamical HREM observations of the microstructure evolution of a grain during the stress relief. The positions of the dislocation cores have been indicated by T. (A) $t=0$ (B) $t=89\text{s}$ (C) IFFT of Figure A and (D) IFFT of Figure B

As shown in Figure 6.3 A and B, the low angle grain boundary which separates the grain at the upper right corner and the one at lower left corner has a tilt angle of about 8 degrees. Our previous observations⁹⁰ has revealed that the grain agglomerates, which formed very rapidly and independently in areas that are experiencing large plastic deformation prior to the fracture in responding to the applied external stress, are very likely to be resulted from diffusion-assistant grain boundary processes. Following the formation of these grain agglomerates, cracks are observed to nucleate and propagate in an inter- or intra-agglomerate manner¹⁰⁷. Thermodynamic considerations indicate that deformation-induced changes in the GB structure would favor the genesis of low-angle GBs from high-angle GBs, allowing for the reduction in free energy of the system. Because all the HREM images were taken from the thin areas produced by deformation, presumably, the grain boundary state observed in Figure 6.3 resulted from the synergic interaction among the local grains in response to the external applied stress.

In order to identify the locations of the various dislocations trapped in this area, the IFFT images corresponding to Figure 6.3 A and B are shown in Figure 6.3 C and D, respectively. Obviously, the dislocations are not in an equilibrium state because dislocations with opposite sign are intermixed with each other. The attractive force for dislocations with opposite sign and close to each other (e.g., several times the magnitude of Burgers vector) can be very large¹⁰⁸. The dislocations marked with a dark T experienced no apparent displacement during the relaxation period of 86s, while those dislocations marked with a white T moved and rearranged (Figure 6.3 C and D). Using the dislocations marked with a dark T as reference, the upper two dislocations marked with white Ts that were very close to each other (Figure 6.3 C) annihilated with each other during the relaxation period (Figure 6.3 D). The lower two dislocations marked by a white T (Figure 6.3 C) moved closer to each other during this time interval (Figure 6.3 D).

The shrinkage and eventual annihilation of trapped dislocations segments during stress relaxation in the nanocrystalline Ni confirm the predication⁷⁷ that dislocation are most probably observed in stressed state. However, it is not appropriate to equal the experimental observation here to those from atomic simulations. This is because of the molecular dynamics simulation can only capture the start of the deformation due to its sub-nanosecond time-scale restriction, and thus exclude certain time-dependent processes. In contrast, due to the intrinsic stability requirements, HREM observations only reveal the dislocation dynamics at the final state of the deformation. Great efforts are still necessary to uncover the entire process from initial deformation to final failure of nanocrystalline materials.

It is interesting to note the dislocation rearrangement occurred in a rather sluggish manner. According the description based on molecular dynamics simulation, once nucleated, the dislocations will usually glide through the grain and absorption in the opposite side of the grain or re-absorbed at the grain boundary source from which they originally nucleated due to the stress relaxation⁷⁷. In both cases, the dislocation should move in a pretty fast manner. Two reasons may be account for this. On the one hand, the Frank-Read mechanism is known to account for the major portion of dislocation multiplication that occurs in crystals. Along with the decreasing of the grain size, the loop radius may exceed the diameter of the grain and therefore the nucleated dislocation has to terminate at the GBs. As a consequence, the dislocation mobility may be decreased by the GBs. On the other hand, nucleation and emission of a dislocation corresponds to the removal of a grain boundary dislocation from the GB nucleation site and a reorganization of the remaining grain boundary dislocations. For the same reason, the absorption of a dislocation will also lead the reorganization of an existed grain boundary. Both of above may lead a sluggish motion of the trapped dislocation besides the intrinsic lattice friction stress.

By monitoring the Bragg peak profiles of x-ray diffraction using the Swiss Light Source during cycle deformation of nanocrystalline Ni, Budrovic et al ⁹² showed that the peak broadening due to dislocations is reversible upon unloading for nanocrystalline Ni with an average grain size of 26nm, but irreversible for coarse Cu with a grain size of 20 μ m. Further, the authors concluded that the deformation process does not build up a residual dislocation network in nanocrystalline materials. This appears in agreement with our HREM observations. However, as shown in their loading-unloading curve (Figure 2 and 3 of ⁹²), the Ni film were fatigued to fracture during the third loading circle. This means that the damage accumulation mechanism was in effect from the start of the loading cycle and may play a critical role for our understanding on the deformation of nanocrystalline materials. However, the authors seems have overlooked this important factors and therefore make their conclusion in a questionable state.

6.4 CONCLUSIONS

In summary, we demonstrate that dislocation dynamics processing can be achieved successfully by exploring a combination of in-situ deformation and in-situ HREM observation. The detection of trapped dislocation in grains as small as 5nm by 10 nm suggested that the as-deposited nanocrystalline Ni may exhibit much higher yield strength than expected. The absence of deformation twinning suggested that twinning may not be a preferred deformation mode even if the nucleation stress for partial is less than that for perfect dislocation. Unlike the molecular simulations which can only capture the very start information of the nanocrystalline materials deformation, the results report here only capture the final state of nanocrystalline materials

deformation. Therefore, further efforts are necessary to reveal the entire process of nanocrystalline materials deformation.

7.0 IN SITU NANO BEAM DIFFRACTION OBSERVATION

7.1 INTRODUCTION

Ever since Herbert Gleiter presented the first concepts for developing nanocrystalline materials over 20 years ago, it has been thought that nanocrystalline materials contained an extremely large fraction of grain boundaries with a special atomic structure. This, plus the experimental observations that grain shapes remain equiaxed before and after deformation^{102,109}, lead to the suggestion^{79,110} that the grain boundaries serve as viscous deformable layers and mass-transport networks, with the central regions of the nano grains behaving like a rigid body during the deformation of nanocrystalline materials. However, more recent experiments^{7,8} suggest that grain boundaries (GBs) in well prepared nanocrystalline materials are not anomalous but similar to those found in their coarse-grained counterparts. This naturally leads to two fundamental questions that, to our knowledge, have hitherto not been fully answered. Do individual nano grains behave differently from that have been expected during deformation? If so, what are the mechanistic contributions of those individual grains to the overall deformation response? Developing an understanding of these related issues would provide valuable insights into the mechanical deformation characteristics of a wide variety of nanocrystalline metals. In addition, investigation of individual grains could also lead to fundamental understanding of the unique mechanical properties of nanocrystalline materials, such as ultra-high strength and hardness.

7.2 EXPERIMENT PROCEDURE

The Ni film and the sample design used in this part of work is exactly same as those used in in-situ BF TEM observation (Chapter 4), i.e., PLD Ni film with its nominal thickness of 60nm glued on the special designed copper substrate. Again, I chose to focus on the grains ahead of branch cracks due to the low local strain rate. Unlike BF and DF TEM observations, nano beam electron diffraction (NBED) can not only monitor the possible rotation of the nano grain involved in the deformation, but also reveal the possible internal structure change of the grain during the straining. The use of the thermal-emission electron gun of the JEOL 2000FX TEM limited the minimum workable probe size for NBED to a diameter of about 20nm. Therefore, only those grains larger than 20 nm can be studied with NBED.

7.3 EXPERIMENTAL OBSERVATIONS

Large variations in the magnitude of grain rotation and internal structure were found. Figure 7.1 are extracted images from a sequence of observations which shows maximum variation. Figure 7.1 A, C, and E are typical BF images showing the feature under investigation (delineated by a dashed line). Figures 7.1 B, D, and F are the corresponding NBED patterns that revealed that the feature under investigation is a single grain. The grain under observation was located about 210nm ahead of a branch crack and had a diameter of about 22nm. Due to the large image shift and the possible contrast change of this grain in response to the displacement steps, other readily identifiable features in the vicinity have been employed as a reference to relocate this grain.

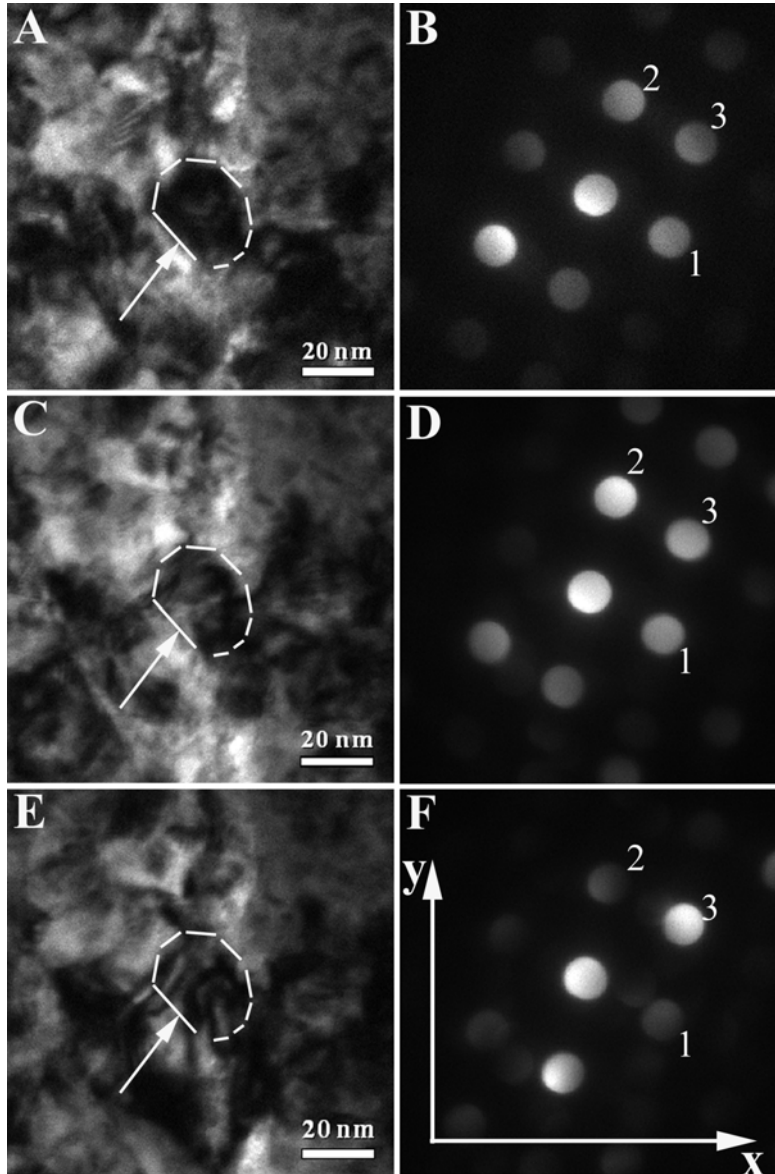


Figure 7-1: Bright-field contrast (A, C, E) and its corresponding NBED pattern (B, D, F) evolution of a grain (delineated by dash line) during straining of as-deposited Ni at room temperature. The diffraction patterns did not match any known f.c.c zone axis. The intensity change of the diffraction spots suggested that the rotation of the grain involves multiple rotation axes. A reference coordinate is shown in figure 2E with its X and Y axis horizontally and vertically, respectively.

It is clear that the contrast of the studied grain has changed significantly with each loading pulse (Figure 7.1 A, C and E). Dramatic changes are also discernible in the accompanying NBED patterns (Figure 7.1 B, D and F). Global rotation (i.e. rotation of the entire region) is not likely to be responsible for the observed contrast change in Figure 7.1, as this will usually cause contrast change across the entire field of view. Lower magnification TEM observations confirmed that the contrast change in response to a displacement pulse occurs only around the center of the band-like thinning area, i.e., the area that is experiencing deformation. For those areas that are a little farther from the deforming area, the image contrast remained nearly constant. The intensity variation of the diffraction spots in the NBED patterns is due to a change in the excitation error associated with each spot (this is the distance of the relevant reciprocal lattice point from the surface of the Ewald sphere⁸⁹) and is sensitive to the crystal orientation of the grain. Therefore, the irregular intensity changes observed in the NBED spots not only confirm that grain rotation has occurred, but also indicate that the grain rotation is multi-axial.

In order to quantify the relative rotation and the possible elastic deformation of the grain, both the angles of diffraction vectors with respect to the reference axis X defined in Figure 7.1 F and the magnitude of the diffraction vectors for eight NBED patterns were measured. Each new NBED pattern corresponds to a different loading state, following the application of one or more loading pulses. The ratios of the diffraction vector lengths and the co-angles between different crystallographic directions were also calculated based on these original data, as shown in Table 7.1. It is surprising to see that no corresponding zone axis direction could be found to produce a diffraction pattern that exactly matched the experimentally collected NBEDP when assuming an undistorted perfect Ni crystal structure, despite the fact that the selected area diffraction pattern clearly indicates that the as-deposited Ni film has the proper FCC structure.

Table 7.1: Summary of measured results of 8 NBED patterns

series	R_1/R_2 (± 0.01)	R_3/R_1 (± 0.01)	R_3/R_2 (± 0.01)	$\theta_{1\&3}$ ($\pm 0.5^\circ$)	$\theta_{3\&2}$ ($\pm 0.5^\circ$)	$\theta_{1\&2}$ ($\pm 0.5^\circ$)
1	1.139	1.330	1.168	51.8	44.1	78.2
2	1.112	1.315	1.183	53.5	46.0	76.5
3	1.148	1.304	1.136	54.7	46.6	75.3
4	1.167	1.328	1.139	54.9	46.2	75.1
5	1.138	1.290	1.133	55.2	47.0	74.8
6	1.104	1.255	1.136	55.0	49.0	75.0
7	1.105	1.267	1.146	54.7	48.3	75.3
8	1.073	1.253	1.168	55.1	50.3	72.4
<110>	1.000	1.155	1.155	54.74	54.74	70.32

After calibration using a known NBEDP from undeformed grains of the same Ni film, the diffraction vector lengths in the experimental NBEDP were found to be closest to those expected for a beam direction of <110>. For comparison, Table 7.1 also lists the theoretical ratio of the diffraction vector lengths and inter-directional angles (co-angles) for the <110> beam direction for perfect FCC Ni. For convenience, the three crystallographic directions are marked 1, 2 and 3, respectively, according to the diffraction vector lengths from short to long (Figure 7.1 B, D and F). The angles of diffraction vectors 1, 2 and 3 with respect to the reference axis X defined in Figure 7.1 F ($\theta_{i\&X}$, $i=1, 2,$ and 3) are plotted in Figure 7.2 A for the sequence of eight NBED patterns. It can be seen that all three diffraction vectors have rotated counterclockwise around the beam direction by at least 1.3 degrees from the first to the eighth NBED pattern. However, the changes are not consistently in phase. $\theta_{2\&X}$ increases monotonically up to 7.5 degree, but $\theta_{1\&X}$ and $\theta_{3\&X}$ both increase and decrease during straining, with $\theta_{1\&X}$ changing in a relatively

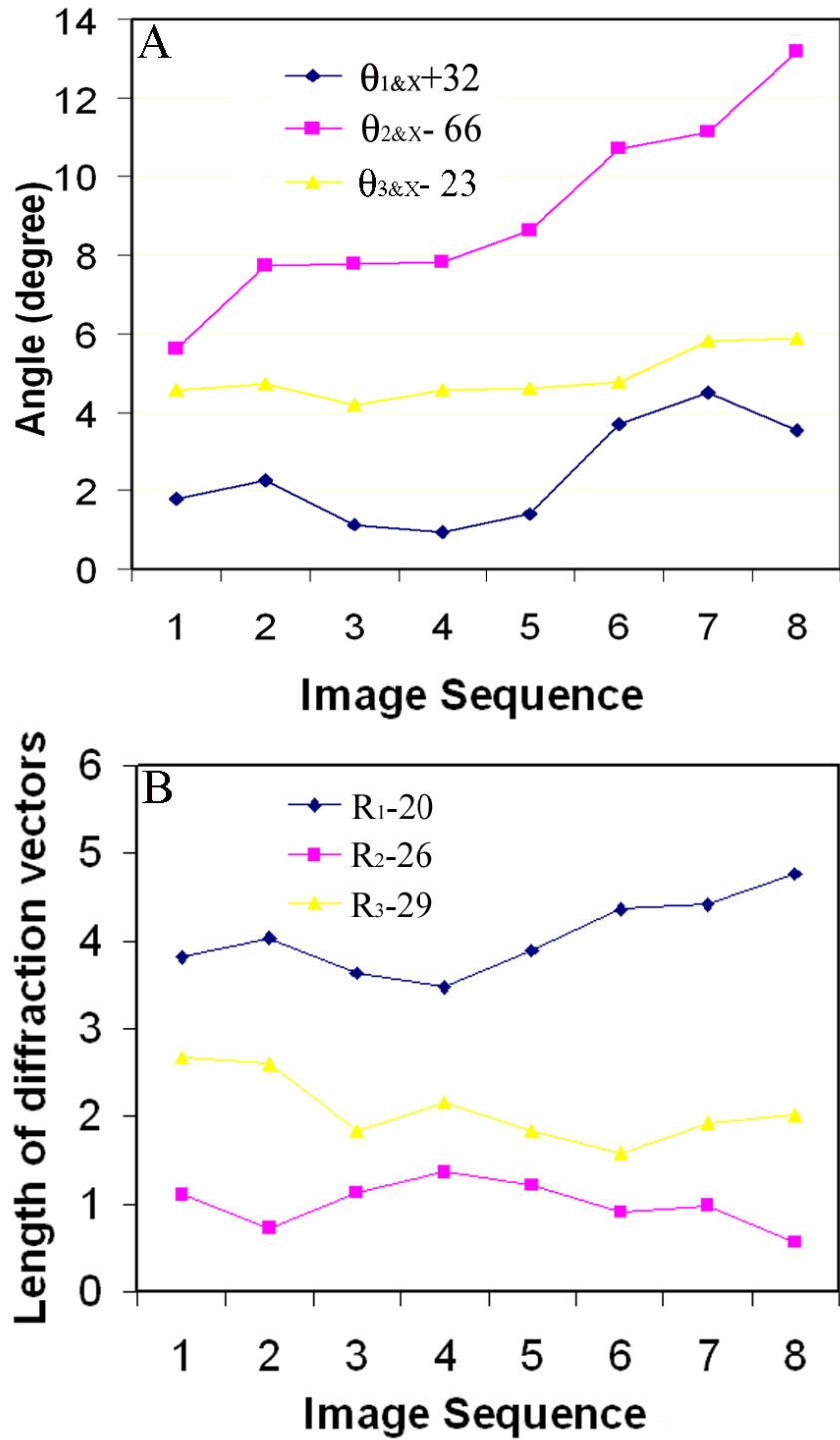


Figure 7-2: (A) Gives the measurements of the co-angle changes between 1, 2, 3 diffraction vectors and the reference X-axis. (B) Gives the measurements of the distances of 1, 2 and 3 diffracted beams from the zero-order beam.

rough manner, as shown in Figure 7.2A. This would be consistent with a non-uniform shear deformation of the studied grain during straining. According to the data collated in Table 1, at the beginning of this sequence, the co-angles of $\theta_{1&2}$, $\theta_{2&3}$ and $\theta_{3&1}$ are 78.2° , 51.8° and 44.1° respectively. After a number of additional displacement pulses, these co-angles have changed in an almost monotonic manner to 72.4° , 55.1° and 50.3° , respectively, at the end of the observations. These co-angles systematically approach the corresponding theoretical values for undeformed Ni grain with a zone axis of $\langle 110 \rangle$ orientation. The apparent elastic strain relaxation of the studied grain indicates that the grain and its neighbors act in a synergistic way to accommodate the loading pulses, resulting in a decrease of mechanical constraint stress acting upon the studied grain.

The measurement in lengths of the diffraction vectors defined as 1, 2 and 3 show that changes occur in a rather irregular manner with additional loading pulses (Figure 7.2 B). Based on Bragg's Law of diffraction of fast electrons in the TEM, the lengths of the diffraction vectors (R_{hkl}) can be converted to interplanar spacing (d_{hkl}) using the well-known relation $Rd = \lambda L$, where λ is the electron wave length and L is camera length⁸⁹. The linear strain in the grain along the particular crystallographic direction normal to the planes (hkl) is given by $\varepsilon_{hkl} = (d_1 - d_0) / d_0$, where d_1 and d_0 are the strained and unstrained interplanar spacing of the (hkl) plane, respectively. Because $Rd = \text{constant}$, it follows that $\varepsilon_{hkl} = (R_0 - R_1) / R_1$. Since the experimentally measured co-angles approach the theoretical values of a perfect Ni crystal with a zone axis of $\langle 110 \rangle$ direction in an approximately monotonic manner, it appears justified to use the measured diffraction lengths of the eighth NBED pattern as the unstrained value, and another extreme value along a particular crystal direction as the strained value to estimate the maximum value of elastic strains along these crystallographic directions. Thus, the largest elastic strains along the directions 1, 2

and 3 direction are about 5.5%, -3.0% and -2.1%, respectively. These are remarkably large strains because annealed single crystals usually yield at elastic strains of less than 0.01%¹¹¹.

7.4 DISCUSSION

Although all calculations presented here are at best first-order approximations, it still appears reasonable to conclude that severe non-uniform elastic deformation occurred in response to the initial displacement pulse in the nanocrystalline grain studied by NBED, which then relaxed over a period of time. The build-up of large elastic strains in crystalline grains in response to suitable externally applied deformation can be understood by considering the size effect of crystals. By assuming that atomic sliding on slip planes is concurrent with, and the cause of, plastic flow, it has been deduced that the theoretical yield strengths of a single crystals of pure materials are about $\mu/10$, where μ is shear modulus¹¹². However, when the mechanical strength of most crystalline solids is measured on a bulk case, the experimental strength is always much smaller (about $10^{-2}\sim 10^{-3}$) than the theoretical strength of a perfect crystal. It has been well experimentally established this is due to the presence of defects within the crystal and on its surface. For example, annealed bulk crystals normally contain from $10^4\sim 10^8$ dislocations per square centimeter¹¹³. It is the motion, interaction, generation and annihilation of those preexisted dislocations that lead the crystalline metal materials show much lower yield strength than that predicted by theoretical prediction. The first experimental verification that materials strengths may approach the theoretical value was achieved by testing the strength of metal tin whiskers (a filament-like single crystal with its diameter about a few micros) over 50 years ago¹¹⁴. After that, the strengths of a large number of whiskers prepared by a variety of methods have been

measured, either by means of bend tests or tensile tests. The maximum values are summarized in Table 7.2. It can be seen the elastic strain for Ni was as large as 1.8%.

Table 7.2: Strength of whiskers¹¹⁴

<i>Material</i>	<i>Max. strain</i>	<i>elastic</i>	<i>Method of testing</i>	<i>Method of growth</i>
<i>Fe</i>	4.9		Tension	Halide reduction
<i>Cu</i>	2.8		Tension	Halide reduction
<i>Ag</i>	4.0		Tension	Halide reduction
<i>Ni</i>	1.8		Tension	Halide reduction
<i>Si</i>	2.0		Tension	Halide reduction
<i>Zn</i>	2.0		Tension	Vapor condensation
<i>NaCl</i>	2.6		Tension	Precipitation
<i>SiO2</i>	5.2		Tension	Vapor condensation
<i>Si2O3</i>	3.0		Tension	Vapor condensation
<i>MoO2</i>	1.0		Tension	Vapor condensation
<i>C</i>	2.0		Tension	Vapor condensation
<i>Sn</i>	2 to 3		Bending	Growth from solid
<i>Ge</i>	1.8		Bending	Halide reduction
<i>ZnO</i>	1.5		Bending	
<i>ZnS</i>	1.5		Bending	Vapor condensation
<i>LiF</i>	3		Bending	Cleavage
<i>MgSO4.7H2O</i>	>2		Bending	Precipitation

In spite of the large scatter in strength, a trend towards higher strengths as the diameter of the whiskers decreases can still be detected clearly¹¹¹. The reason behind this is believed to be

by virtue of the fact that small volume crystals not only have little chance to possess defects, such as dislocations but also are relative difficulty to generating dislocations either internally or at the surface^{111,115}. Therefore, it is reasonable to postulate that if the volume of crystal is small enough to exclude the existence of any defects, then it is possible for the crystalline materials to reach its theoretical strength. It can be seen from Table 7.2, the maximum elastic strain for Ni whiskers is 1.8%. However, comparing the size of whiskers (a few micro meters in diameter and several millimeter in length¹¹¹), the grain we studied here (grains size is about 20 nm) is apparently much smaller and therefore are expected to be similar to a perfect crystal. Based on the atomic model of uniaxial tensile failure, it has been shown the estimated theoretical fracture strengths for Ni is 37.2 GPa¹¹². Taking the Young's modulus of Ni as bulk value 200GPa, and overlooked the nonlinear effect, the maximum elastic stain can be as high as 16.6%. In comparison, the maximum elastic strains we measured here is only about 5.5%. This may be due to the following reasons:

On the one hand, unlike the whiskers, every single nano-grain in nanostructured materials is confined both mechanically and geometrically by its neighboring grains. Any externally applied force exerted upon the material will be transferred to individual grains by their surrounding grains through the grain boundaries. Because materials always choose the easiest way to deform, it is the weaker of the two strengths – that of the individual grains or that of the grain boundaries – that determines the strength and hardness of real materials. For materials with grain sizes of millimeter dimensions down to the sub-micrometer and even into the nanometer regime, it has been well established experimentally that the increase in yield stress is inversely proportional to the square root of the grain size. This relation, known as Hall-Patch relation, is believed to result from the pileup of dislocations at the grain boundaries. For a given dislocation pileup array, the

stress concentration acting upon the lead dislocation is proportional to the number of dislocations in the pile-up and the applied external shear stress ¹⁰⁸. As grains become smaller, especially deeply into the nanometer range, higher stresses are necessary for dislocation nucleation and the space limitations imposed on the extent of a pile up resulting in a reduction of the local stress concentration on the lead dislocation. A higher external applied stress is thus required to nucleate dislocations and to overcome the barrier imposed by the grain boundary before plastic flow occurs. Correspondingly, higher yield stress, increased hardness and larger elastic strain, as observed in our experiments, are expected to occur. Upon reaching a certain critical stress level, i.e., the maximum strength of the material, the local stress accumulation will be released either by the nucleation and motion of dislocations or by grain boundary mediated plasticity. The latter, such as grain boundary sliding and/or grain rotation, is expected to be facilitated by grain boundary diffusion and to increase in prominence with the decreasing grain size ⁹⁰. As a consequence, the material will exhibit macro-scale deformation and the elastic strain accumulated in the single grains then will be released. Details of the elastic strain release depend on the loading mode and the local environment confining the individual grains. Thus, the existence of a peak value of the yield stress or hardness for real materials is an inevitable result of the competition between the stress necessary for the dislocation nucleation and pileup and the strength of the grain boundary barriers. Hence, the position and the magnitude of this peak value will not only depend on the average grain size, but also on the strength of the grain boundaries, i.e., on the grain boundary structure. This indicates that for a given grain size grain boundary engineering may be explored to tailor the mechanical strength of nanocrystalline metals. For instance, if nanocrystalline metals can be designed to contain many special grain boundaries that act as strong barriers to dislocation motion and at the same time exhibit limited ability for

boundary diffusion, which is expected for coherent twin boundaries, higher strength and higher hardness may be obtained than for the same material with a random grain boundary structure at a given grain size. First indications of the beneficial effect of an increased content of twin boundaries have been shown in recent work by Lu et al ⁵⁶, where ultrahigh strength copper was obtained when the fraction of twin boundaries was increased by recourse to pulsed electrodeposition technique.

Due to that higher lattice strength are expected for nano grains, presumably the observed ultra high elastic strain in fact reflects the possible strength of those as-deposited grain boundaries. This, in turn, allows us to critically evaluate two highly cited models, which predict a critical grain size below which dislocation pile up or multiplication cease operation ^{3,4}. By relating the repulsive force between two dislocations to an externally applied force and assuming that the hardness of a materials is about 6 times the shear stress, Nieh et al. ³ predicted that the critical grain size for Ni is about 2.5nm. However, by assuming a Frank-Read type source as dislocation multiplication mechanism and using their measured yield strength value, Legros et al. ⁴ predicted that the cut off value for significant dislocations activity of Ni is about 38 nm. Both of the above calculations assume a constant shear modulus, although theoretically, the nonlinear elastic effect will lead to a decrease in Young's modulus and shear modulus at very large stress level. According to Nieh's model, the relation between the applied external stress (σ) and the equilibrium distance between the two dislocations (l_c) can be expressed as:

$$\sigma = \frac{\mu b}{2\pi(1-\nu)} \cdot \frac{1}{l_c} \quad (7.1)$$

Where μ is the shear modulus, b is the magnitude of the Burgers vector, ν is Poisson's ratio. Because $\mu = E/[2(1+\nu)]$ ¹¹⁶, without losing generality, we can rewrite equation (1) into:

$$l_c = \frac{b}{4\pi(1+\nu)(1-\nu)} \cdot \frac{1}{\varepsilon} \quad (7.2)$$

where $\varepsilon = \sigma/E$ is normal strain and E is the Young's modulus. Taking $\nu = 0.312$ ¹¹⁶, $b = 0.249 \text{ nm}$ and ε equal to the maximum elastic strain measured in our experiments i.e., 5.5%, the lower bound equilibrium distance l_c is estimated as approximately 0.4 nm. This value is unphysically small because $l_c \sim b$. Nonetheless, it indicated that a dislocation pile up mechanism may be valid even at very small grain sizes, based on the large elastic strains measured in our experiment. An additional supporting point is that the Hall-Petch relationship continues to hold up in these same nickel films, even with the small grain size of 10 nm.²² However, an appropriate dislocation multiplication mechanism is apparently necessary to accommodate any dislocation pile up. The Orowan relation for the expansion of a dislocation loop suggests that dislocation multiplication requires Frank-Read-type sources. With an approximation of the source size equal to the grain size (d) (reasonable for nanocrystalline materials, especially for those with grain size less than 20 nm), according to elementary dislocation theory¹⁰⁸, the critical shear stress necessary (τ) to nucleate a dislocation can be expressed as $\tau = 2\alpha\mu b/d$. The parameter α reflects the character of the dislocation ($\alpha = 0.5$ and 1.5 for edge and screw dislocations, respectively). Assuming that $\tau \sim \sigma/2$, then it is readily shown that the grain size $d = 2\alpha b / [(1+\nu)\varepsilon]$. Again, taking $\varepsilon = 5.5\%$, the maximum elastic strain measured in our experiment, the estimated lower bound of grain size for the operation of a dislocation source is approximately 3.5~10.4 nm for nickel, depending on the nature of the dislocations involved. This is in good agreement with our previous observations⁹⁰.

7.5 CONCLUSIONS

Nano-beam electron diffraction has been used to study the behavior of individual grains in nanocrystalline Ni during deformation under low local strain rate conditions. Direct measurement of lattice distortions during straining reveals that grain interiors may experience large elastic distortions during tensile deformation. These results indicate that a peak strength value must exist, with a position and magnitude that depends on both grain size and grain boundary structure. Additionally, the critical size below which dislocation sources cannot operate is determined to be between 3.5 and 10.5 nm for nickel, depending on the type of dislocation.

8.0 FORMATION MECHANISM OF THE DIMPLED FRACTURE SURFACE

8.1 INTRODUCTION

In nanocrystalline metals (i.e. average grain size typically less than 100nm), tensile stress-strain curves at room temperature show very high strengths accompanied by limited uniform deformation^{12,117}. This behavior is very similar to that observed during brittle fracture. Consequently, it may be expected that fracture occurs intergranularly and that the three-dimensional nature of the grains would be revealed on the fracture surface. However, experimental observations of fracture surfaces of nanocrystalline metals typically exhibit dimple features with sizes considerably larger than the grain size^{7,8,20,52,84,118-121}. Fracture surfaces of this type are most frequently characteristic of ductile fracture.

Several explanations have been proposed to account for this apparent paradox of ductile-like dimpled fracture surfaces in nanocrystalline metals that exhibit a brittle response. Studying nanocrystalline Ni, Kumar et al.⁷ proposed that the dimpled fracture surfaces may have resulted from the evolution of those grain boundaries (GBs) and/or triple junction voids which form when intragranular slip (dislocation motion) is coupled with unaccommodated GB sliding. This mechanism reasonably accounts for the experimental observations in nanocrystalline Ni with an average grain size of about 30nm, where dislocation-mediated plasticity has been proven to be the dominant deformation mode⁷. However, it cannot explain the dimple features observed on

the fracture surface of nanocrystalline materials with a much smaller grain size (e.g. less than 10 nm¹²¹). It is expected that GB mediated plasticity (GB sliding and/or grain rotation) will begin to replace dislocation mediated plasticity as the dominant deformation mechanism for such small grain size^{2,5,103}.

Iwasaki et al¹²¹ recently reported deformation and fracture characteristics of an electrodeposited nanocrystalline Ni-W alloy with an average grain size of 8.1nm. The fracture surface also showed dimple features with sizes 2.5 to 25 times larger than the average grain size. Post-mortem high-resolution TEM of the immediate vicinity of the fracture surface showed a long deformation band which aligned primarily along GBs. Hence, the authors¹²¹ proposed that the dimpled fracture surface is a result of grains sliding in clusters and that the dominant deformation mechanism in nanocrystalline Ni-W is GB sliding. However, the authors did not mention how or why grains might slide as clusters, nor directly demonstrate this mechanism in operation.

Molecular dynamics (MD) computer simulations have been used to study the fracture surfaces of nanocrystalline material. Hasnaoui et al.⁸⁴ studied a specimen containing 125 grains with a mean grain size of 6nm. They demonstrated that due to the presence of GBs that are resistant to sliding, local shear planes are concentrated around their neighboring planes, creating a cluster of grains embedded in a sliding environment. Thus, an inherent plasticity length emerges that is on the order of several grain sizes and corresponds to the dimensions of the dimple features documented on experimental fracture surfaces. However, the unrealistically high strain rate (10^7 s⁻¹), very short duration (350 ps), as well as the high temperature (800K) used suggest that the results obtained from the MD simulation should be used only for qualitative guidance, rather than as a validation of the existence of the proposed mechanism⁸.

It is evident from the foregoing discussion that all the proposed explanations have their own limitations. However, if we take all of them ^{7,84,121} into consideration, a common characteristic can be identified: GB sliding plays an important role in the formation of dimpled features on the fracture surfaces of nanocrystalline materials, while no direct experimental confirmation of the role of this mechanism has been reported in these studies. Therefore, confirming the prevalence of GB-related deformation seems to be a key point for uncovering the underlying physical mechanism that dominates the formation of the dimpled fracture surfaces in nanocrystalline metals. With its inherently dynamic character and atomic-scale resolution, in situ transmission electron microscopy (TEM) observations during tensile straining may be expected to provide additional useful insights into the nature of the formation of dimple features on the fracture surfaces of the nanocrystalline materials.

8.2 MATERIALS AND EXPERIMENTAL METHODS

A detailed analysis of previous studies ready to show that GB sliding has been taken as the common mechanism ^{7,84,121} to rationalize the formation of the dimple structures observed on the fracture surface of nanocrystalline metals and alloys although no direct experimental confirmation on such mechanism has been reported in these studies. Therefore, to confirm the activation of GB related deformation seems to be a key point for uncovering the underlying physical mechanism that dominate the formation of the dimpled fracture surface.

In this study, we select to use the Ni samples synthesized by directing a high-energy pulsed KrF excimer laser onto a high purity Ni target under a vacuum with a base pressure of approximately 2×10^{-7} torr and the resulting Ni plasma was deposited onto a [001] NaCl substrate

to a nominal thickness of 150nm. It has been shown ^{9,90} that as-deposited Ni films possess of very high-quality, fully-dense and essentially artifact-free with an average grain size typically less than 10nm.

As for the technique, we choose to employ in situ dynamic dark field TEM (DFTEM) observation because GB sliding, if exists, will naturally lead the reorientation of those involved individual grains and DFTEM is sensitive to this orientation change. Because the {111} and {200} polycrystalline diffraction rings of Ni are very close to each other and the limitation of the select field aperture size, both {111} and {200} diffraction spots were selected as the image forming diffraction vectors. According to the nature of the image formation mechanism of DFTEM images⁸⁹, any grains illuminated with bright contrast is in strong diffracting conditions and exhibit essentially edge-on orientations of their {111} and/or {200} planes.

However, global and local tilting of the sample during deformation are two often encountered problems that hinder us to achieve a successful in situ dynamics DFTEM observation ²¹. Analysis shows they are most probably resulted from the inappropriate sample design. In this study, a special sample design developed in our previous study was adopted ⁹⁰. It has been experimentally proven that this improved sample design can minimize the global and local tilting in maximum extent.

The room temperature tensile loading during in situ TEM experiments was applied with a single-tilt straining stage while continuously imaging the deformed region using a JEOL 3010 instrument operating at 300kV with a point-to-point resolution of 1.9 Å. Still images were obtained with a Gatan 754 Digital CCD camera and videotape images were obtained with a Gatan 622 TV-rate video-intensified camera and recorded with a VCR. The regions immediately

ahead of the crack tip were monitored during in situ straining to identify the active deformation and fracture mechanisms.

8.3 RESULTS AND DISCUSSION

TEM observations (Figure 8.1a) indicate that the as-deposited Ni consists of roughly equiaxed grains. No obvious texture is detected by electron diffraction in the specimens used here. Statistically significant measurements using DFTEM images reveal a narrow, log-normal grain size distribution, ranging from several nanometers to 23 nm with an average value of about 10 nm⁹⁰. High-resolution electron microscopy (HREM) shows that most grains are separated by high-angle GBs (Figure 8.1b). No additional GB phases, no porosity and no intergranular microcracks were detected in these samples⁹⁰.

Due to the sample design, the discernable deformation and the fracture process were usually concentrated in a narrow, long band-like area ahead of the crack tip. Under BFTEM imaging conditions, rapid changes in contrast of many different grains are observed to occur continuously in the band-like area where the local strain rate is usually high upon loading. This type of BFTEM contrast change has been reported previously^{10,21} and has usually been identified as dislocation activity, although it may also result from other strain induced deformation mechanisms, such as GB mediated plasticity.

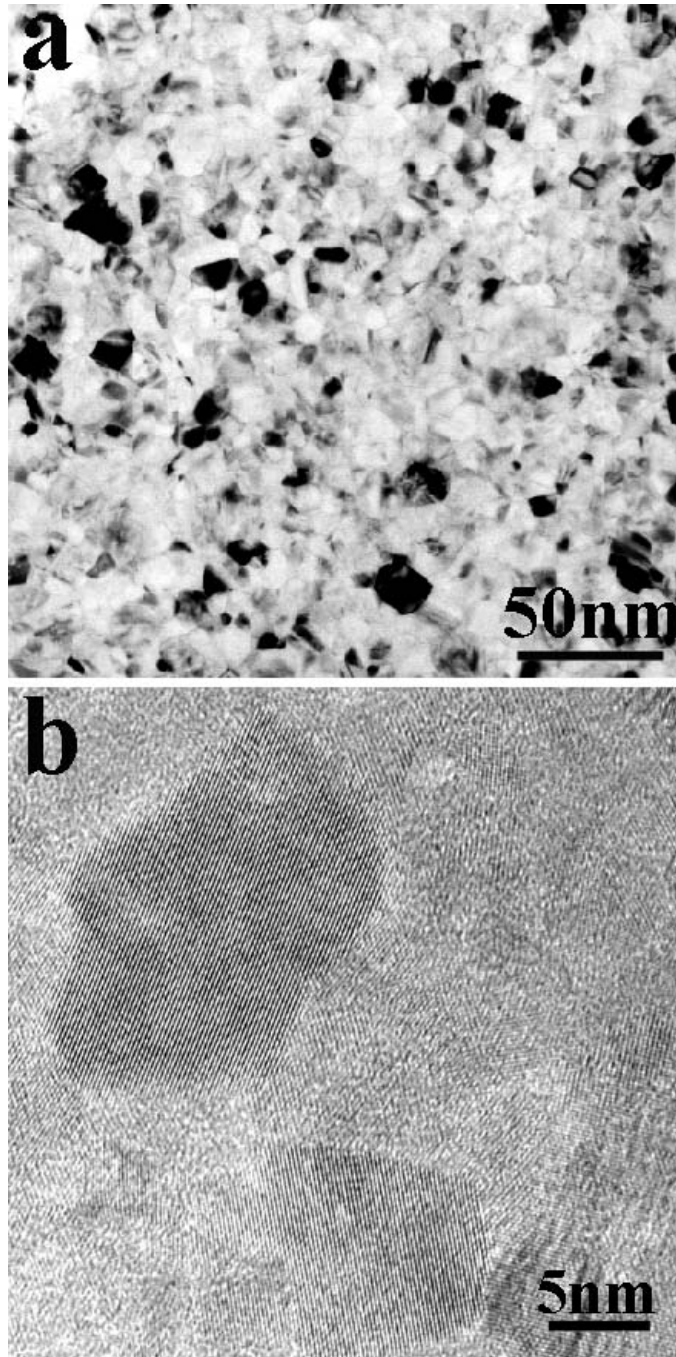


Figure 8-1: Microstructure of as deposited nanocrystalline nickel. (a) Bright field TEM micrograph of the nanocrystalline Ni, (b) Typical HREM image of as deposited Ni.

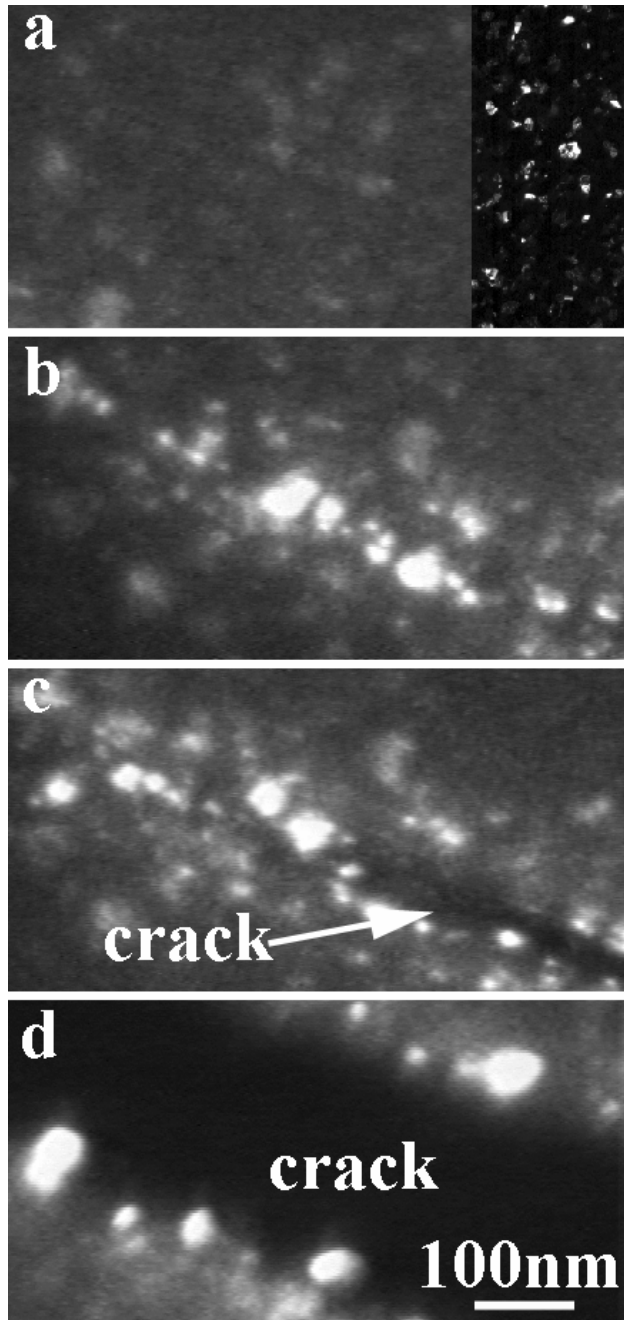


Figure 8-2: DF TEM observation of the deformation and fracture process of as-deposited nanocrystalline Ni.

Figure 8.2 shows DFTEM images extracted from videotape, which depict the dynamic evolution of the deformation and fracture process of nanocrystalline Ni upon loading. Figure 8.2a shows an area before deformation occurred. The right-hand-side inset in Figure 8.2a is a DFTEM image taken from an area that has been thinned using low temperature ion thinning. This micrograph confirms the narrow grain size distribution of the as-deposited nanocrystalline Ni with an average grain size of about 10nm. Upon loading, many bright contrast features form very frequently and rapidly at many locations in the narrow, long band-like area ahead of the crack tip, apparently independent of one another, under the influence of the applied stress as shown in Figure 8.2b. These features have been identified as agglomerates of smaller grains and the details of their formation are discussed in Ref. ^{90,107,122}. Clearly, the size of these bright contrast features (up to about 80 nm in Figure 8.2b) is much larger than the average grain size. Comparison of the undeformed state (Figure 8.2a) and the post-deformation state (Figure 8.2b) indicates that groups of neighboring grains have undergone an orientation change during straining and formed numerous larger grain agglomerates, with the smaller grains in these agglomerates exhibiting essentially edge-on orientations of their {111} and/or {200} planes. Further loading causes the crack to propagate through this band-like thinner area, where the grain agglomerates are concentrated (Figure 8.2c). Careful examination of Figure 8.2b and 8.2c found that, instead of remaining constant after formation, the sizes and shapes of the grain agglomerates changed in a rather irregular manner during the deformation and fracture process. This implies that GB related plasticity mechanisms were active among the groups of smaller grains that constitute the larger grain agglomerates in response to the additional loading pulses. Figure 8.2d shows the final crack propagation path. The bright contrast features at the edges of the propagating crack indicate that some grain agglomerates behave in a collective manner

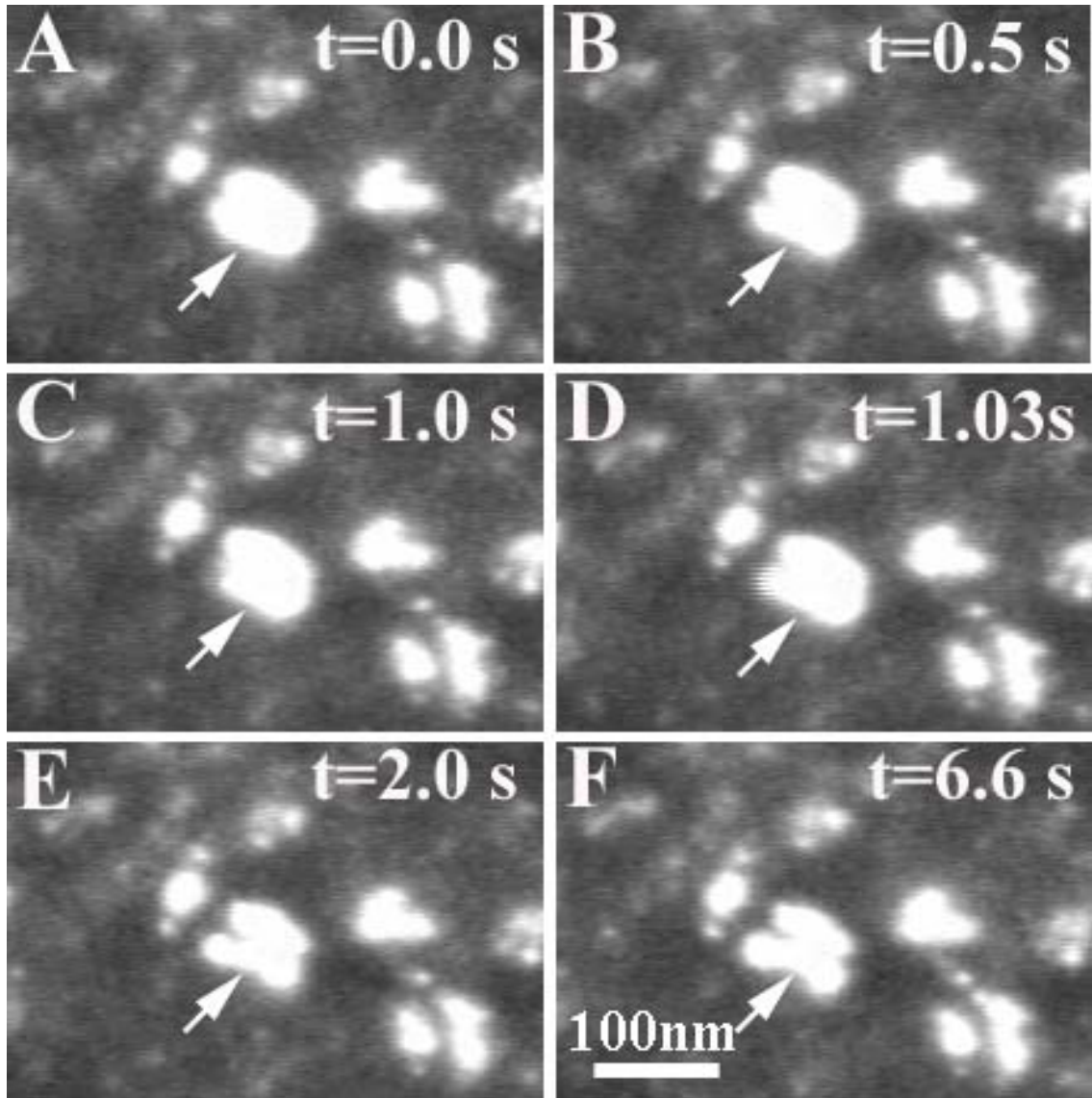


Figure 8-3: DFTEM observation of the intra-agglomerate deformation depicted by individual still frames extracted from a dynamic video-sequence.

during the fracture process and the crack advances around them rather than through them (i.e. in an inter-agglomerate mode of crack propagation and fracture).

However, deformation and fracture through or across the grain agglomerates is also observed. Figure 8.3 shows DFTEM micrographs extracted from a typical dynamic sequence of images taken after the application of a single displacement pulse. The times listed on each still frame are based on the video-acquisition rate of 30 frames per second. At the beginning of this sequence, the grain agglomerate indicated by the white arrow exhibits a slightly oblong shape with an approximate size of 60nm along the short axis and 80nm along the long axis, as shown in Figure 8.3a. Then a v-shape notch begins to form and grows at the middle-left of the agglomerate (Figure 8.3b). Following the growth of the notch, the lower left part of the agglomerate, which has been separated by the growing notch, begins to dim and finally rotates completely out of contrast by $t=1.0$ s (Figure 8.3c). However, only $1/30$ of a second later the lower left part of the grain agglomerate, a region of about 8 nm in size, close to the average grain size, rotates suddenly back into a strongly diffracting orientation again. This sequence implies that the individual grains in the nanocrystalline Ni can suddenly rotate under the influence of the applied stress. During the growth of the middle left notch, another notch at the middle right end began to emerge and grew, as shown in Figure 8.3e ($t=2.8$ s). After this sequence of rapid contrast changes, the evolution of the agglomerate slowed significantly. The image in Figure 8.3f was extracted at $t=6.6$ s when the evolution of the grain agglomerate almost stopped. Note that the surrounding features in bright contrast provide a frame of reference for the evolution of the grain agglomerate we have been considering. They appear nearly constant in shape and position, indicating that any overall bending or rotation of the observed region did not occur. Instead, the

changes in contrast of the grain agglomerate located centrally in Figure 8.3 are due to local grain orientation changes, presumably by rotation. The re-splitting of the grain agglomerate in the center of Figure 8.3 is further strong evidence of GB mediated plasticity^{90,107} and would be completely inconsistent with an interpretation wherein these grain agglomerates were produced simply by grain coarsening or grain growth¹²².

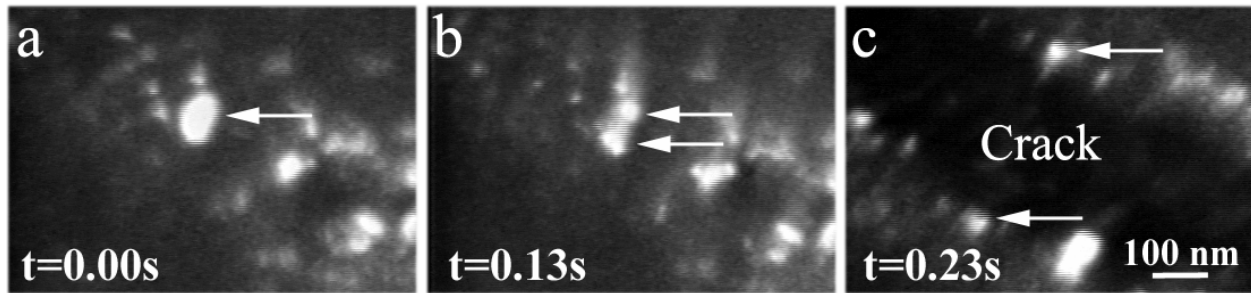


Figure 8-4: DFTEM observation of intra-agglomerate fracture depicted by individual still frames extracted from a dynamic video-sequence. (a) $t=0s$, a agglomerate with dimension of about 60nm by 90nm is indicated by the white arrow. (b) The agglomerate split at $t=0.13s$ (c) $t=0.23s$, the crack propagated across the agglomerate; the residual parts located at the crack edges are indicated by the white arrows.

Figure 8.4 shows DFTEM images extracted from video tape, which demonstrate the dynamic fracture process of as deposited Ni occurring in an intra-agglomerate manner. At the beginning of this sequence, the image of the agglomerate indicated by the white arrow had a dimension of about 60 nm by 90nm (Figure 8.4a). However, only 0.13s later, the agglomerate was observed to split into two parts (Figure 8.4b). It is worth noting that the total size of the two bright, split parts in Figure 8.4b appears smaller than the original agglomerate (Figure 8.4a) due to a gray zone between them. This suggests that grains in the middle of the original agglomerate have rotated out of contrast, and that grain-boundary processes are active in producing the fracture. At $t=0.23s$, a crack has propagated across the agglomerate and the two residual parts of the

agglomerate located at the opposite edges of the crack can be seen clearly, as indicated by the white arrows in Figure 8.4c.

Thermodynamic considerations imply that deformation-induced changes in the GB structure would favor the genesis of low-angle grain boundaries (LAGB) from high-angle grain boundaries (HAGB), allowing for a reduction in free energy of the system. In order to verify the GB structure of the grains constituting the agglomerates, HREM images were taken along the crack edge where, as shown in Figure 2 and Figure 4, inter- and/or intra-agglomerate fractures are expected to occur. An example is shown in Figure 5.

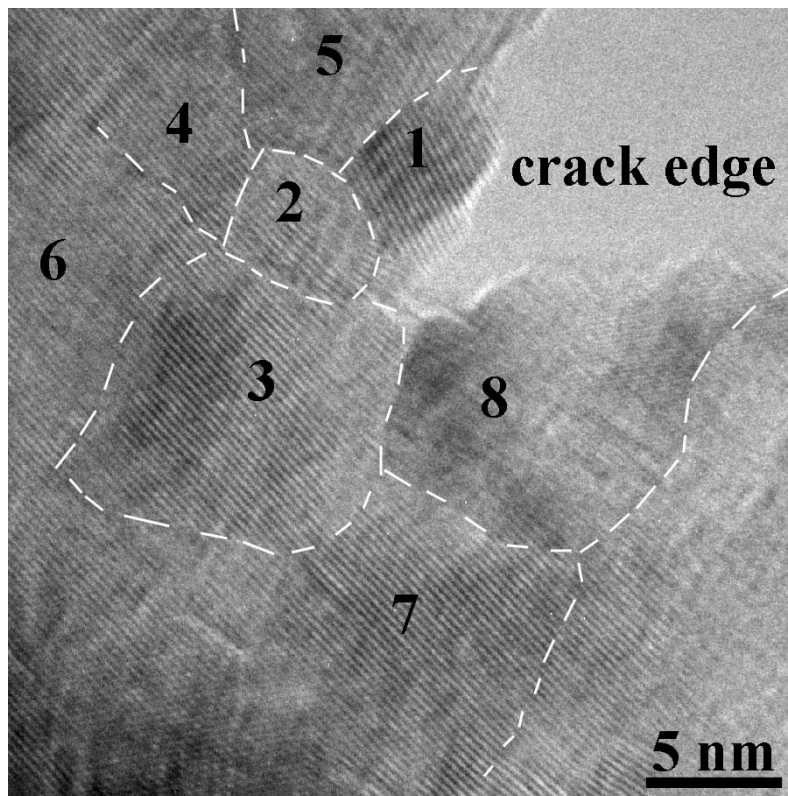


Figure 8-5: Typical HREM image taken from the areas around the propagating crack tip. All the grains identified are divided by low angle grain boundaries and the lattice fringes are belong to {200} type.

In comparison with the as-deposited state (Figure 8.1b), it was surprising to identify more than 8 grains in such a small area and to find that all of the grains appear to be delineated by LAGB. This evidence strongly supports the genesis of LAGB from HAGB during the deformation-induced formation of the larger grain agglomerates. Because of the small diffraction angles for fast electrons used in the TEM, lattice fringe images are produced only for those crystal planes in a nearly edge-on orientation, i.e., those with normals approximately perpendicular to the incident beam direction. After calibrating the magnification, it was found that most of the lattice fringes in the HREM images are consistent with (002) planes of the fcc Ni lattice. This appears unusual since (111) planes are expected to be more readily imaged than (002) planes because of their larger interplanar distance.

Recently, Budrovic et al.⁹² reported that plastic deformation in nanocrystalline nickel with average grain size of about 26nm exhibits reversible peak broadening during tensile straining, which is believed to be caused by a deformation process that fails to produce a network of residual dislocations. However, relative to the undeformed state, they observed a reduction in the (400) full widths at half maximum (FWHM) of the x-ray peaks after the unloading. This additional recovery is seen only in the (200) family of diffraction peaks and not in the (111) family or in the (220) peak. Hence, it appears reasonable to propose that localized (100) textures may develop during the deformation of nanocrystalline Ni, which would be consistent with our observation in Fig. 4 of the unusually high incidence of (002) type planes in an edge-on orientation in the group of nanocrystalline grains constituting an agglomerate. It is notable that improved crystalline alignments of lattice planes appear to be observed by both TEM of thin films (~100 nm) and by x-ray diffraction of thicker electro-deposited films (~200 μm)⁹². This

implies that the deformation processes identified with TEM do yield insights into the behavior of thicker nanocrystalline material as well.

8.4 DISCUSSION

The observations presented above clearly reveal that the grain agglomerates, which formed very rapidly and independently in areas experiencing large plastic deformation prior to the fracture in response to the applied external stress, result from GB-mediated plasticity, such as GB sliding and grain rotation. Following the formation of these grain agglomerates, cracks are observed to propagate in an inter- or intra-agglomerate manner. HREM indicates that these grain agglomerates are very likely comprised of numerous small grains that are separated by LAGB. The mechanistic process envisioned from these observations can be described as follows: The dense network of grain boundaries present in the nanocrystalline material represents a metastable state. This metastable state can be destabilized by an applied external stress. Due to the spatially inhomogeneous distribution of the microstructure, such as grain sizes, grain shapes, grain orientations, grain boundary structure etc., the rearrangement or reorientation of individual grains at certain favored sites can be activated to release the locally accumulated stress resulting from the application of a critical level of external stress, i.e. the critical resolved shear stress may be achieved locally, producing local or micro-yielding in some regions of the nanocrystalline material. This disrupts the former metastable local equilibrium. With or without a short incubation period, which may possibly be facilitated by diffusional processes, individual grains with especially favorable characteristics (size, shape, orientation etc.) rearrange first by GB sliding, grain rotation or even dislocation activities⁹⁰. These grains can then serve as seeds and

eventually trigger an avalanche of interactions in the neighboring grains, followed by further reorientation and/or coalescence. However, the evolution of the grain agglomerates usually spans only a very short time period, as a state of new metastable equilibrium is approached locally.

Our observations of the formation of grain agglomerates, as well as their deformation and fracture characteristics, allow us to speculate on their role in the fracture process. Firstly, the grains that are adjacent to the outer boundaries of the grain agglomerates presumably have a stable structure, i.e. they are not easily deformed. If this were not the case they would likely become incorporated into the agglomerate, favored by an accompanying decrease in the free energy of the system. Rapid diffusion along grain boundaries in nanocrystalline materials^{1,123,124} during the formation of the grain agglomerates will inevitably lead to the transportation of point defects, such as vacancies, to the agglomerate boundaries in order to conserve volume. This renders the boundaries of the agglomerates favorable sites for the nucleation, growth and propagation of voids and cracks. As a consequence, the grain agglomerates, which are much larger than the average grain size, may tend to stay together as a unit during the deformation and fracture process (as shown in Figure 8.2d). If the cracks propagate along the boundaries that surround the agglomerates, the fracture surfaces would be expected to exhibit dimple features on the order of the agglomerate size. The first-order correlation between observed dimple sizes during fracture^{7,84} and the size of the grain agglomerates suggests that this may be the case.

Secondly, the genesis of the LAGB from HAGB inside the grain agglomerates indicates that the smaller grains in some grain agglomerates could share at least some of their available slip systems. This would facilitate dislocation-mediated plasticity within the agglomerates via dislocation transfer across the LAGB's at stress levels that are lower than would be expected for randomly oriented nanocrystalline grains with the same grain size, for instance. Therefore, the

formation of these softer grain agglomerates must inevitably lead to plastic instabilities, causing a catastrophic “brittle-like” failure response due to the excessive localized deformation. Despite the rapid “brittle-like” failure response, the large amounts of associated plastic deformation can be expected to yield a fracture surface characteristic that is more ductile in nature. Thus, the grain agglomerates can lead directly to the formation of the large dimpled features observed on fracture surfaces of nanocrystalline metals.

The foregoing discussion qualitatively explains the underlying mechanism why nanocrystalline materials with their grain size in the regime where grain boundary mediated plasticity are expected exhibit very limited elongation to failure but show dimple structures on the fracture surface. However, what is the mechanism for those materials with their grain size in the regime where dislocation mediated plasticity are dominant? A detailed literature investigation readily to show that almost all of the nanocrystalline materials exhibit limited elongation to failure but with a dimple structure on their fracture surface are prepared by electron deposition^{7,8,20,52,84,118-121}. Besides the intrinsic impurities introduced by this processing method⁷, TEM observations indicated that most of the nanocrystalline grains in these materials are equiaxed and separated by small-angle grain boundaries that consist of dislocations arrays¹²⁵. The impurities in this type of nanocrystalline materials can lead to solid solution strengthening and grain boundary embrittlement. This accounts at least part reason for the very limited elongation to failure. Moreover, the nano grains which are close to each other and divided by dislocation arrays may behave essentially like a larger grain and exhibit ductile characterization in responding to the external applied stress, just similar to the discussion for the grain agglomerates.

Based on the idea that certain kinds of grain boundaries can be resistant to sliding, Hasnaoui et al ⁸⁴ suggested that general HAGB are necessary for good ductility of nanocrystalline materials. However, this is based on the assumption that the structure of the grain boundaries remains stable as the nanocrystalline materials undergo deformation. In real materials, as in our experiments, it is quite likely that the GB structure will change locally at the onset of the deformation by forming numerous grain agglomerates. This instead leads to highly localized plastic deformation of the grain agglomerates and the catastrophic fracture of nanocrystalline materials. Therefore, simply increasing the density of general HAGB may be detrimental to the overall elongation to failure of nanocrystalline materials with a narrow grain size distribution. In order to improve the ductility of nanocrystalline materials and retain high yield stress, other methods such as using multiple scales of grain sizes ¹²⁶ or increasing the density of low energy GB ⁵⁶, may be necessary to produce local strain hardening and spreading of plasticity processes throughout the evolving microstructure of the deforming nanocrystalline metals.

8.5 CONCLUSION

In summary, using in situ tensile straining DFTEM investigations of a free standing nanocrystalline Ni film with a nominal thickness of 150nm, it was found that grain agglomerates formed very frequently and rapidly in many locations, apparently independently of one another under the influence of applied stress at the onset of deformation. Cracks are observed to nucleate and propagate in a combined inter- and intra-agglomerate manner. Post mortem HREM observations show evidence for the genesis of LAGB from HAGB. Guided by the in situ TEM tensile experiments as well as other reported experiments, we propose that the “brittle response”

of nanocrystalline materials during tensile loading results from the formation of grain agglomerations. These observations suggest that simply increasing the number of high-angle grain boundaries in a nanocrystalline metal is unlikely to lead to increased ductility, and that other metallurgical methods (greater control of grain size distribution and increasing the number of low energy GB) may be more fruitful. Understanding the formation mechanisms and role of grain agglomerates in nanocrystalline metals is expected to directly impact the processing methods required to create nanocrystalline metals with improved strength and ductility.

9.0 SUMMARY AND CONCLUSIONS

In summary, the microstructure of the PLD Ni film with its nominal thickness of 60 nm has been characterized by TEM. It was found this high quality Ni sample is essentially fully-dense, artifact-free thin film with its average grain size about 10nm and narrow grain size distribution. The deformation process has been studied by using in situ BF TEM observation under low local strain rates. The observation suggested that grain boundary mediated plasticity, such as grain rotation and grain boundary sliding is very likely to contribute prominently to entire plastic deformation.

In situ dynamic dark field transmission electron microscopy observations of nanocrystalline nickel films with an average grain size of about 10 nanometers confirmed that grain boundary mediated processes have become a prominent deformation mode. Additionally, trapped lattice dislocations are observed in individual grains following deformation. This change in the deformation mode arises from the grain-size dependent competition between the deformation controlled by nucleation and motion of dislocations and the deformation controlled by diffusion assisted grain boundary processes.

The dislocation dynamics processing has been achieved successfully by exploring a combination of in-situ deformation and in-situ HREM observation. The detection of trapped dislocation in grains as small as 5nm by 10 nm suggested that the as-deposited nanocrystalline Ni may exhibit much higher yield strength than expected. The absence of deformation twinning

suggested that twinning may not be a preferred deformation mode even if the nucleation stress for partial is less than that for perfect dislocation. Unlike the molecular simulations which can only capture the very start information of the nanocrystalline materials deformation, the results report here only capture the final state of nanocrystalline materials deformation. Therefore, further efforts are necessary to reveal the entire process of nanocrystalline materials deformation.

Nano-beam electron diffraction has been used to study the behavior of individual grains in nanocrystalline Ni during deformation under low local strain rate conditions. Direct measurement of lattice distortions during straining reveals that grain interiors may experience large elastic distortions during tensile deformation. These results indicate that a peak strength value must exist, with a position and magnitude that depends on both grain size and grain boundary structure. Additionally, the critical size below which dislocation sources cannot operate is determined to be between 3.5 and 10.5 nm for nickel, depending on the type of dislocation.

By employing in situ tensile straining DFTEM investigations of a free standing nanocrystalline Ni film with a nominal thickness of 150nm, it was found that grain agglomerates formed very frequently and rapidly in many locations, apparently independently of one another under the influence of applied stress at the onset of deformation. Cracks are observed to nucleate and propagate in a combined inter- and intra-agglomerate manner. Post mortem HREM observations show evidence for the genesis of LAGB from HAGB. Guided by the in situ TEM tensile experiments as well as other reported experiments, we propose that the “brittle response” of nanocrystalline materials during tensile loading results from the formation of grain agglomerations. These observations suggest that simply increasing the number of high-angle grain boundaries in a nanocrystalline metal is unlikely to lead to increased ductility, and that

other metallurgical methods (greater control of grain size distribution and increasing the number of low energy GB) may be more fruitful. Understanding the formation mechanisms and role of grain agglomerates in nanocrystalline metals is expected to directly impact the processing methods required to create nanocrystalline metals with improved strength and ductility.

10.0 OUTLOOK-QUANTITATIVE INVESTIGATION OF NANOCRYSTALLINE DEFORMATION

10.1 MOTIVATION

The unusual attributes of nanocrystalline materials, such as ultrahigh strength and hardness, low temperature super-plasticity etc. have generate considerable interest in the use of these metallic systems for a wide variety of structural and functional applications. However, despite the extensive efforts over the past decade, reliable properties of nanocrystalline materials are still very limited. This, on the one hand, is due to experimental challenges encountered in processing perfect nanocrystalline materials. For example, i) The microstructure of nanocrystalline materials depends severely on the processing methods; ii) It has been difficult to obtain bulk nanocrystalline materials without processing flaws or contaminations; iii) Only very limited amount of nanocrystalline material can be produced for most processing methods; iv) The standard mechanical testing protocols are often not suitable for measuring the tensile properties of the small nc samples. On the other hand, it is largely due to the lack of understanding of the underlying physical mechanisms that control these mechanical properties of nanocrystalline materials. With the encouraging efforts of pioneer's work, it have been confirmed so far that deformation mechanism of nanocrystalline materials can be divided into three regimes, according to grain size^{2,90}. However, this is largely based on qualitative investigations. For example, i)although it has been confirmed that there exists a cross over regime, between which,

the dominant deformation mode will change from one controlled by the nucleation and motion of dislocation to one controlled by grain boundary mediated plasticity, the exactly grain size boundary of this cross over regime remains unclear; ii) it has been predicted that the diffusion ability of nanocrystalline materials will increase sharply with the decreasing of the grain size, but quantitative experimental data on this are very scarce; iii) based on the assumption that nanocrystalline materials are intrinsic ductile, the limited elongation to failure have been largely attribute to localized deformation which are resulted from the highly non-uniform distributed microstructure of nanocrystalline materials. However, to date, no firm experimental evidence on this has been provided although it is feasible to get such data with a selective technique on a small volume of nanocrystalline materials with uniform microstructure; iv) so far, TEM are the best experimental means for directly revealing the undying physical mechanism that control the solid deformation and it has been argued for a long time that electron irradiation may have import effect on nanocrystalline deformation, but quantitative data, such as how illumination density, time, voltage etc are related to the microstructure of any particular nanocrystalline material during the solid deformation are still very limited.

It is evident from forgoing discussion that very limited quantitative data are available of the physical mechanisms that control the macro properties of nanocrystalline materials, although it is very important for our understanding on this topic. The reason behind this is the limitation of available techniques and the lack of creative experimental design. Therefore, in order to fulfill the specific objective of gaining quantitative data of nanocrystalline deformation, new experimental techniques as well creative idea are necessary.

10.2 EXPERIMENTAL FEASIBILITY

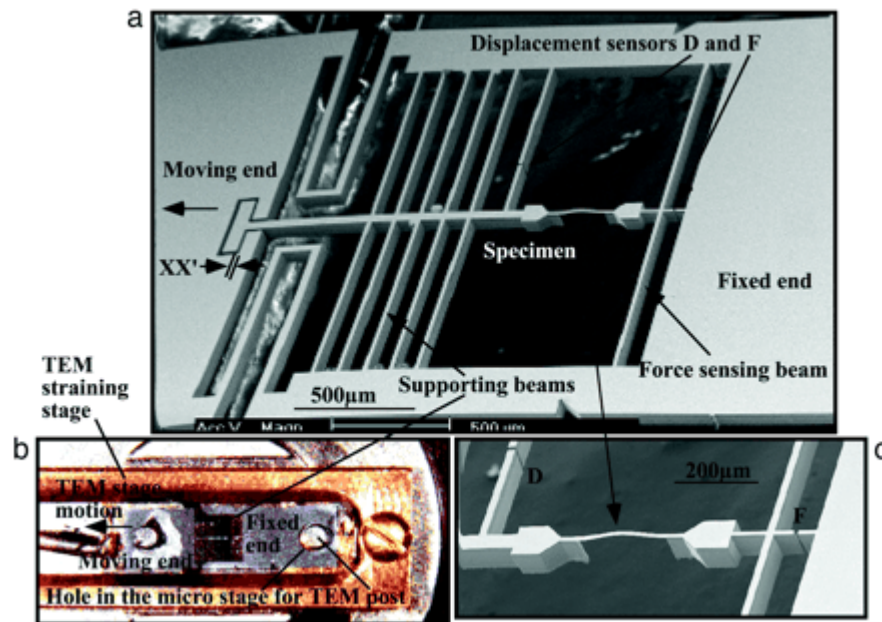


Figure 10-1: (a) Scanning electron micrograph of the microstage showing the freestanding aluminum thin-film specimen being attached to the force sensor beam at one end and to supporting beams at the other. Markers D and F, read displacements at both ends of the specimen. The left end of the microstage is pulled by a piezo actuator of a TEM straining stage. Deflection of the sensor beam (read by marker F), multiplied by its spring constant, gives the force on the specimen. The difference between the two markers' (D and F) gaps gives the elongation of the specimen. The gap XX' prevents accidental straining of the sample during mounting of the microstage on to the TEM straining stage. The TEM straining stage has to move and deform the microstage to close the gap XX' before loading the sample. (b) Microtensile test stage on a TEM straining stage. (c) Zoomed view of the specimen and the two displacement sensors D and F. There is no substrate under the specimen so that the TEM beam can go through the sample for microstructural inspection¹²⁷.

In situ TEM so far has been a major analytical instrument in the research of solid deformation. However, general in situ TEM sample holders usually are not equipped with force displacement sensors. As a result, these holders can only be used as qualitative in situ deforming research

without simultaneous measurement of stress-strain response. In order to perform quantitative analysis, i.e. observing the deformation mechanism during materials testing and measure the stress-strain states in solids at the same time, sample holders that combine quantitative testing of thin films with qualitative TEM observation have to be developed.

Numerous efforts have been made to develop such instruments in the past years¹²⁷⁻¹³¹. Based on a displacement-based uniaxial tensile testing technique, Haque M.A. and Saif M.T.A. developed an in situ TEM (or SEM) tensile instruments in department of mechanical & industrial Engineering, University of Illinois at Urbana-Champaign. Figure 9.1 shows the SEM graph of the instrument. First, a layer of Aluminum was deposited on both sides of the wafers by sputtering. Then a test chip equipped with a force sensor and an actuation mechanism for displacement generation is fabricated through microelectronic technique¹²⁸. Finally, the freestanding specimens are released from the substrate by dry etching with minimal pre-stressing. The specimen is gripped at the two ends by adhesion to the substrate. The novel assembly of a force sensor and structural spring structures ensures perfect alignment of the specimen to the loading direction. So far, quantitative uniaxial tensile tests on nanocrystalline aluminum¹²⁸, gold¹²⁷ have been performed in TEM by recourse to this in situ tensile equipment. Although the present experiments are limited to the complex sample preparation procedure and relative larger grain size (~50nm), potential applications of similar quantitative testing in TEM on nanocrystalline deformation and fracture are very attractive.

Besides in situ TEM tensile instruments, in situ TEM nano-indentation has been also developed. For example, three generations of such devices have been developed at Nation Center of Electron Microscope (NCEM), Lawrence Berkeley National laboratory (LBNL). The first generation (in situ NI-I) was developed mainly by Wall et al.¹³². Their efforts mainly focused on

the development of a stage for the 1.5 MeV high-voltage electron microscope (HVEM) at the NCEM, LBNL. Compared with most of today's electron microscopes, the HVEM has the advantages of its high specimen penetration and large pole gap. As shown in Figure 9.2, the original holder design has a sharp tip mounted onto a long, stiff metal that ran through the shaft of the goniometer. Tip motion along the plane that is perpendicular to the shaft rod (z-plane) was controlled by the screw piezo drives that pushed upon bellows, while the in and out (along the shaft rod direction, z-direction) was accomplished by an ultra-low reduction gear motor drive.

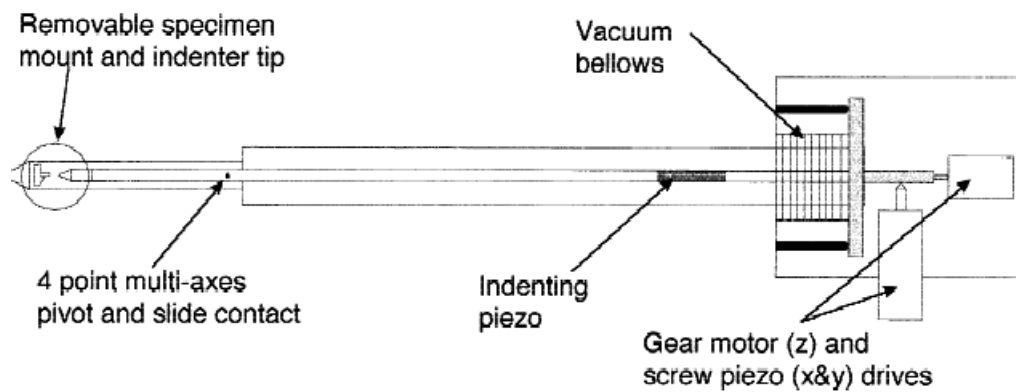


Figure 10-2: Schematic of original in situ nanoindentation holder for the high-voltage electron microscope¹³².

Figure 9.3 presents a schematic of the second generation of in situ nano-indentation (in situ NI-II) holder developed in NCEM, LBNL. In contrast to the in situ NI-I, in which screw drives for coarse Z-plane and a fine gear motor for Z motion were used, the coarse positioning of the indenter tip in NI-II is accomplished with manual screw drives in all three axes. Such a design enables to position the tip mechanically to within about 1 μm of the electron-transparent edge in the z-direction. Another significant improvement in NI-II is to use the piezoceramic tube for the

fine motion of the tip. As a consequence, it is possible to position the tip with about 1nm precision. However, the in situ NI-II is still limited to qualitative analysis.

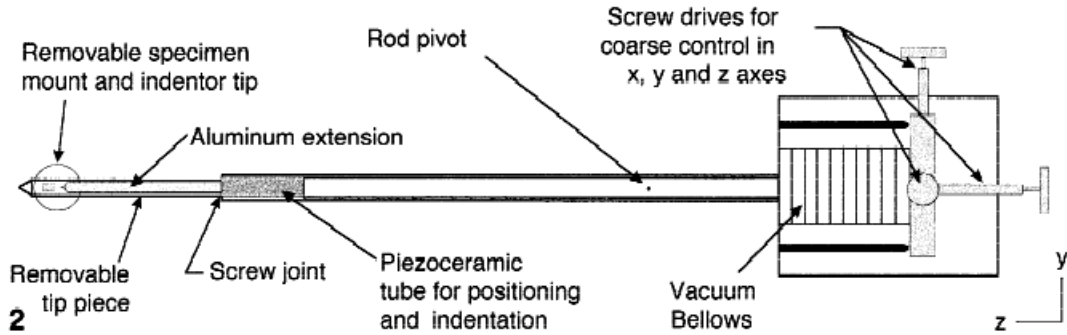


Figure 10-3: Schematic of in situ NI-II holder developed in NCEM, LBNL¹³³.

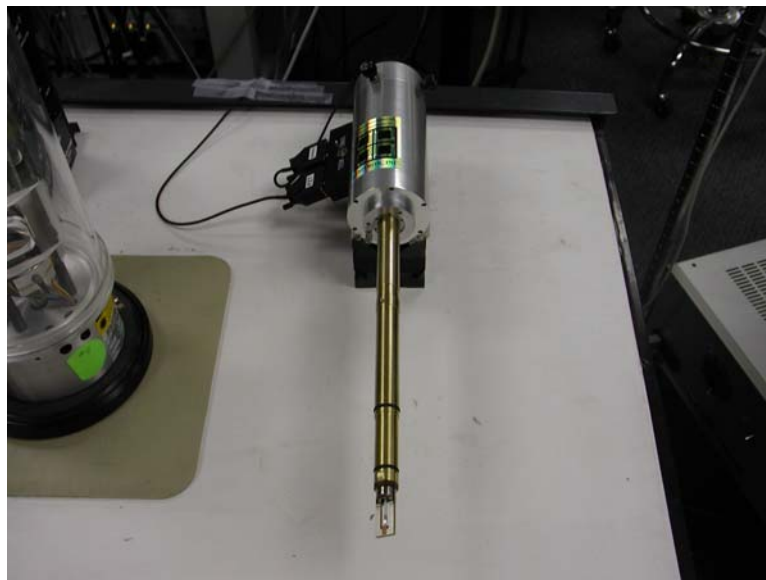


Figure 10-4: New quantitative in situ nanoindentation stage (NI-III), NCEM, LBL.

In order to set up quantitative in situ TEM indentation device, NCEM has tried to find cooperation with Hysitron Inc. which is known to be good at atomic force microscope (AFM). It has been proven that such cooperation is not only necessary but also efficient. The first product resulted from this cooperation has been accomplished recently and is shown in Figure 9.4. This

is the first high accuracy quantitative in situ TEM nano-indentation stage on the world. The load resolution is about 0.2 mN and the displacement resolution is 0.5nm. This new device for the first time provides the possibility of direct correlation of in situ TEM indentation observations with standard load-displacement curves. Figure 9.5 represents some results from the initial test of this novel device. Analysis shows this novel device is even better than some its initial design parameters. It is expected that deformation and fracture study on solid will benefit from those newly developed quantitative devices.

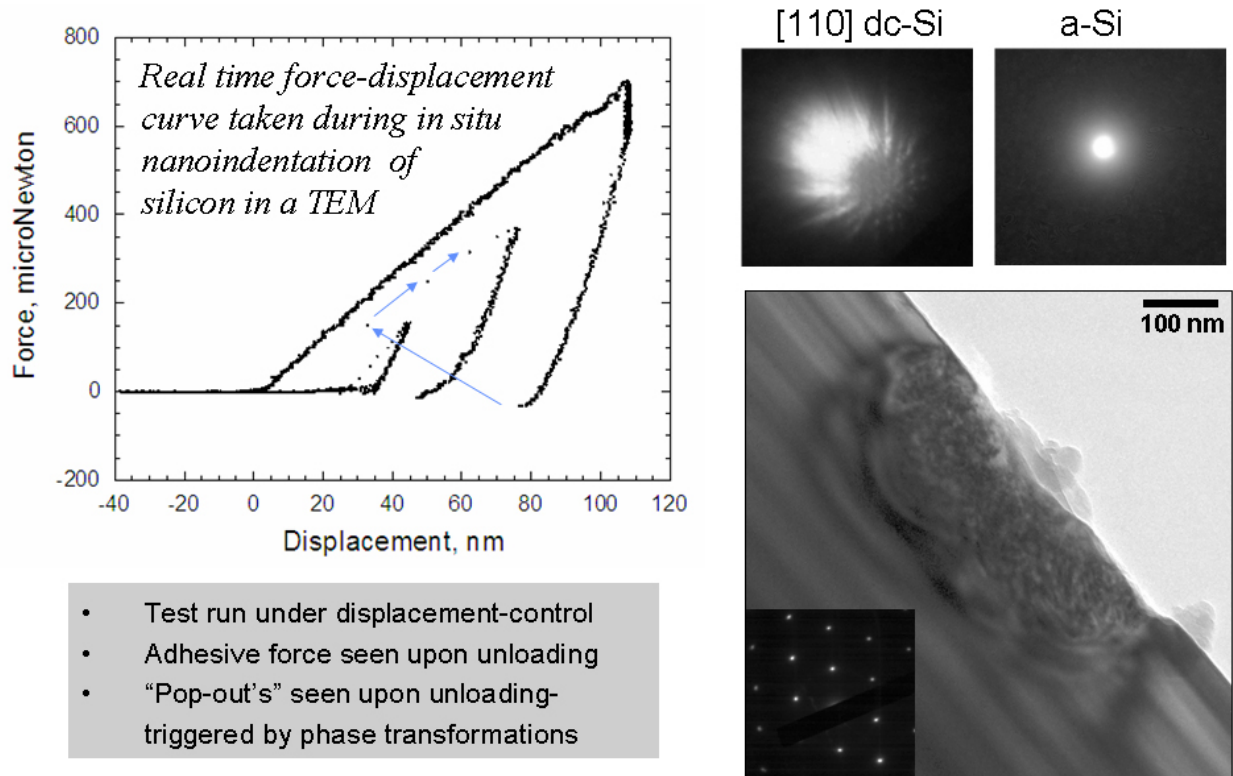


Figure 10-5: Preliminary results of the NI-III quantitative device (This figure was provided by Dr. Minor in NCEM, LBL).

APPENDIX A

COMMENT ON "GRAIN BOUNDARY-MEDIATED PLASTICITY IN NANOCRYSTALLINE NICKEL"

Nanograin rotation via grain boundary sliding has been predicted as an important deformation mode in nanocrystalline materials as grain sizes approach less than 10 nm^{5,103,134}. However, definite experimental evidence beyond molecular dynamics (MD) simulations has been long sought. Recently, Shan *et al.*⁹⁰ reported in situ straining dark-field transmission electron microscope (DFTEM) observations of grain rotation in nanocrystalline Ni and claimed that the plastic deformation of nano-Ni is mediated by this grain boundary behavior. Although the experimental results reported by Shan *et al.* are interesting, their assessment and analysis of the TEM images are problematic. Using the images presented in⁹⁰, we have quantitatively measured the relative displacements and grain sizes. Both results suggest that the grain rotation and associated contrast change reported by Shan *et al.* more likely come from low-temperature nanograin growth, caused by electron-beam irradiation and applied stresses, than from plastic deformation.

In Figure A.1, we show contrast-inverted images from figure 3 in⁹⁰. Small grains with less contrast change are linked with lines to form a trapezoidal frame surrounding grain G, which

exhibited significant contrast change during loading. Overlaying the trapezoidal frame in Figure- ap.1 B and F, shows that all the joint points of the frame match well with the original small grains.

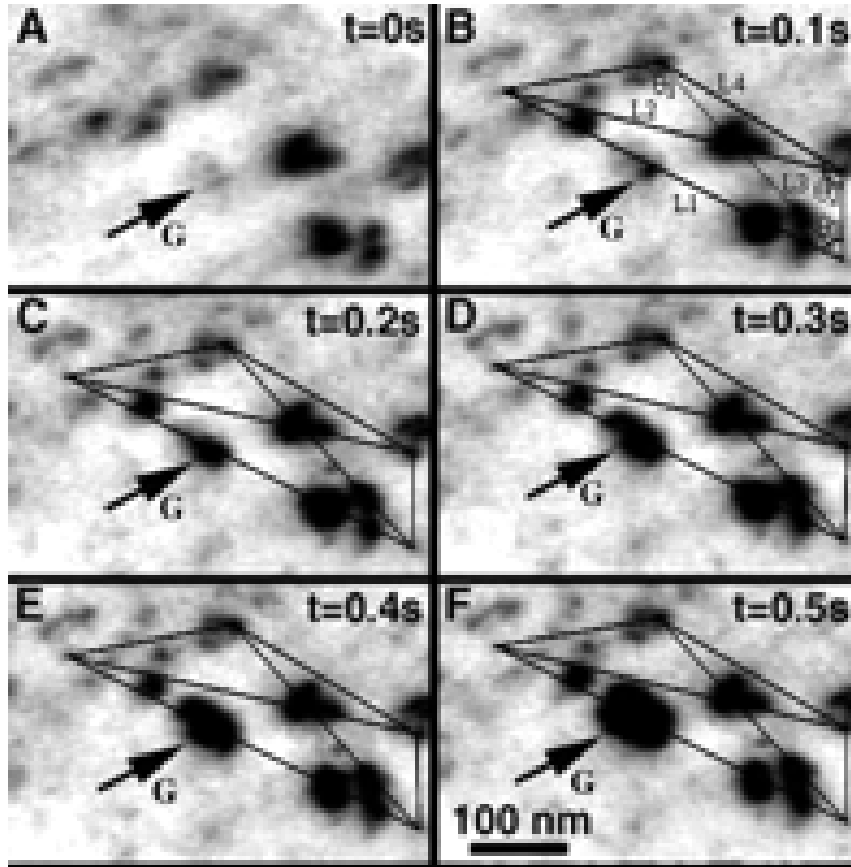


Figure A. 1 Contrast-inverted images of figure 3 in ⁹⁰. The small grains with less contrast change during loading were linked to form a trapezoidal frame.

Precise measurements of the line lengths were performed using NIH Image, and the dependence of the line lengths on loading time was plotted (Figure A.2). The mean error of these measurements is about ± 1 nm and the corresponding strain smaller than 0.5%. The measurements do not suggest any systematic length changes and, thus, any relative displacements and strains.

To rule out the possible bending and torsion deformation, which might not significantly alter the line lengths, we measured the angles marked in Figure A.1 B. We were also unable to

observe any systematic angle changes with time. These measurements unambiguously show that no detectable deformation occurred during loading. If the significant contrast change of grain G were caused by plastic deformation, relative displacements, either in plane or out of plane, should have been observed among the surrounding grains, because plastic deformation cannot be accomplished solely by a single grain rotation.

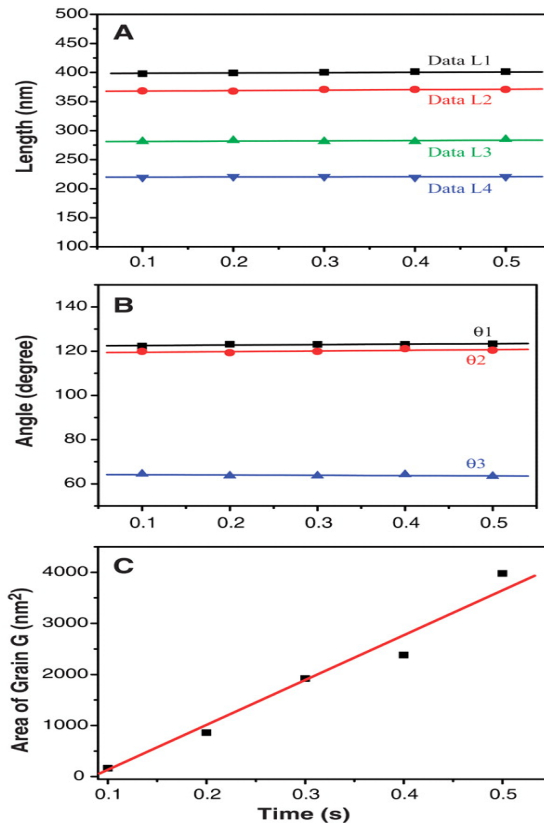


Figure A. 2: Measurements of line lengths, angles, and grain areas using NIH Image. (A) The distance changes between the smaller grains around the marked grain G as a function of loading time (see Figure A.1 B). The slope of each line approaches zero, which suggests that no systematic deformation occurs accompanying the continuous contrast changes of grain G. (B) The relation between the angles (see Figure A.1 B) and loading time. (C) Changes in the area of grain G as a function of time. The linear relation between S and t is consistent with the classical grain growth equation

As several attempts have well demonstrated^{7,10,21}, it is extremely difficult to get uniform plastic deformation in nanocrystalline samples and localized deformation and cracking cannot be

avoided during in situ straining TEM observations. Although the data in Figure A.1 were recorded during in situ tensile tests, it is quite possible that the region observed by Shan *et al.* did not experience visible plastic deformation and that the observed contrast change came mainly from nanograin growth caused by electron-beam irradiation and applied stresses. The time-related size change of grain G, measured using the NIH Image, revealed a linear relation between grain size in the area (S) and time (t) (Figure A.2 C) that is exactly consistent with the classical grain growth equation¹³⁵, $S - S_0 = kt$, where S_0 is the initial grain size and k is a constant.

The diffraction patterns shown in figure 2, B and D, in⁹⁰ also indicate nanograin growth during DFTEM observations. Slightly adjusting the brightness of figure 2D in⁹⁰ to be close to that of figure 2B in⁹⁰ reveals continuous rings with an increasing number of bright spots that correspond to coarsened grains; this, in turn, suggests that the change of diffraction patterns results from the grain growth, rather than the thickness decrease claimed by Shan *et al.*⁹⁰. Additionally, the contrast in the DFTEM [figure 2E in⁹⁰] cannot be solely attributed to the grain boundaries. Crystal defects—for example, dislocations, as revealed by their high-resolution electron microscope image [figure 4C in⁹⁰])—can provide the similar contrast caused by their elastic strain fields⁹⁰. After contrast inversion of figure 2E in⁹⁰, the dark contrast that Shan *et al.* suggested represented grain boundaries shows discontinuous features that are characteristic of dislocations in bright-field TEM. It is not surprising to see dislocations in the nanograin because the grain size, at around 50 nm in diameter, is large enough to contain a number of perfect dislocations. Actually, the appearance of the edge dislocations as observed by Shan *et al.* is also consistent with the rotation growth theory, as suggested by recent MD simulations^{48,136} and the classical rotation growth model¹³⁷.

In summary, the TEM results reported in ⁹⁰ can be interpreted as nanograin growth caused by electron-beam irradiation and applied stresses. Although nanograin growth may not be the whole story, and although a small amount of deformation through grain boundary mediation may occur accompanying the observed grain rotation, the grain contrast change reported by Shan *et al.* appears to result mainly from nanograin coalescence and growth rather than visible plastic deformation.

Mingwei Chen*

Institute for Materials Research
Tohoku University
2-1-1 Katahira, Aoba-ku,
Sendai 980-8577, Japan

Xiaoqin Yan

Institute for Materials Research
Tohoku University
2-1-1 Katahira, Aoba-ku,
Sendai 980-8577, Japan

* *E-mail:* mwchen@imr.tohoku.ac.jp

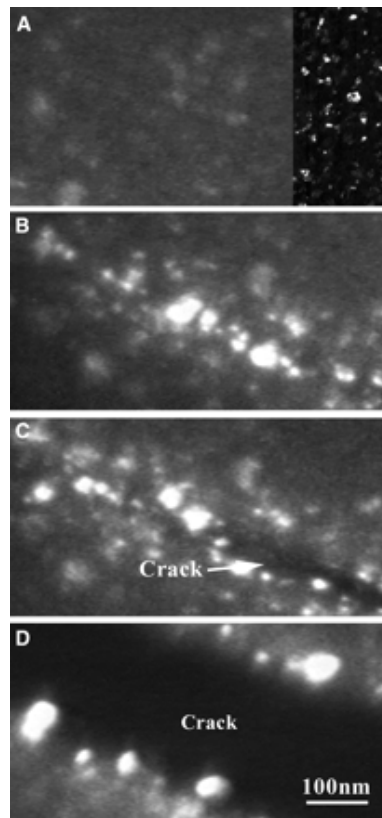
APPENDIX B

RESPONSE TO COMMENT ON "GRAIN BOUNDARY-MEDIATED PLASTICITY IN NANOCRYSTALLINE NICKEL"

Our study⁹⁰ reported on the deformation response of nanocrystalline Ni during in situ dark-field transmission electron microscopy (DFTEM) straining experiments and showed what we view as direct and compelling evidence of grain boundary-mediated plasticity. Based on their analysis of the limited experimental data we presented, however, Chen and Yan¹²² propose that the reported contrast changes more likely resulted from grain growth caused by electron irradiation and applied stress rather than from plastic deformation. Here, we give specific reasons why their assertions are incorrect and discuss how the measurement approaches they have used are inappropriate. Additionally, we present further evidence that supports our original conclusions.

The method Chen and Yan employed to measure displacement merely probes the in-plane (two-dimensional) components of incremental strain occurring during the very short time interval shown [figure 3 in⁹⁰] instead of the accumulated strain. As we noted explicitly in the supporting online material in⁹⁰, the loading was applied by pulsing the displacement manually. After each small displacement pulse, the monitored area always moved significantly within or even out of the field of view. Clear images could be obtained only when the sample position stabilized within the field of view and at that time severe deformation was nearly complete. Thus, little incremental strain occurs during this short image sequence [figure 3 in⁹⁰], as one might expect.

We believe that the images shown in figure 3 of ⁹⁰ are particularly valuable in understanding deformation in nanocrystalline materials. In general, the formation process of grain agglomerates simply occurred too fast to be recorded clearly. Moreover, instead of remaining constant after formation, the sizes of the grain agglomerates changed in a rather irregular manner in responding to the deformation and fracture process (see, for example, Figure A. 3 B and D). This indicates that strong grain boundary-related activity occurred inside the grain agglomerates. Figure 3 in ⁹⁰, a short (0.5 s) extract from more than 6 hours of videotaped



experimentation (imaged ahead of cracks), not only reveals the formation process of a grain agglomerate, but also shows conclusive evidence for grain rotation and excludes the effect of overall sample rotation.

Figure A. 3: Dark-field TEM images showing deformation and fracture of nanocrystalline Ni in response to an applied tensile displacement pulse. Note the growth of larger grain agglomerates along the propagating crack path. Inset in (A) is an image from an undeformed area that has been pre-thinned with low-temperature ion thinning to show more clearly the presence of small grains as well as the narrow grain size distribution.

It should be noted that other small grains still exhibit some minor contrast changes in figure 3 in ⁹⁰. Hence, using them as reference points yields measurements that may not be accurate to ± 1 nm [as Chen and Yan ¹²² claim in their analysis] and limits the accuracy of their conclusions. Chen and Yan also claim that no deformation has occurred, yet simultaneously state that the analysis has a deformation measurement error of 0.5%. This is simply not consistent; even small strains of this order may cause plastic deformation.

In contrast with previous in situ TEM experiments ^{7,10,21}, the special sample design adopted in our investigation ⁹⁰ ensured that all deformation was primarily concentrated in a band like area ahead of the propagating crack. We found that these grain agglomerates were observed only in this band like thinning area as a response to the applied loads (Figure 03 B). No similar phenomena were detected under the electron beam alone or in stressed areas apart from the main deformation area, and these phenomena have not been reported during in situ observations of this same material made by other researchers ²¹. Subsequent cracks were always observed to follow this deformation area upon further displacement pulses (Figure 0.3 C and D). This clearly indicates that the enlarged agglomerates do not result simply from electron irradiation plus stress, but rather from stress-induced deformation.

In their comment, Chen and Yan claimed a linear relation between "grain" area and time based on their measurements made from figure 3 in ⁹⁰ and claimed that these measurements are exactly consistent with the classical grain growth equation. However, as we noted ⁹⁰, the growth

in size of this agglomerate is not isotropic and occurs in an irregular manner. For example, after bright contrast emerged from a grain about 6 nm in diameter, it remained well defined in size as a single, approximately equiaxed grain until $t = 0.1$ s (figure 0.4).

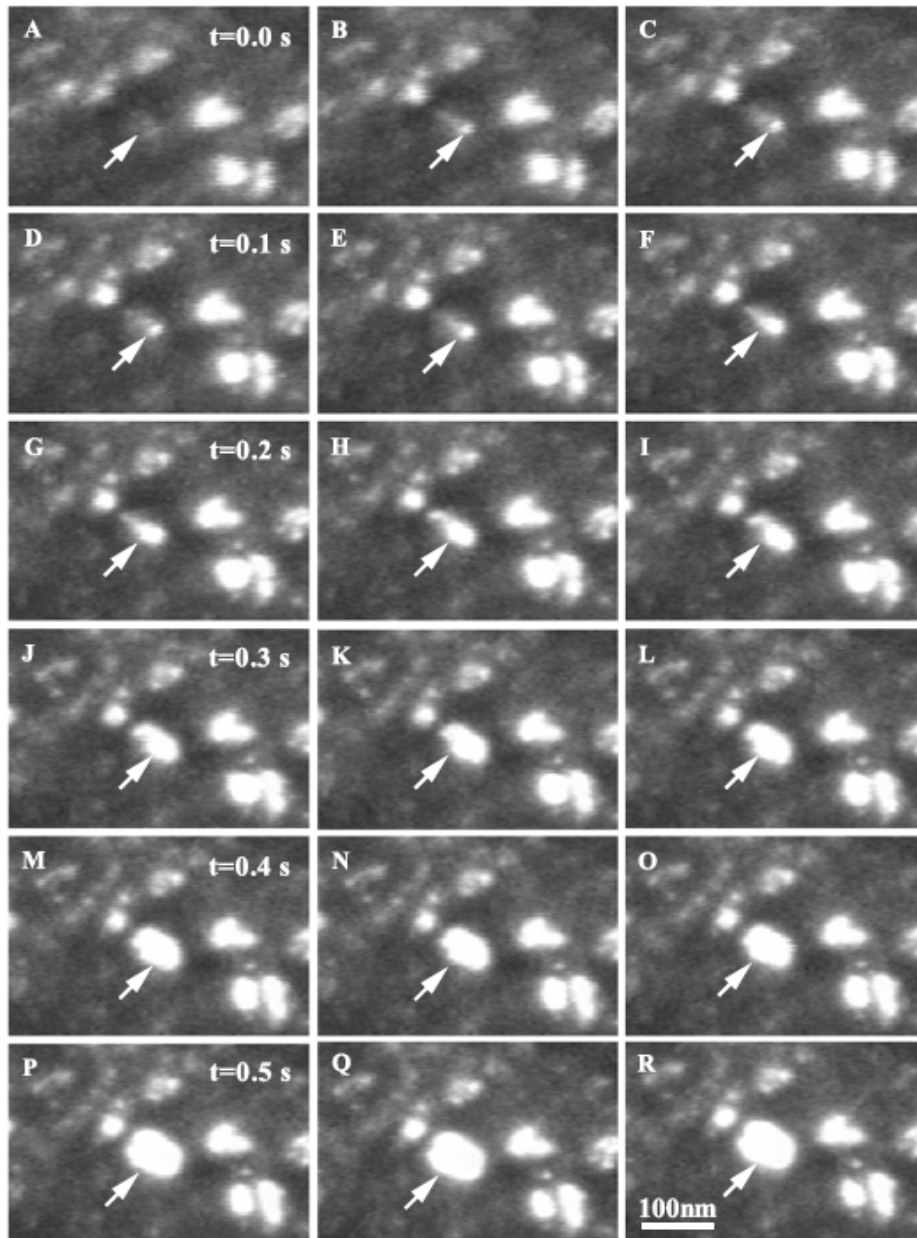


Figure A. 4: Expanded Sequence of dark-field TEM images collected in situ, providing additional detail to evaluate the process of grain grains group of nanocrystalline Ni in response to one displacement pulse. The times listed are based on the videotape record speed (30 frames per second).

We have reproduced the "grain growth" plot of Chen and Yan (Figure A.5) using our entire video image sequence (fig. S1). Clearly, the growth in area of the agglomerate is not consistent with linear grain growth. (Unfortunately, only a portion of these data could be included in the original paper for reasons of space.) Notably, Chen and Yan did not apply a similar "grain growth" analysis to nearby grains; this would have yielded no information in support of their argument, as those grains show essentially no growth.

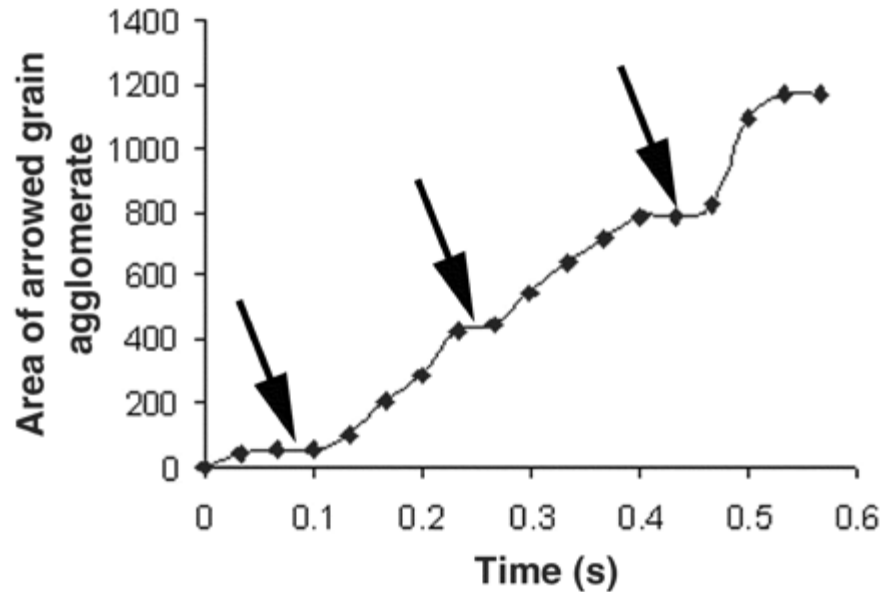


Figure A. 5: Changes in the area of the grain agglomerate as a function of time. Clearly, the growth in area of the agglomerate is not consistent with linear grain growth. Note the "terraces" indicated by black arrows, which suggest an "incubation" time between grain rotations.

In addition, if classical grain growth were occurring during our observations—even though it is not expected at ambient temperature in nanocrystalline nickel^{138,139}—the initial displacement pulse might have added mechanical driving force to overcome an apparent activation barrier that exists for the thermally activated process of grain growth. This additional

mechanical contribution would diminish over time. However, once the appropriate larger grains would have grown to about 6 to 10 times the size of the average grain (see, for example, the large grains in figs. S1 and S2), their growth would be expected to continue at the expense of the smaller grains in their vicinity, because the curvature-derived driving force would be greater, more strongly favoring their continued growth and the reduction of the free energy of the material. However, this was not the case [see, for example, figure 8.3, which was extracted immediately after the sequence shown in figure 3 in ⁹⁰. Without any further displacement pulses, the key grain agglomerate stopped growing and then appeared to split with time. Further loading leads to crack propagation in the band-like deformation area in an inter- or intra-agglomerate manner. Again using the nearby features as references, this subsequent splitting is further conclusive evidence of grain boundary-mediated plasticity and argues against classical grain growth.

The image shown as figure 2E in ⁹⁰ allowed us to state that grain agglomerates, instead of individual large grains, resulted from the applied displacement pulse. To directly compare the undeformed and deformed states, the two diffraction patterns that appeared in our paper [figure 2, B and D, in ⁹⁰ were taken under identical conditions—that is, using the same illumination intensity, the same selected-area aperture size, and the same exposure time. Simply boosting the contrast, as Chen and Yan have done, fundamentally alters the information in these patterns and thus yields an inaccurate conclusion. Presumably they have mistakenly chosen to alter the images out of concern over whether we had taken them in an equivalent manner; unfortunately, their alteration of contrast removes the difference in background intensity, which demonstrates that the material has also thinned and thus has been plastically deformed.

When considering how DFTEM images are formed, it is clear that the smaller grains in the agglomerates exhibit essentially edge-on orientations of their $\{111\}$ lattice planes, their $\{200\}$ lattice planes, or both ⁹⁰. From a thermodynamic view, it is very possible that these grains are divided by small-angle grain boundaries (which would consist of dislocation arrays) or even that some coalescence occurred ¹⁴⁰. However, considering that grain agglomerates, after being formed, change their sizes in a rather irregular way in response to the deformation (for example, Figure A.3 B to D), classical grain rotation-induced grain growth, if it exists, is not likely to be prominent.

The contrast-inverting method used by Chen and Yan ¹²² on figure 2E in ⁹⁰ is poorly chosen. A bright-field image is formed by selecting the direct beam in the selected-area diffraction pattern, which will include contrast information from all diffracting lattice planes. Alternatively, a dark-field image of the type we have used is formed by selecting a small part of the diffraction rings (for polycrystalline materials) using the objective lens aperture. The dark-field image only includes the contrast information from those grains that are oriented such that they contribute to the specific diffraction vectors (direction and length) contained in the small region of the diffracting rings that is selected by the objective lens aperture. Therefore, to obtain bright-field contrast by inverting the dark-field contrast is simply incorrect; bright-field and dark-field TEM images give strictly inverse intensity only when considering a two-beam diffraction condition in the kinematics electron diffraction limit ¹⁴¹. Moreover, diffraction-contrast TEM images display true grain sizes only when the diffraction condition, exposure time, and image intensities are selected correctly. Manipulation of TEM images by software is easy but is fraught with scientific peril and should be done only with great care.

In sum, it is unfortunate that only part of the video frames from our experiments could be included in ⁹⁰, as this omission led to the incorrect deduction by Chen and Yan ¹²² of a false linear grain growth by subsequent measurements. However, the remaining supporting evidence that they present stems largely from inappropriate image contrast adjustments and a misreading of our original paper.

Zhiwei Shan

Department of Mechanical Engineering
University of Pittsburgh
Pittsburgh, PA 15261, USA

E. A. Stach

School of Materials Engineering
Purdue University
West Lafayette, IN 47907

J. M. K. Wiezorek

Department of Materials Science and Engineering
University of Pittsburgh
Pittsburgh, PA 15261, USA

J. A. Knapp

Sandia National Laboratories
Albuquerque, NM 87185-1056, USA

D. M. Follstaedt

Sandia National Laboratories
Albuquerque, NM 87185-1056, USA

S. X. Mao*

Department of Mechanical Engineering
University of Pittsburgh
Pittsburgh, PA 15261, USA

BIBLIOGRAPHY

1. Masumura, R. A., Hazzledine, P. M. & Pande, C. S. Yield stress of fine grained materials. *Acta Materialia* **46**, 4527-4534 (1998).
2. Yip, S. Nanocrystals - The strongest size. *Nature* **391**, 532-533 (1998).
3. Nieh, T. G. & Wadsworth, J. Hall-Petch relation in nanocrystalline solids. *Scripta Metallurgica et Materialia* **25**, 955 (1991).
4. Legros, M., Elliott, B. R., Rittner, M. N., Weertman, J. R. & Hemker, K. J. Microsample tensile testing of nanocrystalline metals. *Philosophical Magazine a-Physics of Condensed Matter Structure Defects and Mechanical Properties* **80**, 1017-1026 (2000).
5. Schiotz, J., Di Tolla, F. D. & Jacobsen, K. W. Softening of nanocrystalline metals at very small grain sizes. *Nature* **391**, 561-563 (1998).
6. Yamakov, V., Wolf, D., Phillpot, S. R., Mukherjee, A. K. & Gleiter, H. Deformation mechanism crossover and mechanical behaviour in nanocrystalline materials. *Philosophical Magazine Letters* **83**, 385-393 (2003).
7. Kumar, K. S., Suresh, S., Chisholm, M. F., Horton, J. A. & Wang, P. Deformation of electrodeposited nanocrystalline nickel. *Acta Materialia* **51**, 387-405 (2003).
8. Kumar, K. S., Van Swygenhoven, H. & Suresh, S. Mechanical behavior of nanocrystalline metals and alloys. *Acta Materialia* **51**, 5743-5774 (2003).
9. Hugo R. C., K., H., Weertman J. R., Mitra R., Knapp J. A., Follstaedt D. M. In-situ TEM tensile testing of DC magnetron sputtered and pulsed laser deposited Ni thin films. *Acta Mater*, **51**, 1937-1943 (2003).
10. Youngdahl, C. J., Weertman, J. R., Hugo, R. C. & Kung, H. H. Deformation behavior in nanocrystalline copper. *Scripta Mater* **44**, 1475-1478 (2001).
11. Gleiter H. *Prog Mater Sci* **33**, 223 (1989).

12. Koch, C. C., Morris, D. G., Lu, K. & Inoue, A. Ductility of nanostructured materials. *Mrs Bulletin* **24**, 54-58 (1999).
13. Suryanarayana, C. Nanocrystalline Materials. *International Materials Reviews* **40**, 41-64 (1995).
14. Wang, Y. M., Chen, M. W., Zhou, F. H. & Ma, E. High tensile ductility in a nanostructured metal. *Nature* **419**, 912-915 (2002).
15. Farhat, Z. N., Ding, Y., Northwood, D. O. & Alpas, A. T. Effect of grain size on friction and wear of nanocrystalline aluminum. *Materials Science and Engineering a-Structural Materials Properties Microstructure and Processing* **206**, 302-313 (1996).
16. Jeong, D. H., Gonzalez, F., Palumbo, G., Aust, K. T. & Erb, U. The effect of grain size on the wear properties of electrodeposited nanocrystalline nickel coatings. *Scripta Materialia* **44**, 493-499 (2001).
17. McFadden, S. X., Mishra, R. S., Valiev, R. Z., Zhilyaev, A. P. & Mukherjee, A. K. Low-temperature superplasticity in nanostructured nickel and metal alloys. *Nature* **398**, 684-686 (1999).
18. Lu, L., Sui, M. L. & Lu, K. Superplastic extensibility of nanocrystalline copper at room temperature. *Science* **287**, 1463-1466 (2000).
19. Lu, L., Li, S. X. & Lu, K. An abnormal strain rate effect on tensile behavior in nanocrystalline copper. *Scripta Materialia* **45**, 1163-1169 (2001).
20. Dalla Torre, F., Van Swygenhoven, H. & Victoria, M. Nanocrystalline electrodeposited Ni: microstructure and tensile properties. *Acta Materialia* **50**, 3957-3970 (2002).
21. Hugo, R. C. et al. In-situ TEM tensile testing of DC magnetron sputtered and pulsed laser deposited Ni thin films. *Acta Materialia* **51**, 1937-1943 (2003).
22. Knapp, J. A. & Follstaedt, D. M. Hall-Petch relationship in pulsed-laser deposited nickel films. *Journal of Materials Research* **19**, 218-227 (2004).
23. Fougere, G. E., Weertman, J. R. & Siegel, R. W. Processing and Mechanical-Behavior of Nanocrystalline Fe. *Nanostructured Materials* **5**, 127-134 (1995).
24. Huang, J. Y. & Zhu, Y. T. Atomic-scale structural investigations on the nucleation of cubic boron nitride from amorphous boron nitride under high pressures and temperatures. *Chemistry of Materials* **14**, 1873-1878 (2002).
25. Elsharik, A. M. & Erb, U. Synthesis of Bulk Nanocrystalline Nickel by Pulsed Electrodeposition. *Journal of Materials Science* **30**, 5743-5749 (1995).
26. Lu, L., Sui, M. L. & Lu, K. Cold rolling of bulk nanocrystalline copper. *Acta Materialia* **49**, 4127-4134 (2001).

27. Lu, K., Zhang, H. Y., Zhong, Y. & Fecht, H. J. Grain size dependence of mechanical properties in nanocrystalline selenium. *Journal of Materials Research* **12**, 923-930 (1997).
28. Lu, K. Nanocrystalline metals crystallized from amorphous solids: Nanocrystallization, structure, and properties. *Materials Science & Engineering R-Reports* **16**, 161-221 (1996).
29. Lu, K., Luck, R. & Predel, B. Thermodynamics of the Transition from the Amorphous to the Nanocrystalline State. *Journal of Non-Crystalline Solids* **156**, 589-593 (1993).
30. Youssef, K. M., Scattergood, R. O., Murty, K. L. & Koch, C. C. Ultratough nanocrystalline copper with a narrow grain size distribution. *Applied Physics Letters* **85**, 929-931 (2004).
31. Wei, Q., Jiao, T., Ramesh, K. T. & Ma, E. Nano-structured vanadium: processing and mechanical properties under quasi-static and dynamic compression. *Scripta Materialia* **50**, 359-364 (2004).
32. Tao, N. R., Sui, M. L., Lu, J. & Lu, K. Surface nanocrystallization of iron induced by ultrasonic shot peening. *Nanostructured Materials* **11**, 433-440 (1999).
33. Li, D., Chen, H. N., Liu, G. & Lu, K. Homogenization of microstructure and hardness of surface layer of SS400 steel welded joint. *Acta Metallurgica Sinica* **37**, 980-984 (2001).
34. Wu, X. et al. Microstructure and evolution of mechanically-induced ultrafine grain in surface layer of AL-alloy subjected to USSP. *Acta Materialia* **50**, 2075-2084 (2002).
35. Liu, G., Lu, J. & Lu, K. Surface nanocrystallization of 316L stainless steel induced by ultrasonic shot peening. *Materials Science and Engineering a-Structural Materials Properties Microstructure and Processing* **286**, 91-95 (2000).
36. Wang, Y. M., Ma, E., Valiev, R. Z. & Zhu, Y. T. Tough nanostructured metals at cryogenic temperatures. *Advanced Materials* **16**, 328-+ (2004).
37. Zhu, Y. T. et al. Nanostructures in Ti processed by severe plastic deformation. *Journal of Materials Research* **18**, 1908-1917 (2003).
38. Valiev, R. Z. & Islamgaliev, R. K. Enhanced superplasticity of ultrafine-grained alloys processed by severe plastic deformation. *Towards Innovation in Superplasticity Ii* **304-3**, 39-46 (1999).
39. Liao, X. Z., Zhao, Y. H., Zhu, Y. T., Valiev, R. Z. & Gunderov, D. V. Grain-size effect on the deformation mechanisms of nanostructured copper processed by high-pressure torsion. *Journal of Applied Physics* **96**, 636-640 (2004).
40. Sergueeva, A. V., Song, C., Valiev, R. Z. & Mukherjee, A. K. Structure and properties of amorphous and nanocrystalline NiTi prepared by severe plastic deformation and

- annealing. *Materials Science and Engineering a-Structural Materials Properties Microstructure and Processing* **339**, 159-165 (2003).
41. Elsharik, A. M., Erb, U., Palumbo, G. & Aust, K. T. Deviations from Hall-Petch Behavior in as-Prepared Nanocrystalline Nickel. *Scripta Metallurgica Et Materialia* **27**, 1185-1188 (1992).
 42. Gertsman, V. Y., Hoffmann, M., Gleiter, H. & Birringer, R. The Study of Grain-Size Dependence of Yield Stress of Copper for a Wide Grain-Size Range. *Acta Metallurgica Et Materialia* **42**, 3539-3544 (1994).
 43. Wang, N., Wang, Z. R., Aust, K. T. & Erb, U. Effect of Grain-Size on Mechanical-Properties of Nanocrystalline Materials. *Acta Metallurgica Et Materialia* **43**, 519-528 (1995).
 44. Bata, V. & Pereloma, E. V. An alternative physical explanation of the Hall-Petch relation. *Acta Materialia* **52**, 657-665 (2004).
 45. Schiotz, J., Vegge, T., Di Tolla, F. D. & Jacobsen, K. W. Atomic-scale simulations of the mechanical deformation of nanocrystalline metals. *Physical Review B* **60**, 11971-11983 (1999).
 46. Van Swygenhoven, H. Plastic deformation in metals with nanosized grains: Atomistic simulations and experiments. *Superplasticity in Advanced Materials* **447-4**, 3-10 (2003).
 47. Yamakov, V., Wolf, D., Phillpot, S. R. & Gleiter, H. Grain-boundary diffusion creep in nanocrystalline palladium by molecular-dynamics simulation. *Acta Materialia* **50**, 61-73 (2002).
 48. Haslam, A. J., Moldovan, D., Phillpot, S. R., Wolf, D. & Gleiter, H. Combined atomistic and mesoscale simulation of grain growth in nanocrystalline thin films. *Computational Materials Science* **23**, 15-32 (2002).
 49. Wilde, G., Dinda, G. P. & Rosner, H. Synthesis of bulk nanocrystalline materials by repeated cold rolling. *Advanced Engineering Materials* **7**, 11-15 (2005).
 50. Erb, U., Palumbo, G., Szpunar, B. & Aust, K. T. Electrodeposited vs. consolidated nanocrystals: Differences and similarities. *Nanostructured Materials* **9**, 261-270 (1997).
 51. Erb, U. Electrodeposited nanocrystals: Synthesis, properties and industrial applications. *Nanostructured Materials* **6**, 533-538 (1995).
 52. Ebrahimi, F., Zhai, Q. & Kong, D. Deformation and fracture of electrodeposited copper. *Scripta Materialia* **39**, 315-321 (1998).
 53. Nieh, T. G. & Wang, J. G. Hall-Petch relationship in nanocrystalline Ni and Be-B alloys. *Intermetallics* **13**, 377-385 (2005).

54. Hibbard, G., Aust, K. T., Palumbo, G. & Erb, U. Thermal stability of electrodeposited nanocrystalline cobalt. *Scripta Materialia* **44**, 513-518 (2001).
55. Karimpoor, A. A., Erb, U., Aust, K. T. & Palumbo, G. High strength nanocrystalline cobalt with high tensile ductility. *Scripta Materialia* **49**, 651-656 (2003).
56. Lu, L., Shen, Y. F., Chen, X. H., Qian, L. H. & Lu, K. Ultrahigh strength and high electrical conductivity in copper. *Science* **304**, 422-426 (2004).
57. Segal VM. *Mater Sci Eng A* **197**, 157 (1995).
58. Valiev, R. Z., Islamgaliev, R. K. & Alexandrov, I. V. Bulk nanostructured materials from severe plastic deformation. *Progress in Materials Science* **45**, 103-189 (2000).
59. Yong, X. P., Liu, G., Lu, J. & Lu, K. Fabrication and characterization of nanostructured surface layer of low carbon steel. *Acta Metallurgica Sinica* **38**, 157-160 (2002).
60. Tao, N. R. et al. An investigation of surface nanocrystallization mechanism in Fe induced by surface mechanical attrition treatment. *Acta Materialia* **50**, 4603-4616 (2002).
61. Wang, Y. M. et al. Microsample tensile testing of nanocrystalline copper. *Scripta Materialia* **48**, 1581-1586 (2003).
62. Lu, K. & Lu, J. Surface nanocrystallization (SNC) of metallic materials-presentation of the concept behind a new approach. *Journal of Materials Science & Technology* **15**, 193-197 (1999).
63. Hall E. O. . *Proc. R. Soc. (Lond.) B* **64**, 9474 (1951).
64. Petch N.J. *J. Iron Steel Inst.* **174**, 25 (1953).
65. Conrad H. *Acta Met* **11**, 75 (1963).
66. Chou, T. C., Nieh, T. G., Tsui, T. Y., Pharr, G. M. & Oliver, W. C. Mechanical-Properties and Microstructures of Metal Ceramic Microlaminates .1. Nb/Mosi2 Systems. *Journal of Materials Research* **7**, 2765-2773 (1992).
67. Wolf, D., Yamakov, V., Phillpot, S. R. & Mukherjee, A. K. Deformation mechanism and inverse Hall-Petch behavior in nanocrystalline materials. *Zeitschrift Fur Metallkunde* **94**, 1091-1097 (2003).
68. Jang, D. & Atzmon, M. Grain-size dependence of plastic deformation in nanocrystalline Fe. *Journal of Applied Physics* **93**, 9282-9286 (2003).
69. Conrad, H. Grain size dependence of the plastic deformation kinetics in Cu. *Materials Science and Engineering a-Structural Materials Properties Microstructure and Processing* **341**, 216-228 (2003).

70. Nieh TG, W. J. Hall-Petch relation in nanocrystalline solids. *Scripta Metallurgica et Materialia* **25**, 955 (1991).
71. Sanders, P. G., Eastman, J. A. & Weertman, J. R. Elastic and tensile behavior of nanocrystalline copper and palladium. *Acta Materialia* **45**, 4019-4025 (1997).
72. Scattergood, R. O. & Koch, C. C. A Modified-Model for Hall-Petch Behavior in Nanocrystalline Materials. *Scripta Metallurgica Et Materialia* **27**, 1195-1200 (1992).
73. Takeuchi, S. The mechanism of the inverse Hall-Petch relation of nanocrystals. *Scripta Materialia* **44**, 1483-1487 (2001).
74. Van Swygenhoven, H. & Weertman, J. R. Preface to the viewpoint set on: mechanical properties of fully dense nanocrystalline metals. *Scripta Materialia* **49**, 625-627 (2003).
75. Van Swygenhoven, H., Spaczer, M., Caro, A. & Farkas, D. Competing plastic deformation mechanisms in nanophase metals. *Physical Review B* **60**, 22-25 (1999).
76. Yamakov, V., Wolf, D., Phillpot, S. R., Mukherjee, A. K. & Gleiter, H. Dislocation processes in the deformation of nanocrystalline aluminium by molecular-dynamics simulation. *Nature Materials* **1**, 45-48 (2002).
77. Yamakov, V., Wolf, D., Salazar, M., Phillpot, S. R. & Gleiter, H. Length-scale effects in the nucleation of extended dislocations in nanocrystalline Al by molecular-dynamics simulation. *Acta Materialia* **49**, 2713-2722 (2001).
78. Van Swygenhoven, H., Spaczer, M. & Caro, A. *Acta Mater* **47**, 3117 (1999).
79. Van Swygenhoven, H. & Derlet, P. A. Grain-boundary sliding in nanocrystalline fcc metals. *Physical Review B* **64**, 024104-1~7 (2001).
80. Van Swygenhoven, H., Derlet, P. M. & Hasnaoui, A. Atomic mechanism for dislocation emission from nanosized grain boundaries. *Physical Review B* **66**, - (2002).
81. Derlet, P. M., Van Swygenhoven, H. & Hasnaoui, A. Atomistic simulation of dislocation emission in nanosized grain boundaries. *Philosophical Magazine* **83**, 3569-3575 (2003).
82. Derlet, P. M. & Van Swygenhoven, H. Length scale effects in the simulation of deformation properties of nanocrystalline metals. *Scripta Materialia* **47**, 719-724 (2002).
83. Hasnaoui, A., Van Swygenhoven, H. & Derlet, P. M. Cooperative processes during plastic deformation in nanocrystalline fcc metals: A molecular dynamics simulation. *Physical Review B* **66**, - (2002).
84. Hasnaoui, A., Van Swygenhoven, H. & Derlet, P. M. Dimples on nanocrystalline fracture surfaces as evidence for shear plane formation. *Science* **300**, 1550-1552 (2003).

85. Van Swygenhoven, H. & Caro, A. Plastic behavior of nanophase metals studied by molecular dynamics. *Physical Review B* **58**, 11246-11251 (1998).
86. Yamakov, V., Wolf, D., Phillpot, S. R. & Gleiter, H. Deformation twinning in nanocrystalline Al by molecular dynamics simulation. *Acta Materialia* **50**, 5005-5020 (2002).
87. Froseth, A., Van Swygenhoven, H. & Derlet, P. M. The influence of twins on the mechanical properties of nc-Al. *Acta Materialia* **52**, 2259-2268 (2004).
88. Ke, M., Hackney, S. A., Milligan, W. W. & Aifantis, E. C. Observation and Measurement of Grain Rotation and Plastic Strain in Nanostructured Metal Thin-Films. *Nanostructured Materials* **5**, 689-697 (1995).
89. Williams, D. B. & Carter, C. B. *Transmission electron microscopy : a textbook for materials science* (Plenum Press, New York, 1996).
90. Shan, Z. W. et al. Grain boundary-mediated plasticity in nanocrystalline nickel. *Science* **305**, 654-657 (2004).
91. Mitra, R., Chiou, W. A. & Weertman, J. R. In situ study of deformation mechanisms in sputtered free-standing nanocrystalline nickel films. *Journal of Materials Research* **19**, 1029-1037 (2004).
92. Budrovic, Z., Van Swygenhoven, H., Derlet, P. M., Van Petegem, S. & Schmitt, B. Plastic deformation with reversible peak broadening in nanocrystalline nickel. *Science* **304**, 273-276 (2004).
93. Raj, R. & Ashby, M. F. On Grain Boundary Sliding and Diffusional Creep. *Metallurgical Transactions* **2**, 1971-1113 (1971).
94. Harris, K. E., Singh, V. V. & King, A. H. Grain rotation in thin films of gold. *Acta Materialia* **46**, 2623-2633 (1998).
95. Moldovan, D., Wolf, D. & Phillpot, S. R. Theory of diffusion-accommodated grain rotation in columnar polycrystalline microstructures. *Acta Materialia* **49**, 3521-3532 (2001).
96. Chen, M. W. et al. Deformation twinning in nanocrystalline aluminum. *Science* **300**, 1275-1277 (2003).
97. Hirth, J. P. & Lothe, J. *Theory of dislocations* (New York : Wiley, c1982., 1982).
98. Murr, L. E. *Interfacial Phenomena in Metals and Alloys* (Addison Wesley, Reading MA, 1975, 1975).
99. Dobson, P. S., Goodhew, P. J. & Smallman, R. E. *Phil Mag* **16**, 9 (1967).

100. Weertman, J. R. Structure and mechanical behavior of bulk nanocrystalline materials. *Mater. Res. Soc. Bull.* **24**, 44-50 (1999).
101. Koch, C. C., Morris, D. G., Lu, K. & Inoue, A. Ductility of nanostructured materials. *MRS Bulletin* **24**, 54-58 (1999).
102. Lu, L., Sui, M. L. & Lu, K. Superplastic extensibility of nanocrystalline copper at room temperature. *Science* **287**, 1463-1466 (2000).
103. Van Swygenhoven, H. Polycrystalline materials - Grain boundaries and dislocations. *Science* **296**, 66-67 (2002).
104. Liao, X. Z., Zhou, F., Lavernia, E. J., He, D. W. & Zhu, Y. T. Deformation twins in nanocrystalline Al. *Applied Physics Letters* **83**, 5062-5064 (2003).
105. Liao, X. Z. et al. Formation mechanism of wide stacking faults in nanocrystalline Al. *Applied Physics Letters* **84**, 3564-3566 (2004).
106. Shan, Z. W. et al. TEM studies of plasticity mechanisms in nanocrystalline Ni during tensile deformation. *MRS Fall meeting, Boston* (2004).
107. Shan, Z. W. et al. Response to Comment on "Grain Boundary-Mediated Plasticity in Nanocrystalline Nickel". *Science* **308**, 356 (2005).
108. Weertman, J. & Weertman, J. R. *Elementary dislocation theory* (Oxford University Press, New York, 1992).
109. Valiev, R. Z., Alexandrov, I. V., Zhu, Y. T. & Lowe, T. C. Paradox of strength and ductility in metals processed by severe plastic deformation. *Journal of Materials Research* **17**, 5-8 (2002).
110. Yang, W. & Wang, H. T. Mechanics modeling for deformation of nano-grained metals. *Journal of the Mechanics and Physics of Solids* **52**, 875-889 (2004).
111. Brenner, S. S. Growth and Properties of "Whiskers". *Science* **128**, 568-575 (1958).
112. Courtney, T. H. *Mechanical behavior of materials* (McGraw-Hill, New York, 1990).
113. Hirsch, P. B. *Prog. in Metal Phys.* **6**, 236 (1957).
114. Herring, C. & Galt, J. K. *Phys. Rev.* **85**, 1060 (1952).
115. Gane, N. The direct measurement of the strength of metals on a sub-micrometre scale. *Proc. Phys. Soc. Lond. A* **317**, 367-391 (1970).
116. Meyers, M. A. & Chawla, K. K. *Mechanical behavior of materials* (Prentice Hall, Upper Saddle River, N.J., 1999).

117. Weertman, J. R. *Mechanical Behavior of Nanocrystalline Metals in Nanostructured Materials: Processing, Properties, and Potential Applications* (William Andrew, Norwich, CT, 2002).
118. Ebrahimi, F., Bourne, G. R., Kelly, M. S. & Matthews, T. E. Mechanical properties of nanocrystalline nickel produced by electrodeposition. *Nanostructured Materials* **11**, 343-350 (1999).
119. Mukai, T. et al. Nanostructured Al-Fe alloys produced by e-beam deposition: static and dynamic tensile properties. *Acta Materialia* **51**, 4197-4208 (2003).
120. Schwaiger, R., Moser, B., Dao, M., Chollacoop, N. & Suresh, S. Some critical experiments on the strain-rate sensitivity of nanocrystalline nickel. *Acta Materialia* **51**, 5159-5172 (2003).
121. Iwasaki, H., Higashi, K. & Nieh, T. G. Tensile deformation and microstructure of a nanocrystalline Ni-W alloy produced by electrodeposition. *Scripta Materialia* **50**, 395-399 (2004).
122. Chen, M. W. & Yan, X. Q. Comment on "Grain Boundary Mediated Plasticity in Nanocrystalline Nickel". *Science* **308**, 356 (2005).
123. Suryanarayana, C. Structure and Properties of Nanocrystalline Materials. *Bulletin of Materials Science* **17**, 307-346 (1994).
124. Cai, B., Kong, Q. P., Lu, L. & Lu, K. Interface controlled diffusional creep of nanocrystalline pure copper. *Scripta Materialia* **41**, 755-759 (1999).
125. Lu, L., Sui, M. L. & Lu, K. Superplasticity extensibility and deformation mechanism of a nanocrystalline copper sample. *Advanced Engineering Materials* **3**, 663-667 (2001).
126. Wang, Y. M. & Ma, E. Three strategies to achieve uniform tensile deformation in a nanostructured metal. *Acta Materialia* **52**, 1699-1709 (2004).
127. Haque, M. A. & Saif, M. T. A. Deformation mechanisms in free-standing nanoscale thin films: A quantitative in situ transmission electron microscope study. *Proceedings of the National Academy of Sciences of the United States of America* **101**, 6335-6340 (2004).
128. Haque, M. A. & Saif, M. T. A. In-situ tensile testing of nano-scale specimens in SEM and TEM. *Experimental Mechanics* **42**, 123-128 (2002).
129. Haque, M. A. & Saif, M. T. A. Application of MEMS force sensors for in situ mechanical characterization of nano-scale thin films in SEM and TEM. *Sensors and Actuators a-Physical* **97-8**, 239-245 (2002).
130. Haque, M. A. & Saif, M. T. A. A review of MEMS-based microscale and nanoscale tensile and bending testing. *Experimental Mechanics* **43**, 248-255 (2003).

131. Minor, A. M., Morris, J. W. & Stach, E. A. Quantitative in situ nanoindentation in an electron microscope. *Applied Physics Letters* **79**, 1625-1627 (2001).
132. Wall, M. A. & Dahmen, U. An in situ nanoindentation specimen holder for a high voltage transmission electron microscope. *Microscopy Research and Technique* **42**, 248-254 (1998).
133. Stach, E. A. et al. Development of a nanoindenter for in situ transmission electron microscopy. *Microscopy and Microanalysis* **7**, 507-517 (2001).
134. Schiotz, J. & Jacobsen, K. W. A maximum in the strength of nanocrystalline copper. *Science* **301**, 1357-1359 (2003).
135. Burke, J. E. & Turnbull, D. *Prog. Metal Phys.* **3**, 220 (1952).
136. Haslam, A. J., Phillpot, S. R., Wolf, H., Moldovan, D. & Gleiter, H. Mechanisms of grain growth in nanocrystalline fcc metals by molecular-dynamics simulation. *Materials Science and Engineering a-Structural Materials Properties Microstructure and Processing* **318**, 293-312 (2001).
137. Li, J. C. M. *J. Appl. Phys.* **33**, 2958 (1962).
138. Dannenberg, R., Stach, E. A., Groza, J. R. & Dresser, B. J. In-situ TEM observations of abnormal grain growth, coarsening, and substrate de-wetting in nanocrystalline Ag thin films. *Thin Solid Films* **370**, 54-62 (2000).
139. Wang, N., Wang, Z. R., Aust, K. T. & Erb, U. Isokinetic analysis of nanocrystalline nickel electrodeposits upon annealing. *Acta Materialia* **45**, 1655-1669 (1997).
140. Haslam, A. J. et al. Effects of grain growth on grain-boundary diffusion creep by molecular-dynamics simulation. *Acta Materialia* **52**, 1971-1987 (2004).
141. Hirsch, P. B. *Electron microscopy of thin crystals* (Butterworths, Washington,, 1965).